SHARING

SELF-ORGANIZED HETEROGENEOUS ADVANCED RADIO NETWORKS GENERATION

Deliverable D3.1

New opportunities, challenges and innovative concepts candidates for Multi-point transmission and reception

Date of delivery	31/07/2014
Contractual date of delivery	31/07/2014
Project number	C2012/1-8
Editor(s)	Yolanda Fernández, Adrián Sánchez (TTI)
Author(s)	Yolanda Fernández (TTI), Adrián Sánchez (TTI), Sandeep Kottath (FT), Thierry Clessienne (FT), Yasser Fadlallah (FT), Nivine Abbas (FT), Serdar Sezginer (SEQ), Cécile Germond (TCS), Grégory Gougeon (SIR), Mathieu Brau (SIR), Yoann Corre (SIR), Yves Lostanlen (SIR), Mohamad Assaad (SUP), Sheng Yang (SUP), Antoine Berthet (SUP), David Gesbert (EUR), Xinping Yi (EUR), Sylvie Mayrargue (CEA)
Dissemination level	PU
Workpackage	3
Version	1.0
Total number of pages	100

Abstract:

This document describes the main challenges and objectives of several promising techniques for multi-point transmission and reception, which will be studied along SHARING project. It details transmitter-side cooperative solutions to suppress or avoid interference with CoMP and advanced MIMO schemes. Moreover the main design concerns for next-generation communication systems in terms of interference cancellation are introduced together with different methods for handling of interference in cellular networks. A proposed ray-based propagation model is presented to allow network operators to properly plan for future network deployments. And finally different key aspects related to RF front-ends and antennas are discussed to support carrier aggregation. Architecture requirements are not included, as they will be presented as a separate document (Excel sheet format).

Keywords: CoMP, coordinated scheduling, joint processing, MIMO, interference cancellation, interference management, channel modelling, carrier aggregation.

Document Revision History

Version	Date	Author	Summary of main changes
0.1	24/04/2014	All	Creation of the Table of Contents (ToC)
0.2	29/05/2014	TTI	TTI contribution
0.3	04/06/2014	SEQ	SEQ contribution
0.6	10/06/2014	TTI	FT contribution
0.7	11/06/2014	TTI	TCS contribution
0.9	13/06/2014	SIR	SIR contribution
0.10	17/06/2014	SUP	SUP contribution
0.11	17/06/2014	SIR	SIR update
0.12	18/06/2014	TTI	Format update
0.13	18/06/2014	SIR	Figure 33 update
0.14	18/06/14	EUR	EUR contribution
0.16	23/06/2014	TTI	Editing update
0.17	30/06/2014	CEA	CEA contribution
0.19	14/07/2014	SEQ and CEA	Internal review
0.22	16/07/2014	SIR	Corrections after internal review
0.24	18/07/14	EUR	Corrections after internal review
0.25	17/07/2014	SEQ	Updated SEQ contribution after internal review
0.30	22/07/2014	SUP	Updated SUP contribution after internal review
0.32	23/07/2014	FT	Updated FT contribution after internal review
1.00	31/07/2014	TTI	Final version

TABLE OF CONTENTS

LIST OF FIGURES

LIST OF TABLES

EXECUTIVE SUMMARY

Deliverable D3.1 "New opportunities, challenges and innovative concepts candidates for Multi-point transmission and reception" presents the preliminary analysis and results for several promising techniques for multi-point transmission and reception as well as interference management techniques, which will be studied within the SHARING project. Furthermore, a realistic simulation framework is evaluated based on a ray-based propagation model to provide tools to network operators for future network deployments. Finally, some key aspects related to RF front-ends and antennas are studied and analysed in order to deal with the challenging RF issues to support carrier aggregation in small cells.

In all studies, detailed descriptions of the different solutions are presented showing their main challenges to improve performance and capacity gains in near-future wireless networks.

WP3 investigates the benefits of cooperation in multi-point transmission and reception schemes from different points of view: transmitter-side cooperation (Chapter 2), interference mitigation at the receiver (Chapter 3) and cross-layer interference mitigation within a transmitter-receiver cooperation framework (Chapter 4). Firstly, different transmitter-side cooperative solutions are analysed to suppress or avoid interference with CoMP and advanced MIMO schemes. These solutions could be distinguished based on the way interference is tackled: via (coordinated) user scheduling or via interference control beamforming (such as coordinated beamforming and joint processing CoMP). Secondly, interference mitigation mechanisms at the receiver are introduced and requirements and challenges of interference handling mechanisms on DL and UL are assessed. Enhanced spatial modulation schemes are also discussed. Thirdly, various interference management techniques are envisaged from different perspectives.

A realistic simulation framework is also evaluated, whose aim is to reduce the gap between real network performance and simulations using simplified models. This approach includes realistic environment and network deployment models as well as a ray-based propagation model. This study could support network operators in future deployments through prediction of network capacity and user's satisfaction. A simulation scenario for heterogeneous networks (HetNets) has also been defined.

Additionally, different key aspects related to RF front-ends and antennas have been discussed in the context of small cells to support carrier aggregation. Some solutions have been proposed to deal with the challenging RF issues such as using meta-materials to optimize the radiation properties of the antenna or adding reconfigurability features at power amplifier to provide energy efficiency enhancements.

The information enclosed in this document will be extended in further deliverables providing results from solutions presented here. Furthermore, it would help cross-WP discussions based on the different proposed innovations.

1 INTRODUCTION

This report presents the main challenges and objectives for multi-point transmission and reception solutions, as well as interference management techniques developed in WP3, presenting some initial evaluation results when they are available. Furthermore some key aspects related to RF front-ends and antennas are studied to support carrier aggregation.

As a reminder, WP3 activities are divided into four tasks:

T3.1: "Multi-point cooperation at the transmitter";

T3.2: "Interference cancellation at the receiver and advanced transceivers";

T3.3: "Flexible interference management concept"; and

T3.4: "RF and antenna design".

In each task, different promising solutions are studied to provide new enhancements for mobile heterogeneous cellular networks.

Chapter 2 presents transmitter-side cooperative solutions to suppress or avoid interference with CoMP and advanced MIMO schemes. Some studies on CoMP methods will be addressed to evaluate the real gains in cellular networks. Based on the settings where interference is tackled, different techniques will be studied: coordinated user scheduling and beamforming based on interference control.

The main design concerns for next-generation communication systems in terms of interference cancellation are introduced in chapter 3, where the requirements and challenges of interference handling mechanism both on DL and UL, and enhanced spatial modulation schemes will be discussed.

Chapter 4 investigates different methods for handling of interference in cellular networks and how to combine these methods in a concept that is flexible in terms of its ability to adapt to diverse deployment scenarios and to combine potentials network elements for cross layer optimization.

The aim of chapter 5 is to study a simulation framework to reduce the gap between real network performance and simulations with simplified models, proposing a ray-based propagation model. This task could allow networks operators to properly plan for future deployments and the assessment of network capacity or user's satisfaction.

In chapter 6, different key aspects related to RF front-ends and antennas to support carrier aggregation are discussed in the context of small cells. Innovative RF front-end solutions are studied to handle bandwidths up to 100MHz allowing reconfigurability in terms of bandwidth and frequency of operation. Meanwhile, meta-materials are considered to reduce the size of multi-band antennas.

For each innovation, the corresponding scenario presented in D2.2 is indicated in the very beginning of the section. This allows easy tracking of the solutions/innovations which will be provided as solutions to the scenarios/problems defined in the beginning of the project. For some of the innovations, there is not a corresponding scenario defined in D2.2, meaning that those innovations have been added later on, mainly due to the late confirmation of the definite participation/funding of some partners to the project.

2 MULTI–POINT COOPERATION AT THE TRANSMITTER

LTE-A commonly referred to as LTE-Advanced (LTE-A) is the Release 10 of 3GPP LTE, introduces techniques [1] which enable to answer the increasing demand for multimedia content available anywhere and anytime.

CoMP (Coordinated Multi-Point) aims at improving the quality of service of users at cell edge (which answers to the above mentioned "anywhere" requirement). Indeed, users located at cell edge experience both lower received signal power and increased inter-cell interference compared to those at cell centre. Cooperation between adjacent cells can mitigate these issues.

The CoMP concept was first mentioned in [2] and introduced in [3]. Generally, CoMP is a word which aggregates various concepts in uplink (UL) and downlink (DL) based on more or less complexity at the receivers side. Several CoMP schemes have been defined already in the 3GPP Release 8 both in DL and UL (Figure 1):

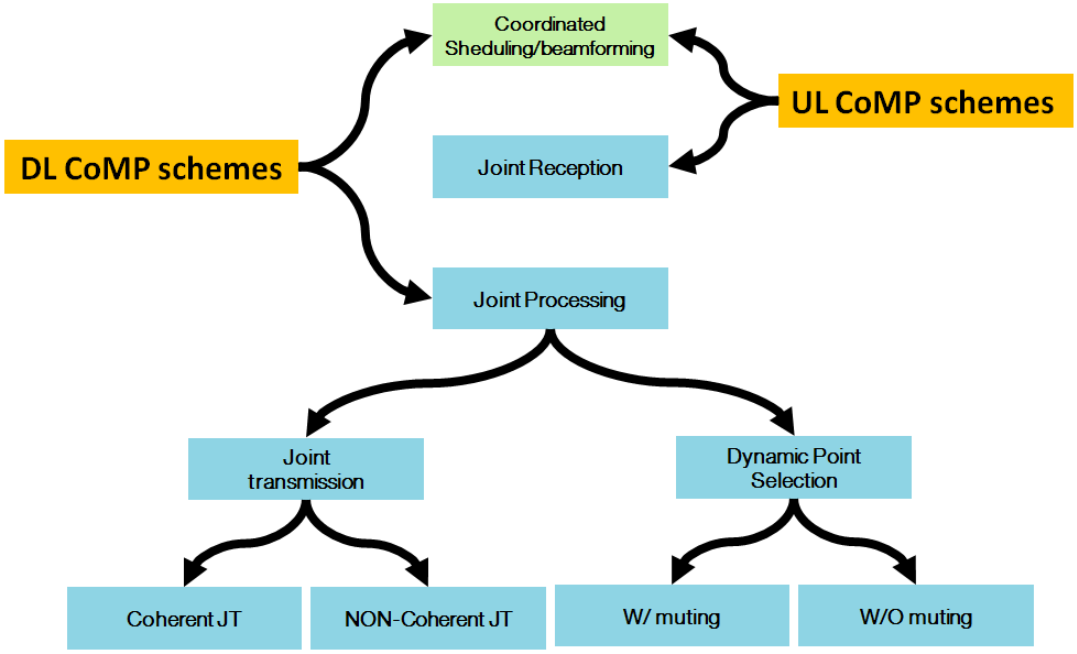

Figure 1 Different CoMP schemes

There are two types of CoMP schemes:

- Joint Processing (JP): Data for a UE is available at more than one point in the CoMP cooperating set (set of - geographically separated - points directly and/or indirectly participating in data transmission to a UE in a given time-frequency resource). Two JP schemes are defined:
  - Joint Transmission (JT): Simultaneous data transmission from multiple points (geographically separated or not) to a single UE or multiple UEs in the same time-frequency resource. Data to a UE is simultaneously transmitted from multiple points, e.g. to (coherently or non-coherently) improve the received signal quality and/or data throughput
  - Dynamic point selection (DPS)/muting: Data transmission from one point (within the CoMP cooperating set) in a time-frequency resource. The transmitting/muting point may change from one subframe to another including varying over the RB pairs within a subframe. Data is available simultaneously at multiple points.
- Coordinated Scheduling/Beamforming (CS/CB): Data for a UE is only available at and transmitted from one point in the CoMP cooperating set (DL data transmission is done from that point) for a time-frequency resource but user scheduling/beamforming decisions are made with coordination among points corresponding to the CoMP cooperating set. The transmitting points are chosen semi-statically.

And these two types are both studied in the present document.

In this task we study transmitter-side cooperative solutions to suppress or avoid interference with CoMP and advanced MIMO schemes. Even though CoMP methods are extremely promising, this is a multi-faceted challenging problem, as can be seen from the fact that despite several years of intense study

under the auspices of 3GPP, it is still not clear what are the real gains to be expected from CoMP in cellular networks or what are the best signal processing and RAN network architectures for it. Through this task and a multi-angle attack we hope to shed some light on this area.

First the settings where interference is tackled via (coordinated) user scheduling, as opposed to beamforming based interference control (such as coordinated beamforming and joint processing CoMP), are distinguished. Coordinated scheduling algorithms are proposed and evaluated which give interference mitigation gains. Clearly the gains depend on the number of users (the more the better for greater multiuser diversity) but also on the information exchange capability between the interfering eNBs. Decentralized scheduling methods, which work with few users, are therefore investigated.

In the case of multi-antenna based interference reduction, we show that a key discriminating factor is the amount of feedback (channel state information at the transmitter (CSIT)) allowed on the uplink. Hence feedback design studies are crucial.

In one innovation, a new form of feedback design for CoMP is investigated based on the notion of wireless broadcast: in this case the user estimates the downlink channels, then broadcasts a quantized version of them on the uplink towards any eNB (hence including interfering eNBs) capable of decoding this feedback. Broadcast feedback is currently non LTE compliant however exhibits interesting scalability advantages for dense small cells networks.

More generally, assuming a standard compliant feedback design, a key objective addressed by this task is to evaluate just how much feedback about each user is required at any eNB for a satisfactory performance. We provide an information theoretic answer to this question with a key notion being the need to coordinate within a limited neighbourhood dictated by the strength of interference.

When the backhaul capabilities do not allow for a full sharing of the CSIT, an interesting question is also to evaluate the loss of CoMP methods compared with the ideal full CSIT setting. In this case, new methods ought to be derived that are capable of producing good transmitter design solution with an incomplete description of the CSIT. There are several strategies in this context: one strategy consists in allowing multiple antenna combining at the RX side, in which case the receivers can handle the interference mitigation task while the transmit antennas can be used for another purpose, such as diversity oriented space time coding, or non-coherent CoMP designs. Such schemes are studied here. Finally another approach consists in forming robust precoders that can handle partial CSIT or delayed CSIT. New algorithms are derived in this context as well.

2.1 Coordinated Scheduling Techniques

2.1.1 Advanced Scheduling for intra and inter-site CoMP

Corresponding scenario in D2.2: 2.1.6 "Multipoint coordination schemes for LTE-A networks"

2.1.1.1 **Introduction**

In this study the performance of the Joint transmission (JT) DL CoMP scheme has been evaluated with a System simulator for intra and inter-site scenarios. The aim of the study is twofold: On the one hand the JT CoMP scheme is evaluated to better understand the benefits of this feature while on the other hand it shows where the gains are achieved between intra or inter site. This last point is the key for the future deployments choice since black fiber and time/phase synchronization are needed to enable the inter-site JT DL CoMP. Note that in this study a perfect backhaul assumption has been used.

2.1.1.2 **Problem description**

CoMP for inter-site scenario requires close coordination between geographically separated eNBs.

Two types of schedulers are considered as shown in Figure 2:

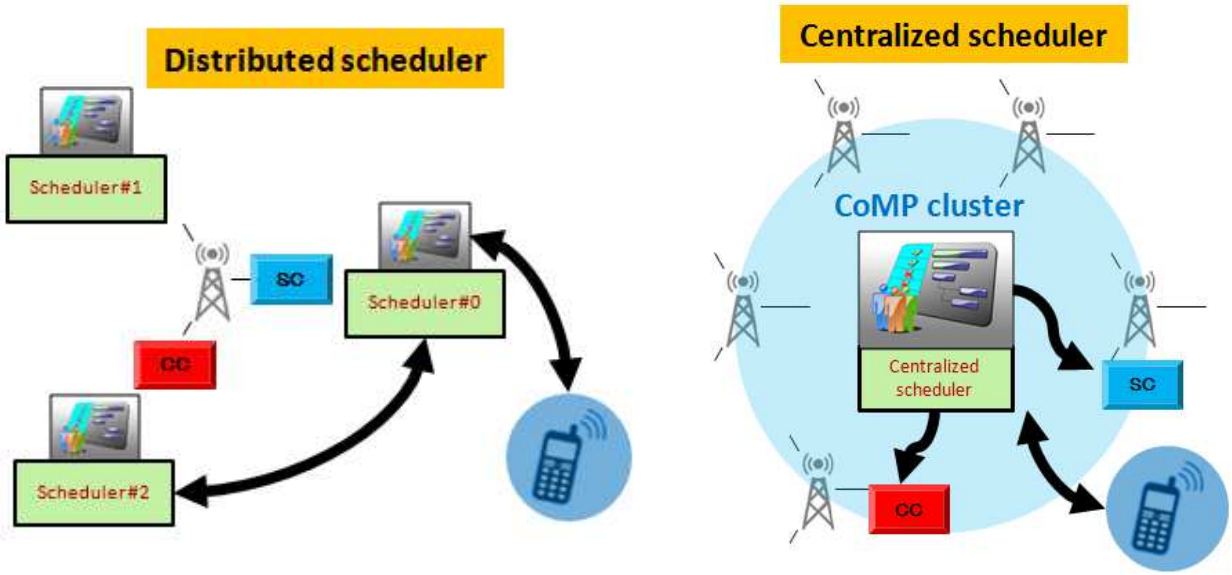

SC = Serving Cell CC = Collaborative Cell

Figure 2 Two scheduling approach for CoMP

In the distributed case the resource allocation is performed per cell in parallel while the centralized scheduler allocates the resource per CoMP cluster.

2.1.1.3 Proposed approach and preliminary analysis

In the case of distributed scheduler, each cell (the serving cell in Figure 2) is associated to one and only one scheduler. The straightforward CoMP scheduler is composed by one distributed scheduler associated by a Call Admission Control process. To assess the CoMP feasibility the serving cell asks to the collaborative cell if the resource blocks are available.

Considering the fact that two UEs populations (nCUEs and CCUEs) have to be scheduled, two strategies are proposed for the distributed case:

- Successive scheduling with prioritization: A strict prioritization is performed. CoMP Candidate UEs (CCUEs) over no-CoMP UEs (nCUEs) then the controversy.
- Simultaneously scheduling: The scheduling is only based on Proportional Fairness (PF) metric without any other consideration.

For these two strategies and depending on the availability of the resource blocks on the serving cell an nCUE will be served or not. At the beginning of a transmission cell a CCUE will become:

- a served CUE (CoMP UE) if SC and CC RBs are available
- a served nCUE if only SC RBs are available
- or stays CCUE if else

During the transmission the UE the status stay the same (a CUE cannot become an nCUE and vice versa). Figure 3 gives the machine state that determines the CoMP status of a given CCUE:

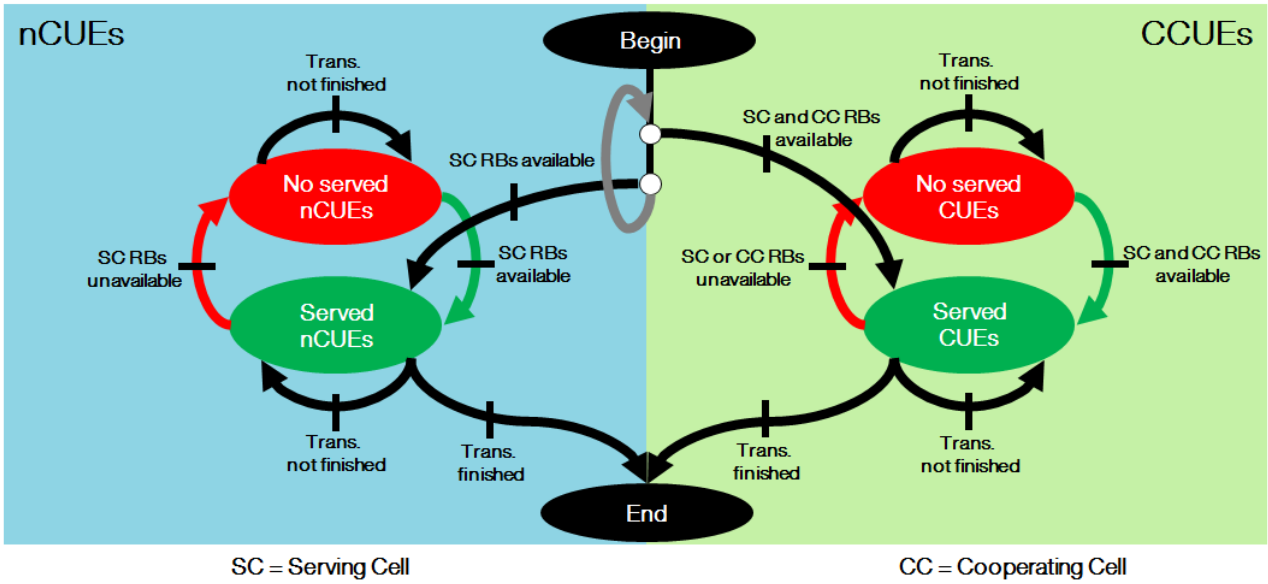

Figure 3 Machine state of the CoMP status determination

2.1.1.4 **Impact of Δ_P on the proportion of CCUEs in the network**

Δ_P is the threshold requirement used to identify the CCUEs: CoMP UEs are selected when the Reference Signal Received Power (RSRP) difference between serving cell and other cells satisfies a threshold requirement, e.g. $RSRP_{UE\_k,\ serving\_cell} - RSRP_{UE\_k,Cell\_i} < \Delta_P$. Figure 4 shows the UEs considered as CoMP candidate depending on the Δ_P.

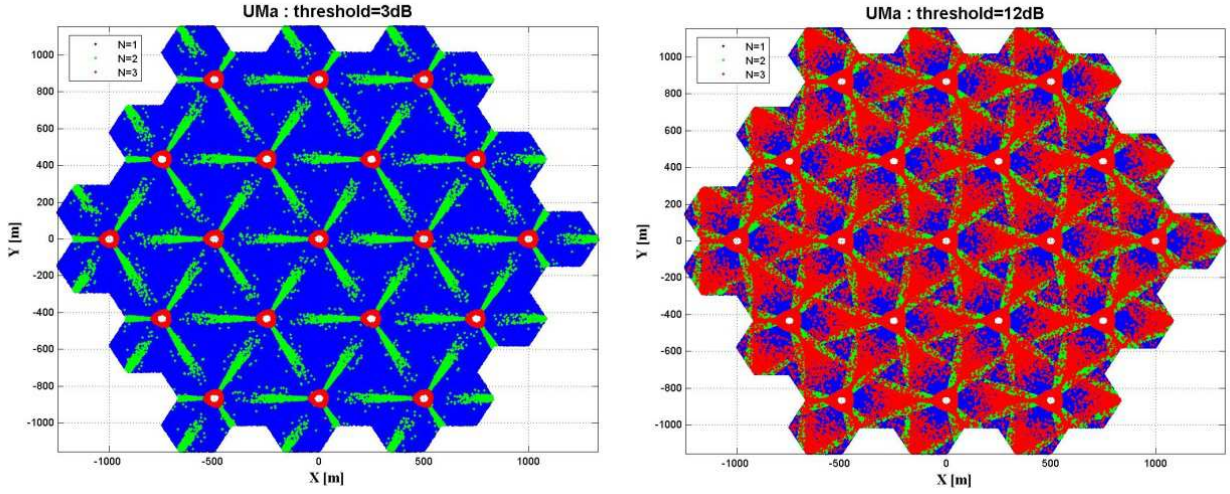

Figure 4 Localization of UEs considered as CoMP candidate

(Blue N=1, Green N=2, Red N=3)

N represents the size of the CoMP measurement set:

- N=1: corresponds to UE without CoMP,
- N=2: the size of the CoMP measurement set equals to 2,
- N=3: the size of the CoMP measurement set equals to 3.

Notice that a ring around each e-Node B exists: in this area the antenna gain does not depend any more on the angle of azimuth, all RSRP received from the 3 cells are equal.

The following figure shows the evolution of the percentage of CCUEs for different values of Δ_P. This percentage increases with Δ_P. For Δ_P = 21dB 100% of the UEs are CCUEs (the maximum attenuation of

the combined antenna pattern is 20dB). In [4], the combined antenna pattern at angles off the cardinal axes is computed as:

$$-\min\left[-\left(A(\theta)+A_e(\phi)\right), A_m\right]$$

$A(\Theta)$ and $A(\phi)$ are respectively the horizontal and elevation antenna patterns and $A_m = 20dB$ is the maximum attenuation. Δ_P has 2 antagonist effects: at one side the number increase (a lot of UEs will take benefice of CoMP) but on another side the complexity of CoMP increases too (for a moment each UE can be CUE).

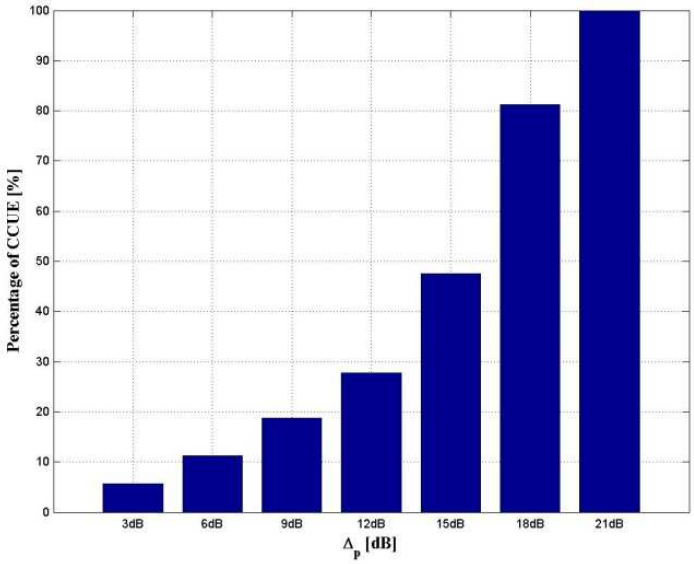

Figure 5 Evolution of the percentage of CCUEs for different values of Δ_P

2.1.1.5 Intra-site CoMP system performance Gain for successive scheduling with prioritization

The studied CoMP category is the Coherent-JT (only one stream sent). Figure 6, Figure 7 and Figure 8 show the Intra-site CoMP system for successive scheduling with prioritization:

(a) nCUEs are first scheduled

(b) CCUEs are first scheduled

(c) Cell-edge user throughput [bps/user] and spectral efficiency [bps/Hz/user].

Cell-edge user throughput (or Gain @ 5%) is the 5-percentile user throughput, obtained from the cumulative distribution function of the user throughput.

For low average cell load situation, CoMP presents gain at cell-edge no matter the scheduling strategy: in this situation there is enough available RB to guaranty the opportunity to be CUE. In opposite site, in high average cell load situation, there is a hard competition between UEs to access to the resource. CUE will inevitably induce a resource sharing.

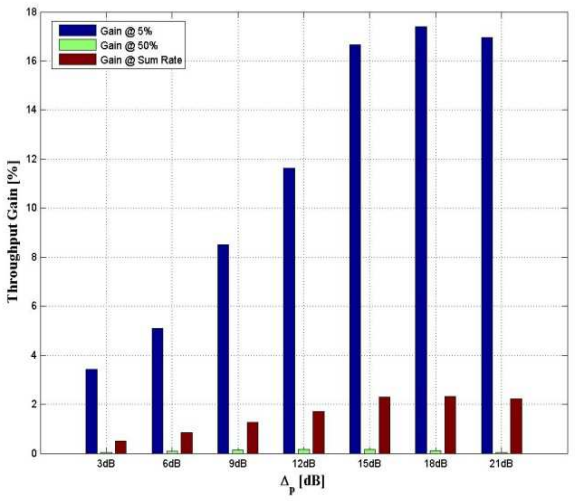

(a) nCUEs are first scheduled

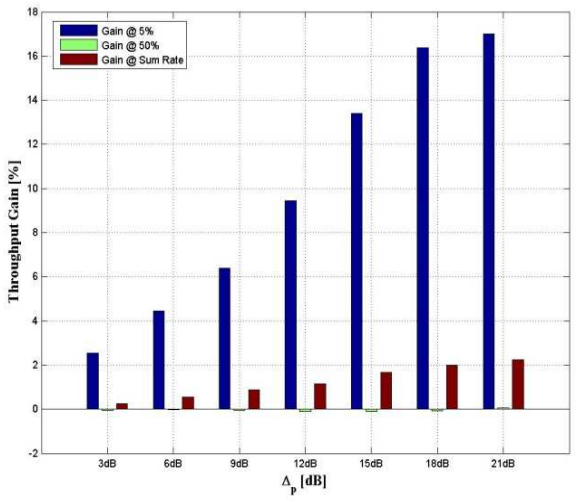

(b) CCUEs are first scheduled

Figure 6 Intra-site CoMP system performance Gain: Average cell load = 20%

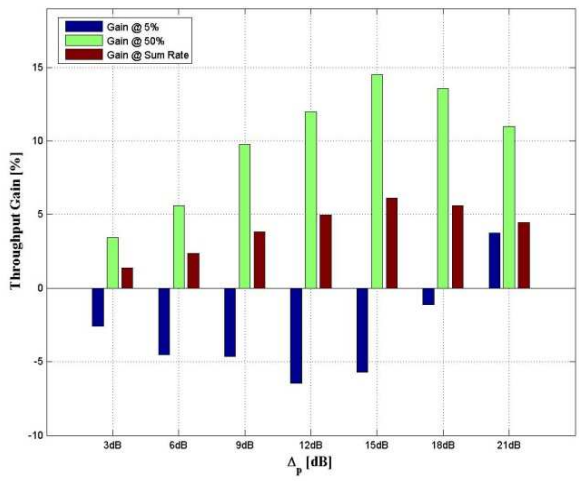

(a) nCUEs are first scheduled

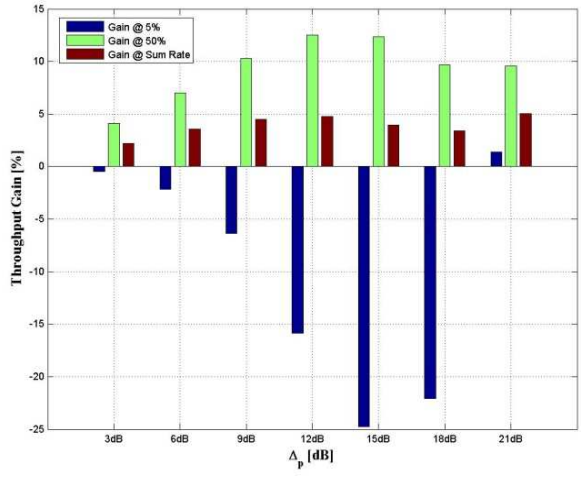

(b) CCUEs are first scheduled

Figure 7 Intra-site CoMP system performance Gain - nCUEs are first scheduled: Average cell load = 60%

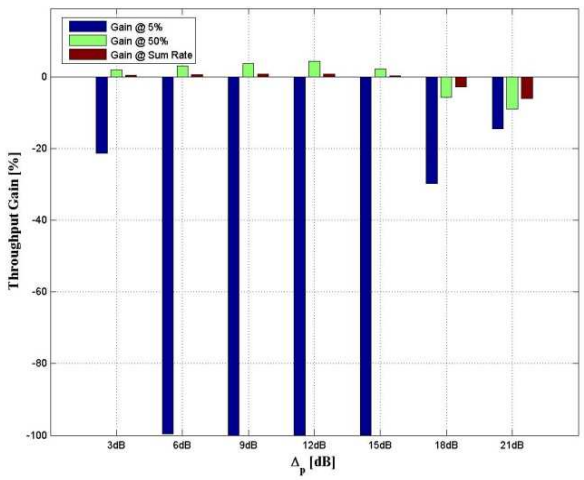

(a) nCUEs are first scheduled

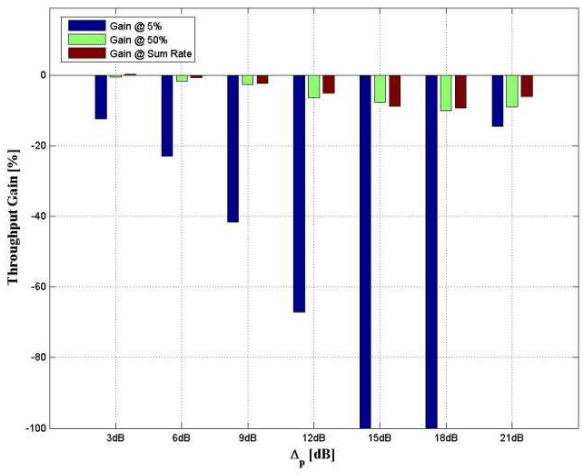

(b) CCUEs are first scheduled

Figure 8 Intra-site CoMP system performance Gain - nCUEs are first scheduled: Average cell load = 100%

The weakness of successive scheduling with prioritization is that in some configuration UEs are not served (there are no more the required resources to serve the least priority UEs):

Table 1 Percentage of no served nCUE – nCUEs are first scheduled

		Average cell load [%]		
		20	60	100
ΔP [dB]	3	0.0	0.0	0.0
	6	0.0	0.0	0.0
	9	0.0	0.0	0.1
	12	0.0	0.1	1.0
	15	0.0	0.9	4.8
	18	0.0	2.1	7.2
	21	0.0	0.0	0.0

Notice that for Δ_P =21dB all the UEs are CCUEs (there is not a prioritization anymore).

2.1.1.6 **Intra-site CoMP system performance Gain for Simultaneously scheduling**

Figure 9 shows the Intra-site CoMP system performance when all UEs are scheduled simultaneously.

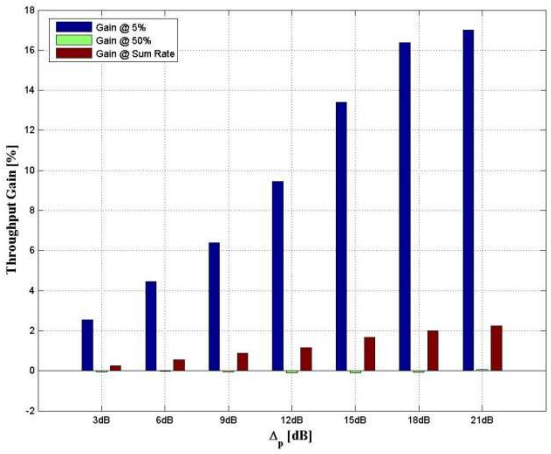

(a) Average cell load = 20%

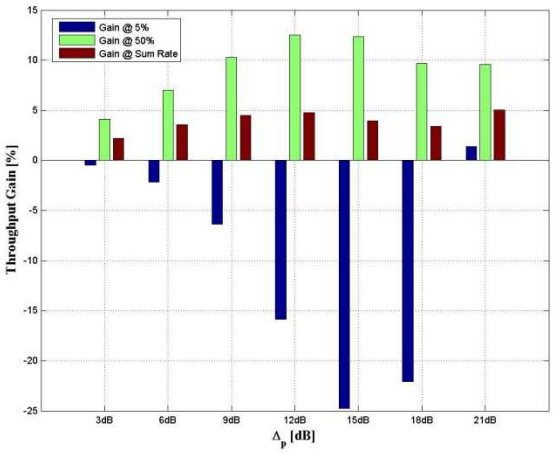

(b) Average cell load = 60%

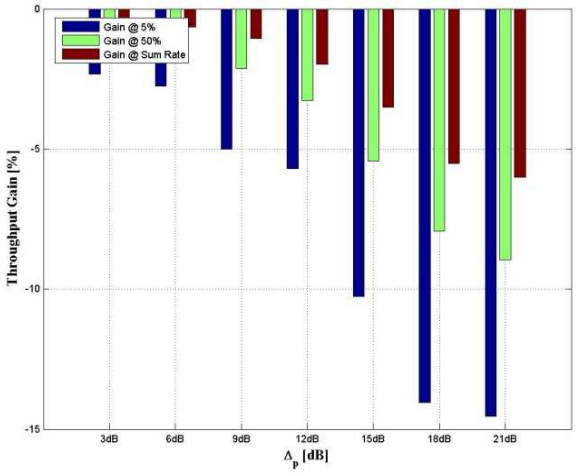

(c) Average cell load = 60%

Figure 9 Intra-site CoMP system performance Gain for Simultaneously scheduling

The last scheduling approach seems to be best approach to avoid the no-served UE situation.

2.1.1.7 **Next steps**

The CoMP transfer function shows the throughput when activating the CoMP function with the distributed scheduling.

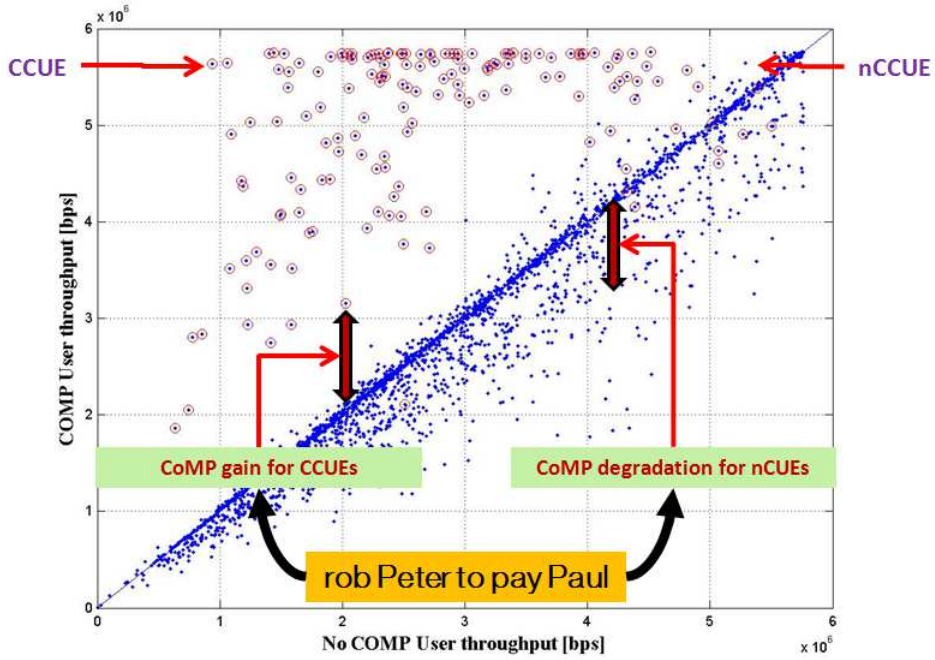

Figure 10 Weakness of the studied scheduler

The improvement of the CoMP performances is made to the detriment of the legacy UEs. The next step will treat the weakness of this scheduler (highlighted by the figure) through a centralized opportunistic approach (to introduce more fairness between the CCUEs and nCUEs).

2.2 Joint Processing Techniques

Joint processing CoMP (JP-CoMP) with shared user's data and channel state information (CSI) is one of the transmitter-side cooperative solutions to mitigate interference. The sharing of the user's data symbols and the CSI to all cooperating transmitters (TXs) imposes huge requirements on the backhaul architecture. The following innovations investigate the problem of feedback design and allocation for JP-CoMP, evaluate the performance loss with limited backhaul, and study a new form of feedback design for CoMP based on the notion of wireless broadcast.

2.2.1 Spatial CSIT Allocation for JP-CoMP Schemes

Corresponding scenario in D2.2: 2.9.11"Joint processing CoMP with limited backhaul and spatial CSIT allocation design"

In this innovation, we address the problem of feedback design and allocation for JP-CoMP. With perfect message and CSI sharing, the different TXs can be seen as a unique virtual multiple-antenna array serving all receivers (RXs), in a multiple-antenna broadcast channel (BC) fashion. However, the sharing of the user's data symbols and the CSI to all cooperating TXs imposes huge requirements on the backhaul architecture, particularly as the number of cooperating TXs increases.

Consequently, the cooperation is usually limited to small cooperation clusters inside which the TXs cooperate. Still, clustering leads to some fundamental limitations. Firstly, there is inevitably inter-cluster interference on the boundaries of the cluster, and secondly, it requires the obtaining at all the TXs inside the cluster of the CSI relative to the entire cluster which means that the amount of CSI feedback required quickly increases with the number of TXs inside the cluster.

The objective of this innovation is to answer the question whether it is possible to overcome the fundamental limitations of clustering by optimizing directly the spatial allocation of CSIT. This means: over how many bits should the channel of user X be represented at base station Y, for any position of X and Y. Hence, we will study the minimization of the CSI shared across the TXs subject to a given required performance. To tackle this intricate question, we will consider the high SNR regime and study the number of degrees-of-freedom (DoF) achieved. We will consider also that the pathloss of the interfering links is parameterized as some function of the SNR, so as to model the network geometry and analyze the generalized DoF. This modelling of the pathloss as a function of the SNR is essential to

model the effect of the network geometry in a DoF analysis where the SNR is assumed to become infinitely large. Indeed, omitting to use such a parameterization and letting the SNR become large makes the pathloss differences (i.e., the network geometry) negligible.

Some preliminary results are provided here, and more contribution and results will be described in the next deliverable.

Here, we provide a CSIT dissemination policy, denoted as *distance-based* allowing to achieve the same generalized DoF as that of a cooperative network with perfect CSI at every TX. This CSIT dissemination policy requires only the sharing of the user's data symbols and of the CSI to within a neighborhood which does not increase with the size of the network. Hence, we show that the pathloss attenuation effectively limits the impact of interference to a local neighborhood around each TX and allows for global interference management with only local cooperation.

In a first step, we study a network with a regular geometry where 36 TX/RX pairs are placed at the integer values inside a square of dimensions 6 × 6. We show in Figure 11 the average rate achieved with different CSIT allocation policies. Specifically, the distance-based CSIT allocation is compared to two alternative CSIT allocations, being the uniform CSIT allocation where the bits are allocated *uniformly* to the TXs, and the clustering one in which (non-overlapping) *regular clustering of size* 4 is used. Both CSIT allocations are chosen to have the same size as the distance-based one.

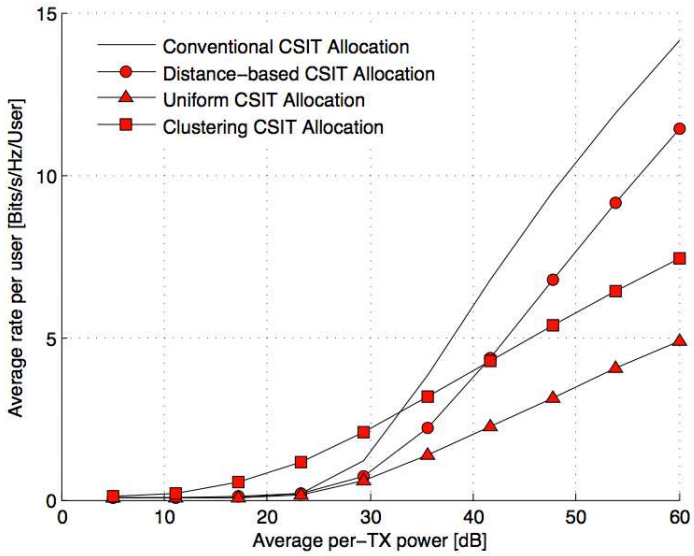

Figure 11 Average rate per user as a function of the SNR for 36 TX/RX pairs. The TX/RX pairs are positioned at the integers values inside a square of dimensions 6 × 6. The 3 limited feedback CSIT allocations used have the same size which is equal to 9% of the size of the conventional CSIT allocation

With these parameters, the size of the distance based CSIT allocation is only equal to 9% of the size of the conventional CSIT allocation. Nevertheless, it can be observed to achieve the maximal generalized DoF while the clustering solution has a smaller slope. The distance-based CSIT allocation suffers from a strong negative rate offset. However, this offset is a consequence of our analysis being limited to the high SNR regime and can be also observed in the fact that JP with clustering outperforms Zero-Forcing (ZF) precoding based on the conventional CSIT-allocation without clustering, which represents in fact the true reference for our scheme. Indeed, using ZF with many users is very inefficient at not-too-high SNR, particularly in a network with strong pathloss. Therefore this strong negative rate offset can be easily reduced by optimizing the precoding scheme and the CSIT allocation at finite SNR. The key element being that the distance-based CSIT allocation does not present the usual limitations of clustering, i.e., edge-interference and bad scaling properties as the size of the cluster increases.

2.2.2 JP-CoMP with Limited Backhaul

Corresponding scenario in D2.2: 2.9.11"Joint processing CoMP with limited backhaul and spatial CSIT allocation design"

The exploitation of multiple antennas for JP-CoMP heavily relies on the availability of sufficiently accurate CSIT. Yet, obtaining the CSIT represents a challenge in fast fading channels. Indeed, in frequency division duplexing (FDD) systems, the channel estimate has to be fed back from the RXs which inevitably introduces some delays and degradations.

The conventional assumption of having a single imperfect channel estimate perfectly shared to all the TXs, which we call hereafter the centralized CSIT configuration, appears as rather optimistic in the case of non-collocated cooperating TXs. As a consequence, we consider here a novel CSIT configuration where every TX receives its own channel estimate of the multi-user channel. This knowledge is then used to compute the transmit coefficients locally without additional communication between the TXs. This setting, referred to as the distributed CSIT scenario, opens new problems and remains little studied despite its practical relevance. The performance has so far only been evaluated in terms of DoF which, although helpful to get insights, is not adapted for practical system design. In particular, it is not known whether the feedback schemes for the BC with centralized CSIT remain efficient when the CSIT is distributed. Answering this question is the main goal of this task.

Due to the CSIT distributedness, the increased amount of leaked interference owing to the less coordinated precoding coefficients is challenging to be quantified, and even worse it is not clear if the analysis for the centralized case can be adapted to the distributed CSIT.

The contribution and results will be described in the next deliverable.

2.2.3 Broadcast Channel Feedback in Cooperated Multiple Antenna Systems

Corresponding scenario in D2.2: 2.9.13 "Broadcast channel feedback in cooperated multiple antenna systems"

We consider an FDD wireless communication network consisting of M base stations and a total of K active users. Each base station is equipped with J antennas and the user terminals are assumed to have a single antenna. We assume that all or a subgroup of base stations serve the users in a Joint Processing CoMP fashion applied through possibly disjoint clusters where the number of clusters may vary from the ideal single cluster case (whole network cooperation) to the extreme case of M clusters (i.e., no cooperation between base stations).

Since we consider an FDD network, channel reciprocity is not valid except in terms of path loss (and hence average SNR). We assume that each user in the network is able to estimate its downlink channel from all the M base stations through a training phase. This channel is quantized and then fed back (broadcast) to all the base stations that can hear this user in the uplink (using non-interfering feedback links).

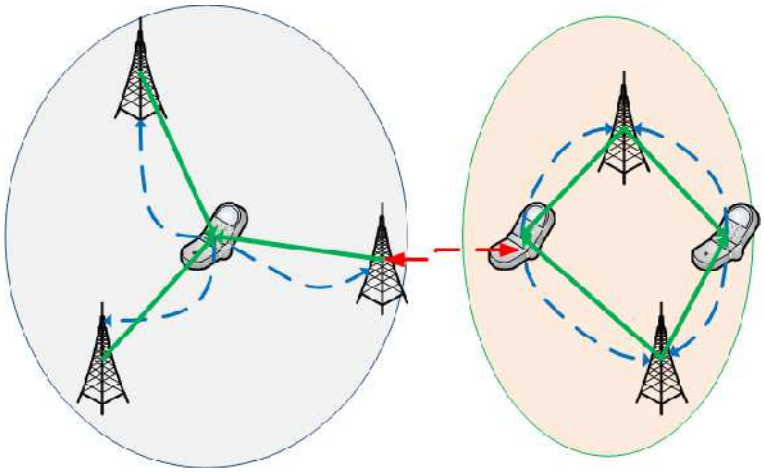

Figure 12 Example of joint CSIT and cooperation cluster. The dashed arrows represent successfully decoded broadcast feedback on the uplink. The solid (green) arrows represent BS serving users in the downlink, belonging to one of two joint CSIT clusters

If B is the number of feedback bits per user and Cmk is the uplink channel capacity [in bits/channel use] from kth user to mth base station, our feedback model is simplified into a simple comparison as follows:

- If Cmk < B then BS m is not able to decode the feedback sent by terminal k (no feedback) and will not attempt to serve it.
- If Cmk >= B then BS m decodes the feedback from terminal k without error.

The knowledge of a given user channel at one particular base station clearly conditions the ability of the base station to serve (jointly with other cooperating bases) that user. We consider a clustering approach where cluster formation is dynamic and based on the availability of channel knowledge; hence the notion of CoMP cluster and joint CSIT cluster will coincide. We define a joint CSIT cluster as follows:

- A Joint CSIT Cluster Sn is defined as a disjoint subgroup of users and base stations such that feedback from all users in the cluster has been successfully decoded by all the base stations in the cluster. We assume that there is coordination between the base stations to exchange the cluster information.

We are interested in finding the best possible disjoint cooperation clusters naturally arising out of the CSI feedback pattern in order to perform JP-CoMP. The description of the proposed algorithm in order to achieve this goal can be found in [5]. The main results from the paper are summarized below.

The distributed broadcast feedback model exhibits an interesting novel trade-off between feedback accuracy and consistency. If the channels are quantized finely (B large), this will favor the accuracy of feedback at the base stations which are closest to the terminal, but will result in some base stations not being able to obtain CSIT and hence the cluster size will reduce. This will increase other-cluster interference (OCI) but reduce intra-cluster interference (ICI). On the other hand a coarser quantization (B small) will lead to a consistent (yet less accurate) estimation of the channel state at more base stations. This will increase ICI due to imperfection in the precoder design but reduce OCI. This points to the existence of an optimum number of bits, B_opt which, if we quantize the CSI, will yield the highest sum rate, which is confirmed from our simulations below.

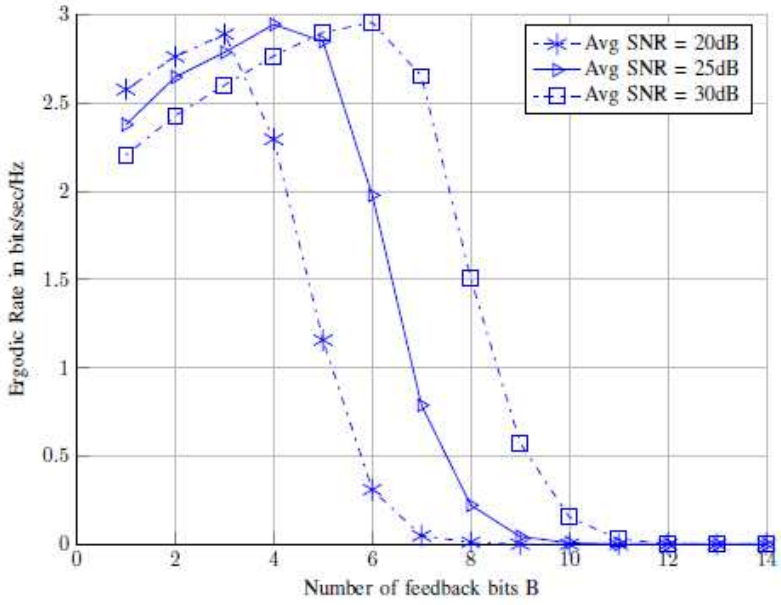

Figure 13 Ergodic rate as a function of B, showing an optimum feedback bits behaviour for a 19 cell network

As it can be seen in Figure 13, the ergodic rate achieved by a user reduces when we increase number of feedback bits beyond B_opt. In this latter region, we can say that the channel quality (SNR) is the limiting factor. Hence, there is no point in increasing the feedback bits more than B_opt. When there is a better channel (higher SNR), we can increase the number of feedback bits again and get better performance. We have also derived a lower bound of this achieved rate to get more insights into the problem, and to allow obtaining B_opt using analytical expression (without running simulations).

We have proposed the concept of broadcast feedback for use in multi-cell CoMP systems. We have shown that this particular design approach naturally leads to a distributed precoding framework for multi-cell MIMO networks. Quantized broadcast channel state feedback leads to a novel trade-off between feedback consistency and accuracy which is specific to the multi-transmitter cooperation scenario.

2.3 Downlink Multi-user CoMP with Interference Aware Receiver

Corresponding scenario in D2.2: 2.1.7 "Joint processing CoMP algorithm, combined with interference cancellation at the receiver"

In this study, we will focus on two techniques: CoMP (Cooperative Multi-Point), and MU-MIMO ((Multi-User MIMO), that were introduced in LTE-A in order both to improve cell edge users quality of service, and to increase cell spectrum efficiency. We will use them jointly, and study their performance when used with a user terminal whose receiver has interference rejection capability.

2.3.1 Problem Description

2.3.1.1 CoMP

As was recalled in the introduction of this section, there are two types of CoMP schemes, namely Joint Processing, and Coordinated scheduling/ Beamforming. We will focus in the following on a subcase of the first category of schemes, Joint Processing-Joint Transmission, where data for a UE are available at more than one point of the CoMP cooperative set of base stations.

From the definition of JT CoMP, it is clear that the price to pay to obtain improved quality at cell edge is a loss of resources in the set of cooperative eNBs considered as a whole, since the same resource block is used in each eNB to serve a single user. Therefore, in order to compensate for this loss of resources, it is necessary to complement JT CoMP with MU-MIMO.

2.3.1.2 MU-MIMO

The first multi antenna scheme to be introduced in 3GPP was beamforming, in RAN #13 meeting (September 2001): N correlated antennas at the base station enable to steer a beam towards a user, thus improving its SINR roughly by a factor N (antenna gain).

SU-MIMO (Single User MIMO) was introduced in LTE release 8. In this scheme, the link capacity is increased by exploiting signal diversity between an antenna array at the transmitter side and an antenna array at the receiver side. Considering the downlink, with 2 to 4 antennas at the base station (Release 8), up to two transport blocks are mapped on up to 4 layers (antennas). The terminal, which has up to 4 receive antennas, is able to decode the two transport blocks, provided that the channel matrix rank is at least two. In order to facilitate the decoding process, Transmitted Mode 4 (closed loop spatial multiplexing) uses a predefined pre-coder matrix. The selection of the precoder is performed by the eNB, after receiving feedback from the terminal: RI (Rank Indication) and PMI (Precoding Matrix Indication). RI is calculated by the terminal based on channel matrix measurements, and determines the number of layers. PMI is based on channel matrix measurement and knowledge of precoder matrix: the terminal chooses its preferred precoder matrix. Since the number of precoder matrices is small, only its index has to be fed back, thus reducing the signalling load.

MU-MIMO could be viewed as a hybrid between SU-MIMO and beamforming. Indeed a MU-MIMO system is formed by a multiple antenna base station communicating with several single antenna terminals, forming a distributed multiple antenna system. Here we will consider MU-MIMO LTE Transmission Mode 5 (codebook-based closed loop spatial multiplexing with one layer dedicated for one UE). Similar to SU-MIMO Transmission Mode 4, transmitted data are precoded by the eNB before transmission. As in the SU-MIMO case, the PMI takes into account the resulting SINR, i.e. not only the best steering vector towards the user, but the best steering vector towards the co-scheduled users. The difference with SU-MIMO is that the eNB has the capability to choose, among all users, which ones to co-schedule. However, this latter issue belongs to RRM and will not be addressed in this contribution.

2.3.1.3 Combined CoMP and MU-MIMO

Figure 14illustrates in a simplified way a MU-MIMO CoMP network. Three eNBs are serving in the same time/frequency resource three UEs. UEs 2 and 3, at cells edge, are served in CoMP JP-JT. Each eNB uses a precoding matrix to realize a MU-MIMO transmission toward two UEs (the transmissions are here schematized by antenna diagrams).

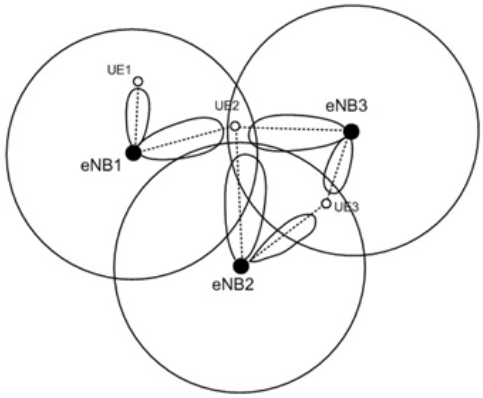

Figure 14 MU-MIMO network. All transmission are made in the same time/frequency resource

If, on paper, the idea of using the potential of MIMO systems to realize Multi User cooperative transmissions is seducing, it turns out that many practical obstacles arise when it comes to practice. In [6] some of these obstacles are described.

First, the mandatory presence of data in several distant points at the same time requires a backhaul link with high capacity and short latency. Synchronization in time and frequency of transmitters must also be considered. For time synchronization, the choice of the cooperating points is restricted by the size of the cyclic prefix of OFDM symbols.

Most critical aspects however are the estimation of channels at the UE side, the quantity of information to feedback to the eNBs and the frequency of this feedback. In the ideal world, eNBs would have a perfect and instantaneous knowledge of downlink channels and would then be able to choose at any time the best UEs to co-schedule i.e. to compute precoding matrices that maximize the useful signal and minimize the interference. In reality, in FDD mode, eNBs cannot benefit from the reciprocity between downlink and uplink channels as in TDD mode. They must then wait that UEs feedback them the information necessary for the choice of the UEs to schedule. To estimate downlink channels, the UE can rely on different types of pilots (Reference Signals: RS) [7], Cell-specific Reference Signal (CRS)/UE-specific DeModulation Reference Signal (DM-RS) and CSI Reference Signal (CSI-RS). The design of time/frequency patterns of RS must take into account the number of antennas, the coherence time and the coherence bandwidth of the channel. The LTE standard [3] allows for an explicit and an implicit channel state/statistical information feedback. The former, called explicit feedback is the feedback of the channel as observed by the receiver. The latter is the feedback of a reduced quantity of information (CQI, PMI …). The implicit feedback helps minimize the occupied bandwidth on the uplink but causes a loss of reliability due to the compression of the information. In addition, the frequency of this feedback must be taken into consideration. A high frequency allows a fast update of the precoding matrices, but in return requires a higher bandwidth on the uplink.

In order to minimize this feedback, the LTE standard [7] provides the use of a quite reduced set of precoding matrices. Unfortunately, in addition to the drawbacks given above, the very poor resolution of these precoders gives rise to interference at the co-scheduled receivers.

2.3.2 3GPP-LTE Network Assisted Interference Cancellation and Suppression

Advanced receivers for interference management have been introduced in release 11 studies [8]. The idea beyond these studies is to increase the role of the receiver in the mitigation of interference in the network. Indeed, the major benefit of receiver side techniques in the DL is the dramatical decrease of the required UL feedback signalling in the network. Linear interference suppression (IS) receivers have first been introduced in [8]. A step forward in increasing the role of the receiver was the specification of interference rejection combining (IRC) receivers. Non-linear interference cancellation receivers have then been shown to provide significant gain over linear receivers.

More recently, in [9], 3GPP has defined scenarios for network-assisted interference cancellation and suppression (NAICS). In this document, 3GPP gives a framework for assessing the performance of advanced receivers with various degrees of knowledge about interfering transmissions. Information that may be provided to the receiver are for example the presence and the characteristics of interference, its resource allocation scheme, its reference symbols (for enabling channel estimation), and its modulation format and/or coding rate. Providing more information to the receiver nevertheless implies defining new

signalling in the DL. NAICS then requires standardization effort. Future work in 3 GPP may include evaluation of the trade-off between network-assisted receivers and "blind" receivers, in terms of complexity, performance and signalling overhead

NAICS receivers can be divided into three categories [9]. Each receiver type realizes a trade-off, to be evaluated, between performance, complexity, network coordination and network signalling.

2.3.2.1 Interference Suppression (IS) receivers

These receivers apply linear filtering to the received signal to suppress the interference. They do not explicitly cancel the interference. IS receivers can be categorized as follow:

- Linear MMSE-IRC (LMMSE-IRC). It is the receiver used as a baseline for MMSE-IRC study in [8].
- Enhanced LMMSE-IRC (E-LMMSE-IRC). These receivers explicitly consider interferer channel estimates and other interferer knowledge. Interference parameters that can enable interferer channel estimation are needed, including, for example, its DMRS or CRS with PMI/RI.
- Widely linear MMSE-IRC (WLMMSE-IRC). WLMMSE-IRC exploits the additional degrees of freedom from the real and imaginary part of the received signal to enhance suppression of interference. Real-valued modulation may be used to increase performance of the WLMMSE-IRC receiver.

2.3.2.2 Maximum Likelihood (ML) receivers

These are non-linear receivers. They can be divided into three categories:

- ML. Useful and interference signals are entirely and jointly detected, following the ML criterion. Interference parameters that can enable interferer channel estimation and interferer detection at symbol level (e.g. modulation) are needed.
- Reduced complexity ML (R-ML). The same receivers as previously but with reduced complexity. The same level of knowledge of interference as ML receivers is required.
- Iterative ML and iterative R-ML. Iterative MAP detection and decoding of useful and interference signals. Both successive and parallel processing implementations may be applied. More interference information than for ML is required, i.e. interference knowledge that can enable code word demodulation and decoding is needed. Assumptions on network coordination may also be necessary.

2.3.2.3 Interference Cancellation (IC) receivers

IC receivers are non-linear receivers. They can be divided into four categories:

- Linear Code word level SIC (L-CWIC). Receiver utilizing successive application of linear detection (e.g.: LMMSE-IRC), decoding, re-encoding, and cancellation. The same interference knowledge as Iterative ML and Iterative R-ML is required and assumptions on network coordination may be necessary.
- ML-CWIC. Receiver utilizing successive application of ML or reduced complexity ML detection, decoding, re-encoding, and cancellation. The same interference knowledge as L-CWIC is required and assumptions on network coordination may be necessary.
- Symbol level IC (SLIC). Successive cancellation receiver utilizing successive application of linear detection, reconstruction, and cancellation. The same interference knowledge as ML/R-ML is required.
- Parallel interference cancellation (PIC). Parallel IC as opposed to successive IC, otherwise it is similar to SIC. PIC receivers can be categorized into L-CW-PIC, ML-CW-PIC or SL-PIC similar to SIC

2.3.3 Related studies in the literature

DL MU-MIMO must be used together with NAICS receivers in order to suppress the intra-cell interference resulting from the poor granularity of precoders used at the eNB.

[10] considers receivers to combat the mutual interference between co-scheduled users in MU-MIMO. They demonstrate the equivalence of IRC and MMSE receivers in such a case.

[11] proposes a low-complexity interference-aware receiver structure which is characterized by the exploitation of the structure of residual interference. They evaluate, among other things, the performance of their receiver with (Figure 15) and without the knowledge of the interfering

constellation. The authors furthermore introduce a new design of the precoder codebook for forthcoming standardizations of LTE incorporating more levels of transmission.

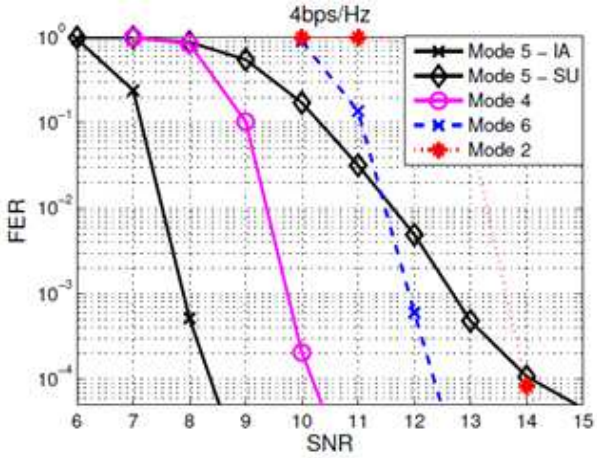

Figure 15 Downlink fast fading channel with the dual-antenna eNodeB and 2 dual-antenna UEs. IA indicates the low-complexity interference aware receiver while SU indicates the single-user receiver. 3GPP LTE rate 1/3 turbo code is used with different puncturing patterns [11]

[12] investigates performances of various types of receiver for LTE MU-MIMO. Based on the assumption that 3GPP standard does not provide information on interfering constellation; they derive a modulation estimation-based joint receiver (Figure 16). The authors also prove that performance of receivers increases with the level of knowledge of the interfering constellation.

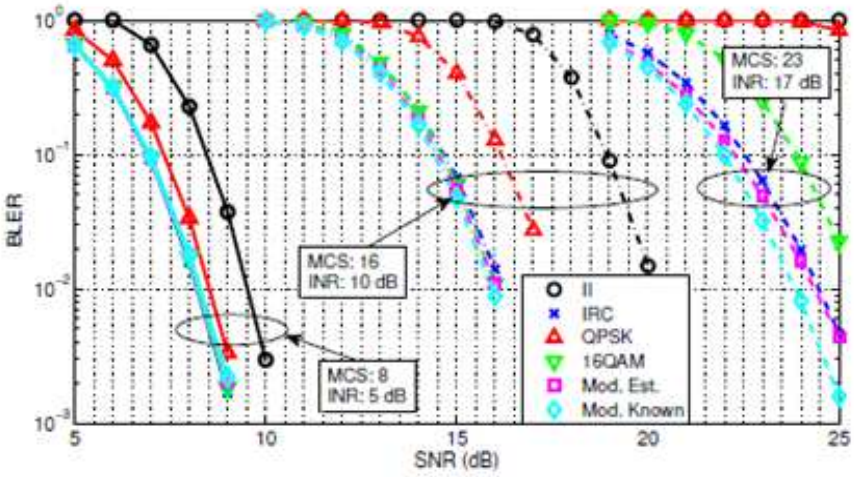

Figure 16 Interference modulation: 64QAM. II: Interference Ignoring, IRC Interference Rejection Combining, QPSK: interference modulation estimated to be QPSK, 16QAM: interference modulation estimated to be 16QAM [12]

[13] is concerned with defining a link level abstraction for system level simulation of systems that are interference-limited rather than noise-limited. MU-MIMO systems are part of this former category.

2.3.4 Proposed Method

The scenario studied is provided within the context of chapters 5, 6 and section 7.5 of [9]:

- Inter- and intra-cell interference conditions will be studied via respectively CoMP and MU-MIMO (LTE Mode 5). The scenario is given by Figure 17, where three UEs are co-scheduled in the same time and frequency resource. We consider a homogeneous network, with macro cell only and an ISD of 500 m. Ideal backhaul between sites is supposed.
- The receiver of interest on Figure 17is UE0. Receiver structures that are able to cancel or suppress the interference from co-scheduled UEs, UE1 and UE2 will be implemented. The eNBs

are equipped with N_T transmit antennas ans the UEs with N_R receive antennas. The grey arrows represent the array broadside of the antenna arrays at eNBs. In order to estimate the trade-off between performance and downlink signaling, their performance will be assessed with different levels of knowledge of the interference:

- o constellation
- o coding rate
- o precoding vectors, ...

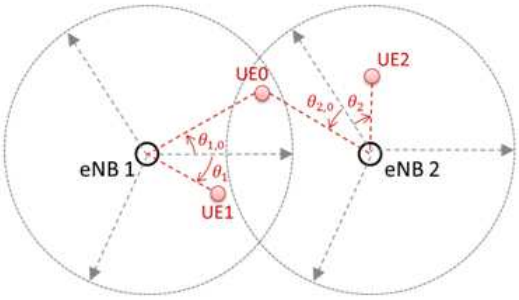

Figure 17 DL MU-MIMO network with CoMP

The study will attempt to prove that MU-MIMO CoMP, despite all the obstacles described above, is a viable technique. To this end, special attention will be paid to designing low computational complexity algorithms at the receiver side. The feedback required at the eNBs for the choice of the precoders will also be the object of particular consideration.

2.4 Cross-layer Performance Evaluation of CoMP

Corresponding scenario in D2.2: 2.1.4 "Cross-layer performance evaluation of multi-cell cooperative schemes in LTE macro cell networks"

2.4.1 Introduction

CoMP is a promising concept to improve cell edge user data rate and spectral efficiency. The main idea of CoMP is that a UE in the cell-edge region receives signals from multiple cell sites and its transmission can be received at multiple cell sites, so if we take the advantage of this multiple reception and transmission, we can improve the link performance. However, with each coordinating site, one more resource is lost. Thus, we should find a trade-off between serving a CoMP user and losing extra resources. This trade-off varies depending on the mobility of the users.

2.4.2 Intra-cell mobility

In order to model the intra-cell mobility, we consider a scenario where a user can move from the center of the cell to the edge and vice versa, and in each region, based on his channel quality as depicted in Figure 18. That user will be served differently with a specific modulation and coding scheme (MCS).Thus each region can be modeled by a different queue with specific average service time depending on the MCS adopted.

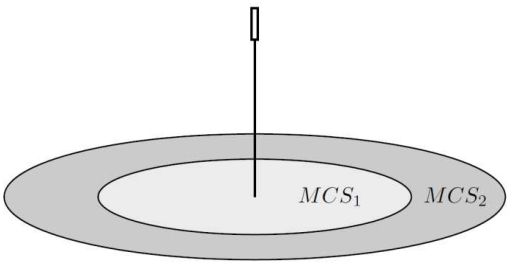

Figure 18 Intra-cell mobility

Since users in both regions share the same resources, each cell can be modeled by a queuing system with coupled processors as shown in Figure 19.

We modeled the center region by a queue of mean service rate μ_1, and we supposed that data flows of the users in the center arrive according to a Poisson process of intensity λ_1, so the corresponding load is $\rho_1 = \frac{\lambda_1}{\mu_1}$. On the other hand, the cell edge region where the users are supposed to arrive with an arrival rate λ_2 is modeled by a queue of mean service rate μ_2, thus the corresponding load of this queue is: $\rho_2 = \frac{\lambda_2}{\mu_2}$.

The two queues are coupled through the mobility mechanism, where ν_1 and ν_2 are the mobility rates, or more precisely the mean speeds at which users moves from one region to another.

Let $X_1(t)$ and $X_2(t)$ be the number of on-going flows in the center region and in the cell edge region respectively, at time t, thus $X(t) = (X_1(t), X_2(t))$ is a two-dimensional Markov process.

Since, load varies from one scenario to another, and between scheduling methods, we took as reference, the load corresponding to a scenario without mobility: $\rho = \rho_1 + \rho_2$.

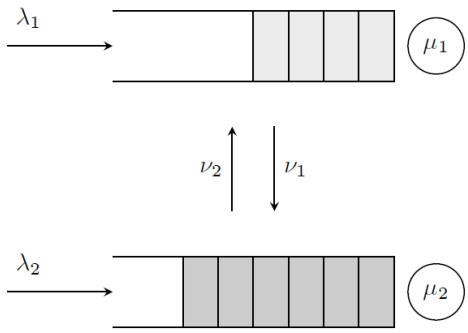

Figure 19 Queuing system modeling intra-cell mobility

We try to compare two scheduling methods, the first (Max C/I) is an opportunistic scheduling which prioritize users with better channel conditions, which means users in the center, while the second method (Proportional Fairness), tries to dynamically allocate resources between the two types of users based on the number of users in each class without taking into account the channel conditions, thus users in the center are served the fraction $\phi_1 = \frac{x_1}{x_1+x_2}$ of the time where cell edge users are served the fraction $\phi_2 = \frac{x_2}{x_1+x_2}$ of the time. Note that those values of ϕ_1 and ϕ_2 are obtained by maximizing $\sum_{i=1,2} x_i \log \phi_i \mu_i$, and with a processor sharing service discipline each user in the system is allocated the fraction $\frac{1}{x_1+x_2}$ of the time which is equivalent to serve users in the cell in Round Robin.

In terms of global performance, there is no big difference between the two described methods when users are immobile (Figure 21). Nevertheless, simulations prove that in the case of a scenario with mobile users, opportunistic scheduling brings significant gain (Figure 20), since prioritizing users with better channel conditions, enable them to be served first and then to profit from their good conditions before leaving the center region, while giving time to the mobile cell edge users to get better channel conditions and then profit from a better service time. This allows to increase the overall bit rate of the system.

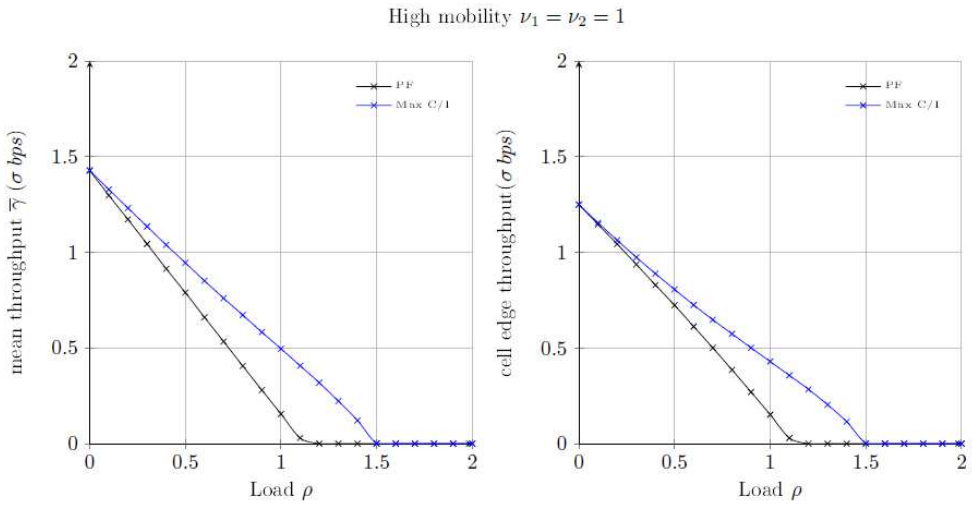

Figure 20 Average and cell edge throughput for mobile users

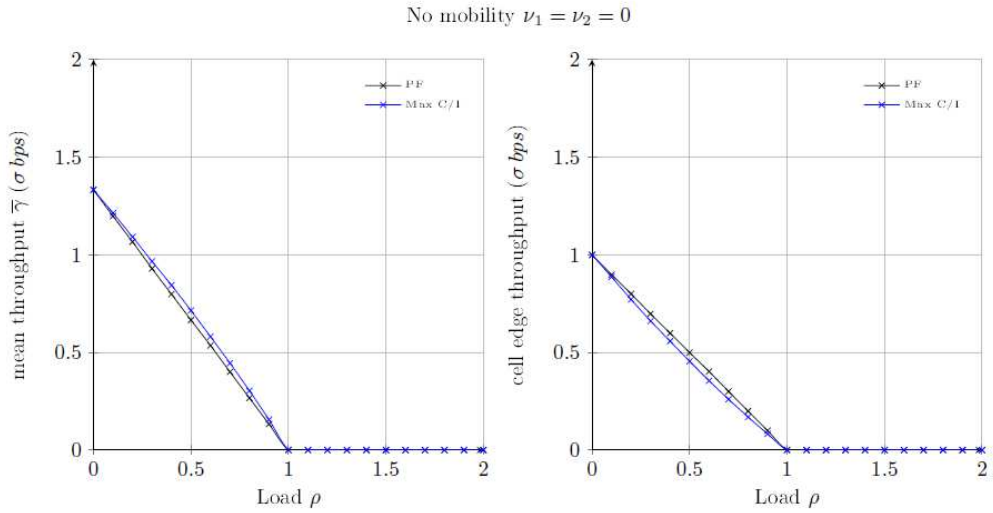

Figure 21 Average and cell edge throughput for static users

2.4.3 Inter-cell mobility &CoMP transmission

In order to study the inter-cell mobility inevitably engendering CoMP transmissions, in our case, we focused on the area represented by Figure 22.

Thus, we modeled the center region of each cell by a queue of mean service rates μ_1 and μ_2, and we supposed that data flows arrive according to a poisson process of intensity λ_1 and λ_2. Hence, the corresponding loads will be $\rho_1 = \frac{\lambda_1}{\mu_1}$ and $\rho_2 = \frac{\lambda_2}{\mu_2}$.

The third queue models the edge regions of both cells, in other words, it models the region where users of mean arrival rate λ_0 can be served as CoMP users at a mean service rate μ_0. The corresponding load is $\rho_0 = \frac{\lambda_0}{\mu_0}$.

We define four mobility rates α_1, α_2, β_1, β_2 as shown in Figure 22.

We took as reference of load: $\rho = \max(\rho_0 + \rho_1, \rho_0 + \rho_2)$.

$X(t) = (X_0(t), X_1(t), X_2(t))$ is a three-dimensional Markov process.

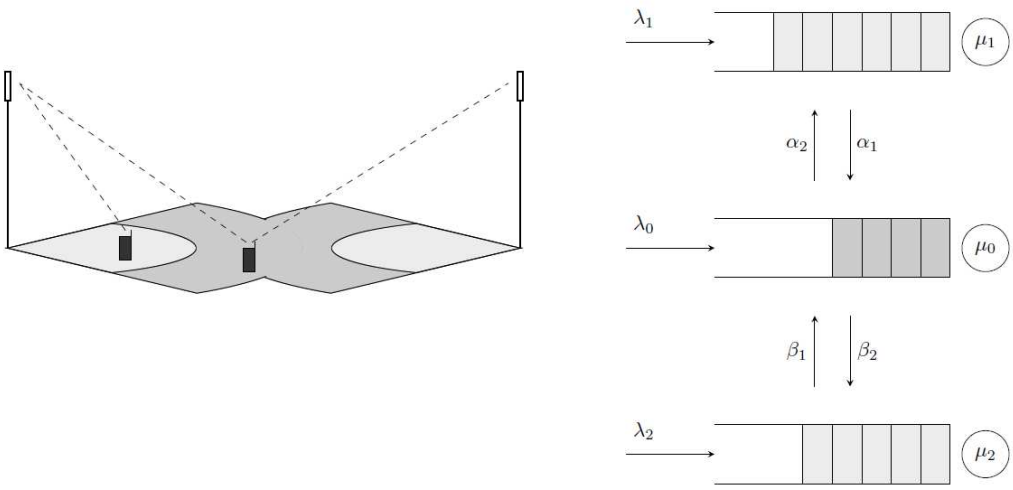

Figure 22 Queuing system modeling inter-cell mobility and CoMP transmission

In the context of a CoMP transmission and for the same reason explained above, it has been proved that prioritizing the users in the center regions is the best method in terms of global performance, when users are supposed to move across the network. This means that it is not worth losing a resource in order to serve a CoMP user if that user is supposed to move to the center and then to profit from better channel conditions, unless the resource is available. However, in the case of a scenario with static users, using a dynamic resource allocation scheme between CoMP and non-CoMP users (PF) proved to be better.

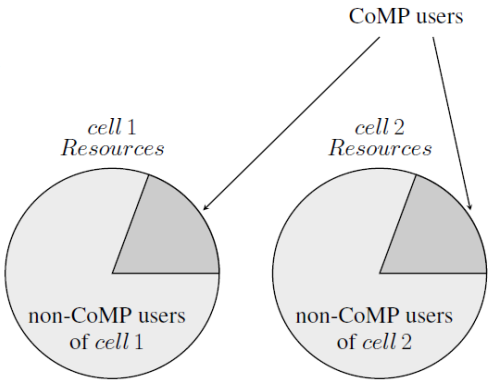

Figure 23 Resource allocation

We try to compare three resource allocation methods as shown in Figure 24: Max C/I which prioritizes users with better channel conditions, proportional fairness PF where resources are dynamically allocated between CoMP and Non-CoMP users based on the number of waiting users in each queue, and fixed allocation (FA) where the shares of CoMP and Non-CoMP users are fixed, so that Non-CoMP users in each cell are allocated $1-\gamma$ of their cell resource, where CoMP users are allocated the fraction γ of each cell resource, since both cells are considered as transmission points for a CoMP user. This fixed allocation creates a considerable waste of resources especially at low load: a user cannot benefit from the share of the other class even if it is available.

For $\gamma = 0.5$:

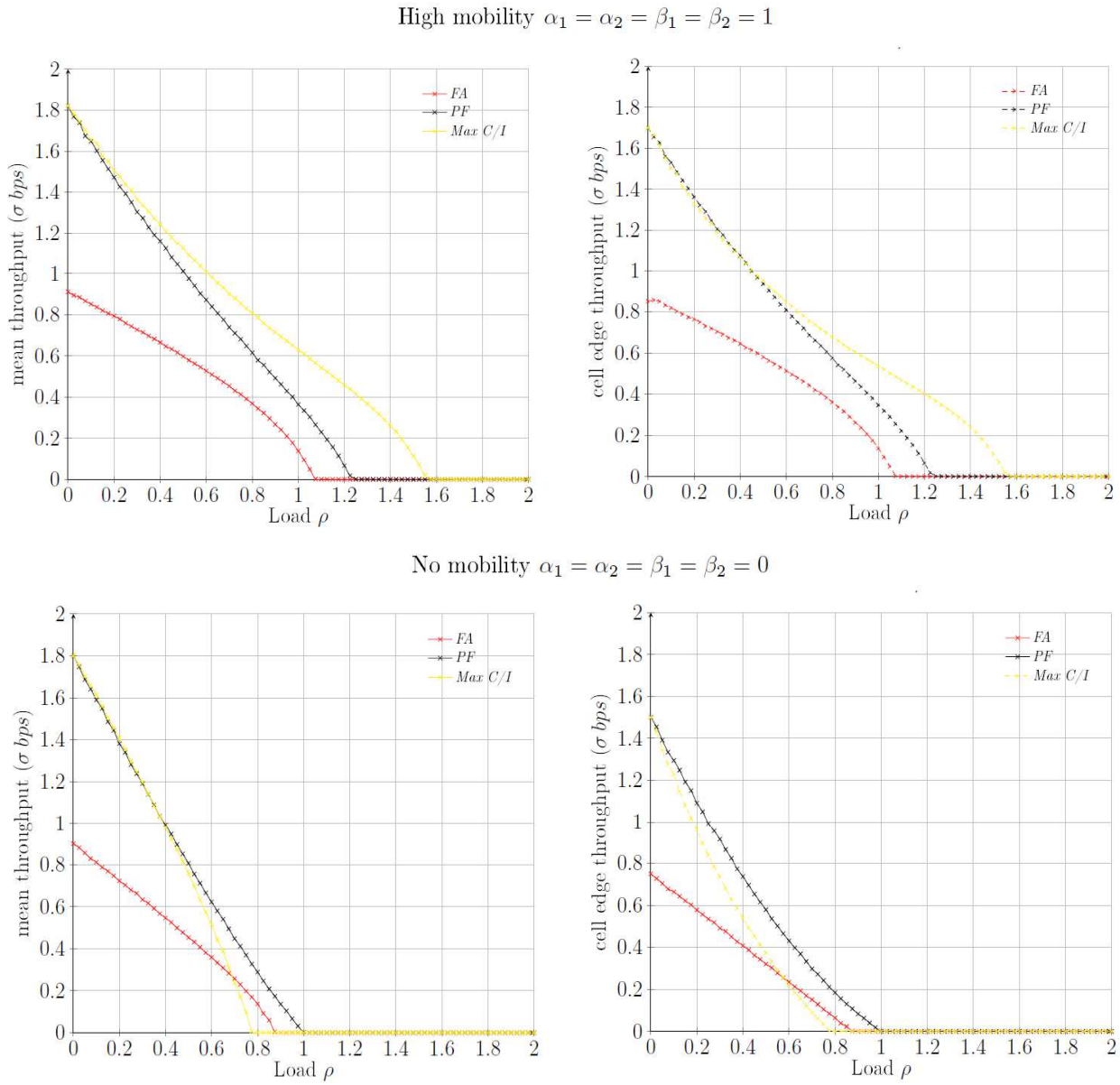

Figure 24 Average and cell edge throughput for different resource allocation methods

We will try to evaluate new scheduling methods that take into account the mobility of the users, supposing that there are two classes of mobility. Moreover, we will try to evaluate these theoretical results using a system level simulator.

2.5 Advanced MIMO Schemes

2.5.1 Transmitter-side Solutions to Suppress or Avoid Interference with Advanced MIMO Schemes

Corresponding scenario in D2.2: 2.1.5 "Interference reduction in LTE through link level processing"

A study about a transmitter-side solution for the suppression or avoidance of interference with advanced MIMO schemes will be carried out. Recently, promising developments have been made on schemes that combine the use of linear dispersive spatial temporal codes at the transmitter and widely linear (WL) processing at the receiver [14]. Such schemes are of great interest:

- They achieve a better link budget, and thus improve the quality of the transmission.
- They allow for mitigating both intra network and inter network interference.
- They work in open loop, hence their implementation is much easier than closed loop schemes.
- They can work with a limited number of antennas at the receiver side, which is also a great advantage when dealing with implementation issues.

The work will be based on TCS previous work, and more especially on a widely linear Alamouti receiver for the reception of Real-Valued constellations corrupted by interferences. The combination with linear dispersive (LD) codes will be analyzed in the project.

Linear dispersive are very promising MIMO schemes. They provide a trade-off between spatial multiplexing gain and a gain in spatial diversity, and can also provide a temporal diversity gain.

The linearity allows the use of medium complex processing at the receiver (Successive Interference Cancellation or Maximum Likelihood implemented with sphere decoder).

Codes are designed for any number of transmit Ne and receive antennas Nr:

Let A_q and B_q be the dispersion matrices of dimension (Nr, Ne)

Let s_q be the symbols to transmit

$$s_q = \alpha_q + j\beta_q, q = 1 \dots Q$$

The coded symbols are built as follows:

$$S = \sum_{q=1}^{Q} (\alpha_q A_q + j\beta_q B_q)$$

LD codes are defined by Q, A_q and B_q.

The receivers associated to LD at transmission are widely linear for any kind of constellation.

These methods will be studied by simulation for OFDM LTE like waveforms and their performance will be assessed regarding interference mitigation.

2.5.2 Fundamental Limits of Advanced MIMO Schemes with Various CSI

This task aims at investigating the performance of a broadcast or interference channel with secrecy constraint, i.e., the message for one user should be kept secret to the others. This analysis is of interest in the context where for example several small cells are interfering with each other. The channel state information is assumed to be imperfect at the transmitter's side. In most practical scenarios, perfect channel state information at transmitter (CSIT) may not be available due to time-varying nature of wireless channels and limited resource for channel estimation. In fast fading scenarios, the channel training/feedback process incurs a delay larger than the coherence time and CSIT may be further outdated. Although delayed CSIT has received a significant attention recently [15][17], the underlying assumption that delayed channel state provides no information on current channel state is rather pessimistic as most of practical channels exhibit some form of temporal correlation. Motivated by such observation, a recent work [16] has studied the degrees of freedom in the two-user time-correlated multiple-input single-output (MISO) broadcast channel under delayed and some current CSIT. The work has been extended to the MIMO broadcast /interference channel [18]. Some wireless applications must guarantee not only reliability but also confidentiality of data such that the message for one user must be kept secret to the unintended users.

In this task, we wish to develop the framework under such scenario and quantify the loss of the throughput due to this additional secrecy constraint. Note that our preliminary work [19] in the two-user multi-antenna broadcast channel with confidential messages showed that completely outdated CSIT, i.e., independent of the current channel state, is useful to increase the secrecy capacity in the high SNR regime, in analogy to the studies in various network systems without secrecy constraint (see [18] and references therein). We then wish to characterize the best achievable secrecy rate and identify the corresponding schemes in the multi-antenna broadcast channel under delayed and partial current CSIT. It is worth noticing that the efficient schemes in this context are expected to be quite different from the conventional ones without the constraints. Our preliminary works have focused on secrecy degrees of freedom (SDoF), capturing the secrecy rate in the high SNR regime, as a performance metric [20]. It is of theoretical and practical interest to refine the analysis and look at the achievable secrecy rate. We will

also study the asymmetric setting when the users have different CSI qualities due to the feedback rate for example.

3 INTERFERENCE CANCELLATION AT THE RECEIVER AND ADVANCED TRANSCEIVERS

With the explosive growth of wireless data traffic, there is a considerable need to densify access nodes to improve the wireless network capacity. One of the main design concerns for next-generation communication systems is the interference cancellation. In addition, enhancement of transceiver schemes are still under investigation considering the usage of higher modulation orders, spatial modulation techniques, etc.

In this section, the requirements and challenges of interference handling mechanisms both on DL and UL, and enhanced spatial modulation schemes are discussed.

3.1 Interference Cancellation within Imperfect Channel Information in LTE DL Transmission

3.1.1 Introduction

Inter-cell interference cancelation techniques play a critical role in future-generation mobile networks. In current wireless network deployments, the main focus is on transmit strategies, e.g., fractional frequency reuse (FFR) and multi-user MIMO (MU-MIMO). However, it is essential that user equipment (UE) can detect, report and suppress interference. This has been recently agreed in 3GPP community and simple interference rejection combining scheme has been included as the required baseline receiver for Release 11 of LTE specifications in interference limited scenario.

A well-known approach is iterative decoding or so called turbo reception, which can be found in [21] for MIMO-OFDM systems. The receiver employs an iterative channel and covariance estimation for maximum a posteriori (MAP) detection, which suppresses interference while detecting the data. Although the corresponding theory is well understood, the high implementation cost has hindered its application in UEs. Another approach for UEs is the interference suppression via noise whitening or equalization. This scheme, known as interference rejection combining (IRC), can be found in [22]. In this scheme, the interference is modelled as a Gaussian noise process with spatial and temporal correlations. The UE receiver estimates the covariance matrix of interference plus noise in order to mitigate interference by the spatial diversity of multiple antennas.

The IRC scheme is attractive for many reasons. First, it is feasible for UE implementation even when interference statistics are not known, and it significantly improves the throughput performance of the cell-edge users compared to the simple minimum mean square error (MMSE) receiver that treats interference as additive white Gaussian noise (AWGN). Also, it is suitable for the asynchronous interference case and does not require high complexity or accurate synchronization to the interfering eNodeB (eNB). However, for the conventional IRC scheme, it may be too optimistic to assume that interference in all time and frequency slots has the same statistical properties. Indeed, this stationary assumption does not hold in practice; in particular, the statistics of the pilot and the data parts from an interfering eNB are quite different. This considerably impacts the possible improvements of interference-aware receivers. Also, estimation errors, e.g., channel estimation, and interference estimation, need to be considered and to be compensated. Yet, how to optimally manage the interference with multiple statistical properties has not been fully investigated.

In this study, we aim to investigate novel IRC-like receivers in interference limited scenarios where each transmitter and receiver has multiple antennas in order to manage different kinds of interference, such as the interfering pilot signal and the interfering data signal. We also aim to develop efficient schemes, which take into account channel estimation errors and the errors in covariance estimation of interference plus noise.

The rest of this contribution is organized as follows. First, we give a brief review on the conventional schemes. Then, we present a preliminary study to show how to manage interference with multiple statistical properties. Finally the research plan and goals of the project are described.

3.1.2 Problem description

We consider a two-user interference channel for MIMO-OFDM systems. The $N_r \times 1$ received waveform of the UE can be expressed as

$$\boldsymbol{y} = \boldsymbol{h}x + \alpha\bar{\boldsymbol{h}}\bar{x} + \boldsymbol{z},$$

where $\boldsymbol{h} = \boldsymbol{Hp}, \boldsymbol{H}$ is the $N_r \times N_t$channel matrix between the user and the serving cell, $\boldsymbol{p}$ is the precoding vector and x is the desired data; on the other hand, $\bar{\boldsymbol{h}} = \bar{\boldsymbol{H}}\bar{\boldsymbol{p}}$ is the interfering compound channel with the precoding vector $\bar{\boldsymbol{p}}$ and $\bar{x}$is the interfering data. We use α for the strength of interference and assume that each entry of $\boldsymbol{z}$ is i.i.d. Gaussian of the form$\mathcal{N}_c(0, N_0)$.In the sequel, we take a 2x2 MIMO system ($N_r = N_t = 2$) as an example. Specifically, it is a two-user interference channel with two base stations and two mobile users, where each node has two antennas.

Let us start with two baseline cases: 1) simple LMMSE, and 2) IRC.

Simple LMMSE: This is the classical approach where the receiver treats interference as AWGN. The resulting output of simple LMMSE is as follows:

$$\hat{x}_{LMMSE} = \hat{\boldsymbol{h}}^H\left(\hat{\boldsymbol{h}}\hat{\boldsymbol{h}}^H + N_0\boldsymbol{I}\right)^{-1}\boldsymbol{y},$$

where $\hat{\boldsymbol{h}}$ is the serving cell compound channel estimate. Although simple LMMSE can suppress noise plus interference with enough receive antennas, it is not an efficient way to exploit its spatial diversity.

IRC: In this case, the receiver learns about the statistical properties of interference. It assumes interference as a Gaussian process instead of AWGN. The output of IRC can be written as:

$$\hat{x}_{IRC} = \hat{\boldsymbol{h}}^H\left(\hat{\boldsymbol{h}}\hat{\boldsymbol{h}}^H + \hat{\boldsymbol{\Sigma}}_{\boldsymbol{V}}\right)^{-1}\boldsymbol{y},$$

Where $\hat{\boldsymbol{\Sigma}}_{\boldsymbol{V}}$ is the variance estimate of interference plus AWGN. This approach can outperform simple LMMSE due to exploitation of more information about interference, such as the mean and the variance.

Here, one can wonder how more information can be exploited about interference in order to provide a more efficient and effective approach for interference suppression. At a first glance, the answer seems to be positive, because exploiting more information about interference helps the receiver to perform better suppression. For example, there would be no interference if the interference term of $\alpha\bar{\boldsymbol{h}}\bar{x}$could be estimated perfectly. However, having complete information about interference is too optimistic, and also estimating all parameters for modelling interference is not practical.

In the following, we show a preliminary scheme to improve the system performance in the presence of interference. This suggests that knowing the pilot/data index from the interfering eNB can provide benefit in suppressing interference.

3.1.3 Proposed approach and preliminary analysis

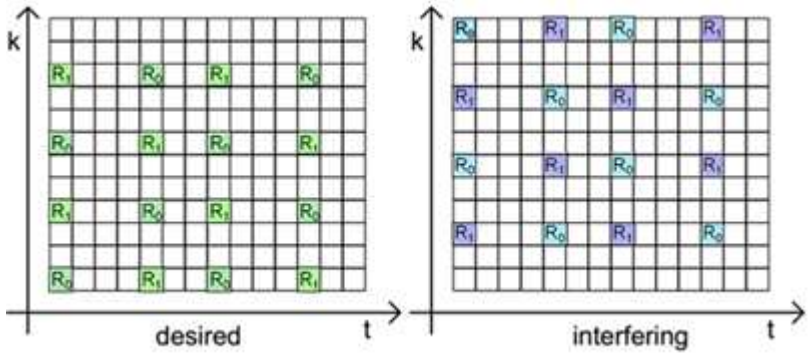

Figure 25 Mapping of the serving and interfering pilot symbols, where R_0 and R_1 indicate the pilot positions corresponding to the 1st and 2ndtransmit antennas, respectively.

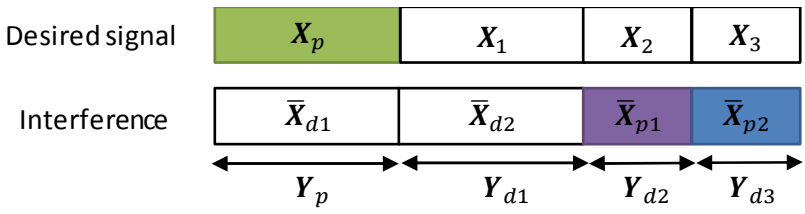

Figure 26 One-dimensional model arranging pilot and data symbols.

The novelty in this proposal is that a new concept is introduced into the receiver design investigation involving statistical properties of interference: interfering signals, such as the control signal, the data signal, etc., can be grouped and be suppressed statistically. With this new concept, the conventional IRC can be improved and some new results can also be obtained under different channel models and the non-synchronized scenario.

We assume that the channels are static over time and frequency within one resource block (RB), and the pilot symbols from two eNBs are non-overlapping. Therefore, it can be observed from Figure 25 that the received signal is subject to three different covariance matrices caused by the interfering pilot and data signals. According to assumption above, the system model can be equivalent to the partition shown in Figure 26, denoted by the one-dimensional model. The pilot/data structure of the desired signal and the interference signal are given as follows:

$$\begin{aligned}\boldsymbol{Y}_p &= \boldsymbol{H}\boldsymbol{X}_p + \alpha\bar{\boldsymbol{h}}\bar{\boldsymbol{X}}_{d1} + \boldsymbol{Z}_{\boldsymbol{p}}\\ \boldsymbol{Y}_{d1} &= \boldsymbol{h}\boldsymbol{X}_1 + \alpha\bar{\boldsymbol{h}}\bar{\boldsymbol{X}}_{d2} + \boldsymbol{Z}_{d1}\\ \boldsymbol{Y}_{d2} &= \boldsymbol{h}\boldsymbol{X}_2 + \alpha\bar{\boldsymbol{H}}\bar{\boldsymbol{X}}_{p1} + \boldsymbol{Z}_{d2}\\ \boldsymbol{Y}_{d3} &= \boldsymbol{h}\boldsymbol{X}_3 + \alpha\bar{\boldsymbol{H}}\bar{\boldsymbol{X}}_{p2} + \boldsymbol{Z}_{d3}\end{aligned}$$

where we use $\boldsymbol{X}_p$for the serving pilot signal, and $\bar{\boldsymbol{X}}_{\mathrm{pi}}$ as the interfering pilot signals. The problem we consider here is to find the optimal linear combination of the data of interest, i.e., $(\boldsymbol{X}_1, \boldsymbol{X}_2, \boldsymbol{X}_3)$. Note that we have three different covariance matrices of the received signal because of the difference between the interfering signals, $\bar{\boldsymbol{X}}_{d2}$, $\bar{\boldsymbol{X}}_{p2}$, and $\bar{\boldsymbol{X}}_{p2}$. In this case, the conventional IRC (which treats interference as a single Gaussian process) naturally leads to limited system performances.

Treating interference as Gaussian noise, the proposed approach has the following form:

$$\begin{cases}\widehat{\boldsymbol{X}}_{1,d\mathrm{l}} = \widehat{\boldsymbol{h}}^H\left(\widehat{\boldsymbol{\Sigma}}_{\boldsymbol{Y}_{d1}}\right)^{-1}\boldsymbol{Y}_{d1}\\ \widehat{\boldsymbol{X}}_{2,d\mathrm{l}} = \widehat{\boldsymbol{h}}^H\left(\widehat{\boldsymbol{\Sigma}}_{\boldsymbol{Y}_{d2}} + \nu\mathbf{I}\right)^{-1}\boldsymbol{Y}_{d2}\\ \widehat{\boldsymbol{X}}_{3,d\mathrm{l}} = \widehat{\boldsymbol{h}}^H\left(\widehat{\boldsymbol{\Sigma}}_{\boldsymbol{Y}_{d1}} + \nu\mathbf{I}\right)^{-1}\boldsymbol{Y}_{d3}\end{cases}$$

where ν is the diagonal loading (DL) value to compensate sample covariance errors. Note thatin the first equation of$\widehat{\boldsymbol{X}}_{1,dl}$, there is no DL value involved in it. This is because the impact of DL is not significant compared to the others, meaning for $\widehat{\boldsymbol{X}}_{2,dl}$ and $\widehat{\boldsymbol{X}}_{2,dl}$. Also, finding the optimal DL value is not trivial, but it is basically related to the sample covariance errors. One common solution is to use the inverse condition number (ratio of the largest to the smallest singular value) of the covariance estimate [23].

As a preliminary analysis, we consider a constant channel which is non-time-varying and frequency non-selective within one RB. The data format follows the LTE specifications given in Figure 25 and Figure 26. The data of interest are modulated with Gray-coded 4-QAM. The interfering data matrices are modulated with Gray-coded 16-QAM.The results are obtained without channel coding. In Figure 27, we compare the conventional schemes: LMMSE (which treats interference as AWGN), IRC, and the proposed approach IRC-DL. BER performances are presented as a function of SNR for SIR = 0 dB. These curves show the improvement of the proposed scheme over the conventional solutions. The performance gain is mainly based on proper grouping of different interfering signals.

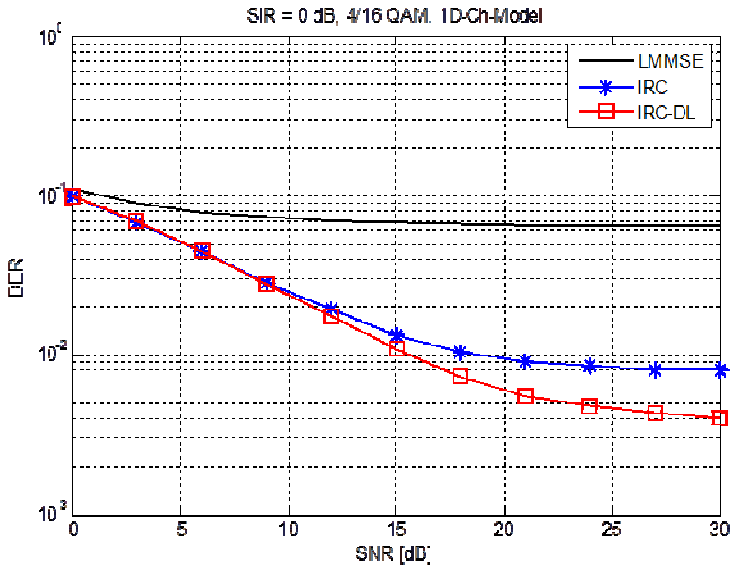

Figure 27 BER vs. SNR in the strong interference region, SIR = 0 dB.

3.1.4 Next steps

In this study, further investigation will be carried out focusing on the fundamental limits of the proposed one-dimensional model. Different suppression strategies and algorithms will be developed and their performance will be investigated in different scenarios including non-synchronized cases and triply selective channels where both the serving and the interfering channels are time variant, frequency selective, and with spatial correlation.

3.2 Enhanced Spatial Modulation Schemes

3.2.1 Introduction

The remarkable growth of mobile data traffic in the cellular industry has motivated researchers in recent years to develop multiple input multiple output (MIMO) technologies that increase the transmitted data rate in a given bandwidth and/or performance over fading channels. Also, energy consumption as well as transmitter and receiver complexities have become very important issues in dense cellular networks, i.e., in small cells and heterogeneous networks. In this environment, a new type of MIMO technique, referred to as Spatial Modulation (SM) has recently attracted considerable attention, particularly due to the low complexity that it promises for both the transmitter and the receiver sides.SM exploits the multiple transmit antennas in a novel manner. It transmits information from a small subset of the transmit antennas in order to reduce the number of radio frequency (RF) chains. Specifically, some of the information bits are used to select the active transmit antennas, and the remaining information bits are mapped onto the constellation symbols transmitted from the selected active antennas. However, this technique has a spectral efficiency loss with respect to spatial multiplexing (SMX) with the same number of transmit (Tx) antennas, and when the modulation order is increased to achieve the same spectral efficiency, it loses in terms of the bit error rate (BER).

A comprehensive survey on SM research can be found in [24], which reviews the main pioneering papers in the field. An inter-channel interference (ICI)-free SM, which transmits information bits using a single active transmit (Tx) switching was introduced in [25]. It shows that the single-RF SM has a significant reduction in receiver complexity. The SM concept described in [25] and [26] was comprehensively studied by using a two-step demodulator, which further reduces its processing complexity. These papers report results demonstrating the potential advantages of SM in terms of BER performance and processing complexity compared to the well-known SMX technique and Alamouti's transmit diversity. In [27], the authors develop the maximum likelihood (ML) demodulator and provide a detailed analysis demonstrating that significant performance improvements can be expected over sub-optimum demodulators. In [28], the concept of Space Shift Keying (SSK) was introduced, in which only the index of the active antenna transmits information. In [29], Generalized SSK (GSSK) was proposed

by allowing more than one Tx to be active and by encoding the information bits onto various combinations of multiple active Tx antennas. The authors show that for the same number of Tx elements, the rate can be improved at the expense of increasing the number of RF channels.

The goal of this study is to explore a new type of SM (referred to as Enhanced SM), which provides a more flexible combination of active Tx antennas and increases the transmitted data rate. In particular, we would like to increase the number of bits transmitted per channel use compared to conventional SM. Note that conventional MIMO techniques including SMX and SM employ a fixed signal constellation. In our proposed technique, some information bits select not only the index(es) of the active antenna(s), but also the constellations to be transmitted from each of them. We also aim to develop the system performance analysis and the complexity analysis to demonstrate that the proposed technique achieves better performance than conventional MIMO schemes.

The rest of this contribution is organized as follows. Next, we give a brief review on the conventional schemes. Then, we present a preliminary study to show how to increases the spectral efficiency. Finally the research plan and goals of the project are described.

3.2.2 Problem description

Considering a MIMO system operating on Rayleigh fading channels, the received signal is

$$\boldsymbol{y} = \boldsymbol{H}\boldsymbol{s} + \boldsymbol{n},$$

where $\boldsymbol{H}$ is the channel matrix, $\boldsymbol{s}$ is the transmitted signal with normalized power, i.e., $\boldsymbol{s} = \frac{1}{\sqrt{E_s}}\boldsymbol{x}$, and $\boldsymbol{n}$ is the additive white Gaussian noise (AWGN). We define the transmit energy by $E_s = E[\boldsymbol{x}^H\boldsymbol{x}]$. Note that the main difference between SM and conventional MIMO using SMX is that in the former not all transmit antennas are activated simultaneously, which means that there are some zero elements in the transmit signal vector $\boldsymbol{x}$.

For SMX with 2 transmit antennas and 4 bpcu, the transmitted symbols can be written as:

$$\boldsymbol{x}_{\mathrm{smx}} \in \left\{ \begin{bmatrix} x_{qpsk}^{(1)} \\ x_{qpsk}^{(2)} \end{bmatrix} \right\},$$

where the entries $\left\{x_{qpsk}^{(k)}\right\} \in \{\pm 1 \pm i\}$ are the QPSK constellation points. The total energy per transmitted symbol vector is $E_s = E[\boldsymbol{x}_{smx}^H \boldsymbol{x}_{smx}] = 4$.In summary, SMX in this case enables two active antennas and transmits two bits on each of them.

On the other hand, in conventional SM with 2 transmit antennas and the QPSK signal constellation, the transmitted symbol vectors can be written as:

$$\boldsymbol{x}_{sm} \in \left\{ \begin{bmatrix} \boldsymbol{x}_{qpsk}^{(1)} \\ 0 \end{bmatrix}, \begin{bmatrix} 0 \\ \boldsymbol{x}_{qpsk}^{(2)} \end{bmatrix} \right\} \triangleq \mathcal{S}_{qpsk},$$

where, as previously, the entries $\left\{x_{qpsk}^{(k)}\right\} \in \{\pm 1 \pm i\}$ are the QPSK constellation points, and the zero entries correspond to the silent TX element. Here, $\mathcal{S}_{qpsk}$ denotes the signal space. In this scheme, 3 information bits are sent per channel use: 1 bit selects the index of the active antenna and 2 bits select a QPSK symbol to be transmitted from that antenna. The principle is illustrated in Table 2, where C1 and C2 represent the combinations of the signal constellations transmitted from TX1 and TX2.

Table 2 Conventional SM, 2TX-3bpcu

	TX1	TX2
C1	QPSK	0
C2	0	QPSK

Here, using the same modulation, SM transmits less information than SMX. As a natural consequence, the major requirement for further enhancement of SM appears to increase the transmitted data rate. In the following, we show a preliminary scheme to boost up spectral efficiency. This suggests that using one or two active transmit antennas and multiple constellations can provide benefit in a larger number of combinations than in conventional SM systems.

3.2.3 Proposed approach and preliminary analysis

The novelty in this proposal is that a new concept is introduced into SM investigation on transmit constellations: the proposed technique allows multiple signal constellations to be used by different active antenna combinations and selecting the reduced-size signal constellations simultaneously used by two active antennas to have zero overlap with the primary signal constellation used during the single active antenna periods. With this new concept, the conventional SM can increase the number of transmitted information bits per channel use (bpcu) and maintain the low-complexity advantage.

ESM-2TX: With QPSK as primary modulation, our proposed ESM technique transmits 4 bpcu, i.e., one bit more than SM, by using a higher number of combinations of active TX elements and associated constellations. In addition to the two combinations used by conventional SM (given in Table 2), we use two more antenna/constellation combinations as shown below:

$$\boldsymbol{x}_{2t4b} \in \left\{ \mathcal{S}_{qpsk}, \begin{bmatrix} x_{b_0}^{(1)} \\ x_{b_0}^{(2)} \end{bmatrix}, \begin{bmatrix} x_{b_1}^{(1)} \\ x_{b_1}^{(2)} \end{bmatrix} \right\},$$

where $\left\{x_{b_0}^{(k)}\right\} \in \{\pm 1\}$, $\left\{x_{b_1}^{(k)}\right\} \in \{\pm i\}$. We refer to the signal constellations $x_{b_0}^{(k)}$ and $x_{b_1}^{(k)}$ as BPSK0 and BPSK1, respectively. The three signal constellations used in ESM are shown in Figure 28, and the four antenna/constellation combinations are illustrated in Table 3.

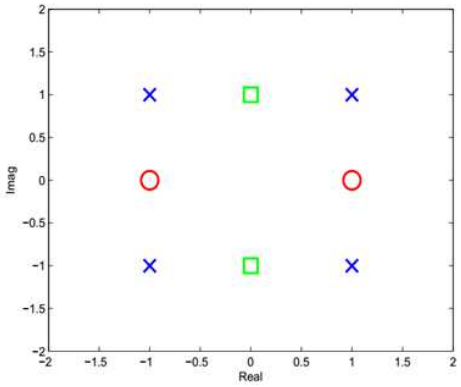

Figure 28 An illustration of the constellations used: The crosses represent QPSK and the circles (resp. squares) represent the BPSK0 (resp. BPSK1) signal constellations.

Table 3 Enhanced SM, 2TX-4bpcu

	TX1	TX2
C1	QPSK	0
C2	0	QPSK
C3	BPSK0	BPSK0
C4	BPSK1	BPSK1

In the first two combinations, a QPSK symbol is sent from one of the two transmit antennas as in conventional SM. In the third combination, denoted C3, two BPSK0 symbols are simultaneously transmitted using the two antennas. Similarly, in the fourth combination, denoted C4, two BPSK1 symbols are transmitted simultaneously. Note that in all combinations, the number of information bits associated to the symbol(s) transmitted by one of the antennas or by both antennas is two. Obviously, selection of one combination out of four requires two other bits, and in this way, the proposed scheme transmits 4 bpcu, compared to the 3 bpcu capacity of conventional SM.

Table 4 Enhanced SM, 4TX-6bpcu

	TX1	TX2	TX3	TX4
C1	QPSK	0	0	0
C2	0	QPSK	0	0
C3	0	0	QPSK	0
C4	0	0	0	QPSK
C5	BPSK0	BPSK0	0	0
C6	BPSK0	0	BPSK0	0
C7	BPSK0	0	0	BPSK0
C8	0	BPSK0	BPSK0	0
C9	0	BPSK0	0	BPSK0
C10	0	0	BPSK0	BPSK0
C11	BPSK1	BPSK1	0	0
C12	BPSK1	0	BPSK1	0
C13	BPSK1	0	0	BPSK1
C14	0	BPSK1	BPSK1	0
C15	0	BPSK1	0	BPSK1
C16	0	0	BPSK1	BPSK1

With four TX antennas and QPSK signal constellation, conventional SM transmits 4 bpcu, because two bits determine the active antenna index and two other bits determine a QPSK symbol to be transmitted from that antenna. In this case, ESM uses 16 combinations of active antennas and constellations transmitted from these antennas, which are shown in Table 4. The first four combinations in this table are those of conventional SM. They simply correspond to the transmission of a QPSK symbol from one of the four TX antennas. Next, we have 6 combinations for transmission of two simultaneous BPSK0 symbols from two TX antennas, and similar combinations for transmission of two simultaneous BPSK1 symbols. Therefore, ESM transmits 6 bpcu, compared to the 4 bpcu capacity of conventional SM: 4 information bits are needed to select one of those 16 combinations, and 2 bits are used to select a QPSK symbol, or a pair of BPSK0 symbols, or a pair of BPSK1 symbols.

Below, preliminary performance results are shown using Rayleigh fading MIMO channel with 4 receive antennas, and considering perfect CSI at the receiver. We compare the BER (with the proper bit labelling in ESM with QPSK as primary modulation) and the PEP performances of different MIMO transmission schemes, based on the same number of transmitted bpcu.

Figure 29 illustrates the BER curves corresponding to 2TX-4bpcu case. The constellation used in each scheme is given in the legend. In particular, SM uses 8PSK (denoted SM-8PSK) and from the 4 bits per channel use 1 bit is used for antenna selection and 3 bits select an 8PSK constellation point to be transmitted from the selected antenna. Similarly, SMX uses 4QAM (denoted SMX-4QAM) and it transmits two 4QAM streams using the two transmit antennas. These curves show that ESM outperforms conventional SM 1.5 dB at BER of10^{-4} and provides the same performance as SMX.

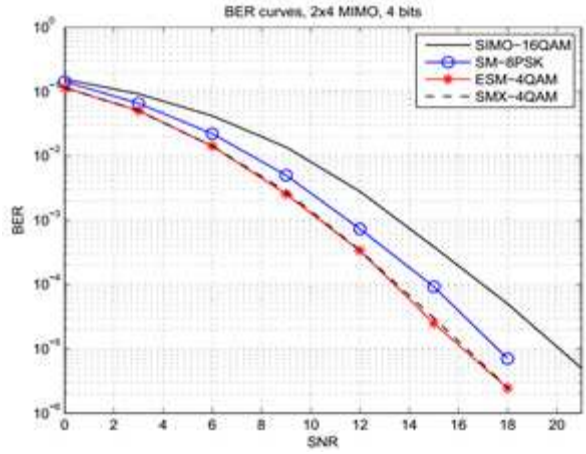

Figure 29 The BER performance of 2TX-4bpcu.

In Figure 30, the PEP curves of 4TX-6bpcu case show substantial improvements of the SM family (both SM and ESM) over SMX. Specifically, ESM gains around 3 dB over SM and approximately 4 dB over SMX at PEP of 10^{-3}. This means that SM gains about 1 dB over SMX while using fewer RF chains.

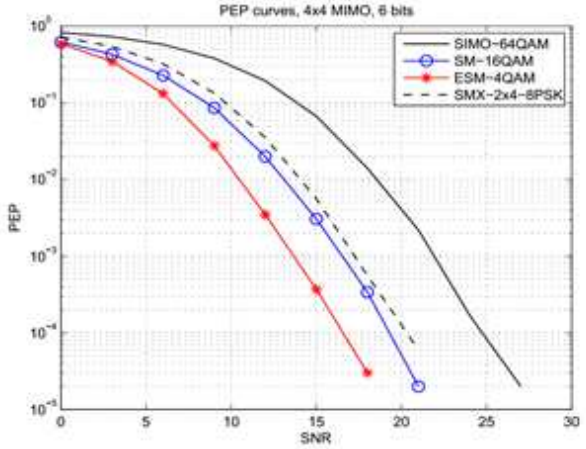

Figure 30 The PEP performance of 4TX-6bpcu.

3.2.4 Next steps

The objective of the coming contributions will be the exploration of more complex constellation. New constellation will be investigated for higher throughput. In addition, the usage of more antennas both at the transmitter and receiver side will be tackled. The assessment of the proposed algorithms will be based on performance analysis and complexity evaluation.

3.3 Advanced Interference Mitigation in the UL

Corresponding scenario in D2.2: 2.1.5 "Interference reduction in LTE through link level processing"

This work will deal with the design of a new interference mitigation technique for single carrier waveforms on frequency selective channel. The solution will be based on frequency equalisation together with multi antenna processing. Such a solution will be of specific interest for LTE in the uplink.

The work will be based on TCS know-how on interference rejection techniques, and more especially on a spatial-temporal technique based on a filtered sequence of reference [30].

The method will be adapted to frequency selective channels with single carrier waveforms and frequency domain equalization. The processing will be designed and its performance studied by simulations.

A special focus will be made on the implementation issues of such techniques, regarding the computation requirements, as well as the requirements on the radio frequency chain.

4 INTERFERENCE MANAGEMENT TECHNIQUES

Various interference management techniques are envisaged in this section. First, section 4.1 focuses on iterative linear minimum mean square error interference cancellation receivers in the MIMO case. These receivers are known to exhibit good performances. However, finding an abstraction layer (actual value interface) that allows them to be taken into account easily within system level simulations is challenging. The study proposed here will tackle this issue as well as the way to use this new metric. Section 4.2 addresses Interference Alignment (IA), which is a means of combating interference at the transmitter side. However, IA needs full channel knowledge at each multi-antenna transmitter to compute the set of precoders. The algorithm developed here will focus on a specific case of restricted channel knowledge and show that perfect alignment is still attainable. Section 4.3 also addresses the imperfect channel knowledge at the transmitters issue in the context of various interference management schemes. It plans to use information on users' topology to decide whether certain interference channels can be considered as null, thus alleviating the requirements in terms of channel information. Section 4.4 seeks first to determine users' location using all available information from radio networks, and then to combine location and interference level knowledge to build radio maps that can be used for various radio management purposes. Finally, section 4.5 plans to investigate the performance of an interference channel with a relay.

4.1 Link adaptation and scheduling for turbo-CWIC receivers

Corresponding scenario in D2.2: 2.9.5 "Flexible interference management schemes for downlink communications"

4.1.1 Introduction

Cross optimization between physical (PHY) and medium access control (MAC) layers, sometimes referred to as cooperative resource allocation, is currently one of the most exciting research topics in the design of multiuser multiple-input multiple-output (MIMO) systems. One reason may be that the computational complexity of solving the cross-layer optimization problem represents a challenge for future generations of mobile communications. In order to build bridges between PHY and MAC layers, it is mandatory that the link-level metrics be accurately modeled and effectively taken into account in higher-level decision-making mechanisms. Only a limited amount of contributions address this issue and, when they do it, most often restrict their study to simple linear receivers (see e.g., [31] and [32]) or, if dealing with more sophisticated non-linear receiver structures, e.g., successive interference cancellation (SIC) [33], idealize some parts of the decoding process, typically assuming continuous-input channels with zero-error Gaussian codebooks, and neglecting error propagation, which leads to inaccurate (i.e., too optimistic) predicted throughputs.

Real systems though involve discrete-input channels and non-ideal finite-length modulation-coding schemes (MCS). In 4G wireless mobile standards (e.g., LTE-A), the family of MCS is constructed out of powerful turbo codes [34]. Due to their particular structure, turbo codes cannot be optimally decoded except for very limited block length. In practice, a suboptimal iterative decoding is applied, where probabilistic soft information is exchanged between the constituent decoders. Besides, in the light of the substantial improvement they can bring in terms of system throughput or performance compared to conventional receivers (i.e., linear receivers or non-linear SIC receivers), *iterative* (turbo) linear minimum mean-square error (soft) interference cancellation and decoding algorithms (in short iterative LMMSE-IC) are likely to become an integral part of the assumptions made on the PHY layer. Clearly, joint iterative LMMSE-IC and turbo decoding gives rise to a complicated receiver structure with at least two interwoven iterative processes.

The contribution of this work is twofold. Firstly, we propose a stochastic modeling of the whole turbo receiver using EXIT charts (and variants) [35]. Our approach is inspired from earlier works dealing with multiple concatenated codes and the convergence analysis of their iterative decoding (see e.g., [36][37][38]). Secondly, we formulate the task of joint spatial precoder selection and rate allocation as a non-trivial (discrete) optimization problem and detail an exhaustive search procedure to accurately predict the average link level performance with this class of doubly iterative receivers.

4.1.2 System model

We consider a single-user transmission over a MIMO block Rayleigh fading multipath AWGN channel with n_b fading blocks, n_t transmit and n_r receive antennas. Partial state information is assumed at the transmitter through a low rate feedback. Perfect channel state information is assumed at the receiver. The total number n_s of channel uses available for transmission is fixed and the number of channel uses per fading block is given as $L = n_s/n_b$. The adressed space time bit interleaved coded modulation (STBICM) scheme with spatial precoding is depicted in Figure 31. The adopted precoding codebook is based on the antennas selection criterion which is a simple form of spatial precoding. The proposed work can be readily extended to more complicated precoding codebook.

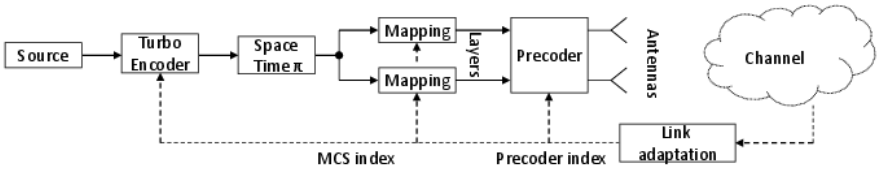

Figure 31 Link adaptation – STBICM with spatial precoding (antennas selection)

Transmission occurs over a MIMO block Rayleigh fading multipath AWGN channel. For the b-th fading block at the instant l, the $n_\tau + 1$ finite-length impulse response (FIR) describes the small-scale multipath fading

$$\mathbf{H}_b(l) = \sum_{\tau=0}^{n_\tau} \mathbf{H}_{b;\tau}\delta(l-\tau)$$

Each tap gain $\mathbf{H}_{b;\tau}$ is an $n_r \times n_t$ random matrix whose entries are modeled as i.i.d. circularly-symmetric complex Gaussian random variables with zero-mean and variance $\sigma^2_{b;\tau}$ under the constraint $\sum_{\tau=0}^{n_\tau} \sigma^2_{b;\tau} = 1$. Let $\breve{\mathbf{H}}_{b;\theta}(l)$ be the precoded channel FIR. In $\breve{\mathbf{H}}_{b;\theta}(l)$, $\breve{\mathbf{H}}^{\theta}_{b;\tau} = \mathbf{H}_{b;\tau}\mathbf{\Phi}_\theta$ denotes the τ-th precoded channel tap , where $\mathbf{\Phi}_\theta$ is the precoding matrix. The discrete-time vector $\mathbf{y}_{b;l}$ received by the destination at b-th fading block and time $l = 1,\ldots,L$, is expressed as

$$\mathbf{y}_{b;l} = \sum_{\tau=0}^{n_\tau} \breve{\mathbf{H}}^{\theta}_{b;\tau}\mathbf{s}_{b;l-\tau} + \mathbf{w}_{b;l}$$

with proper boundary conditions. In previous equation, the source vectors $\mathbf{s}_{b;l}$ are i.i.d. random vectors (uniform distribution) with $\mathrm{E}[\mathbf{s}_{b;l}] = \mathbf{0}_{n_{t,\theta}}$ and $\mathrm{E}[\mathbf{s}_{b;l}\mathbf{s}^{\dagger}_{b;l}] = \mathbf{I}_{n_{t,\theta}}$, and the noise vectors $\mathbf{w}_{b;l}$ are i.i.d. random vectors, circularly-symmetric Gaussian, with zero-mean and covariance matrix $\sigma^2_w\mathbf{I}_{n_r}$.

4.1.3 LMMSE-IC based turbo receivers

Within the class of LMMSE-IC based turbo receivers, we often distinguish between log *extrinsic* probability ratios (LEXTPR) based and log *a posteriori* probability ratios (LAPPR) based iterative LMMSE-IC algorithms. The two algorithms differ by the type of probabilistic information fed back by the decoder for soft interference regeneration and cancellation, namely LEXTPR or LAPPR on coded bits. Empirical evidence reveals that the LAPPR-based iterative LMMSE-IC algorithm can significantly outperform its LEXTPR-based counterpart for highly loaded multiantenna or multiuser systems. In such scenarios indeed, using LAPPR instead of LEXTPR leads to more reliable MMSE symbol estimates. This is due to the extra information gleaned from the equalization/detection process, which allows to cancel out more interference at each iteration. The LAPPR-based iterative LMMSE-IC principle is illustrated in Figure 32. The set $\mathbf{\Lambda}_{D,DEC}$ of all LAPPR on the coded bits becomes after interleaving the set $\mathbf{\Lambda}_{D,LE}$ of all log "a

priori" probability ratios on labeling bits used for (soft) interference regeneration and cancellation, although LAPPR contain "observation".

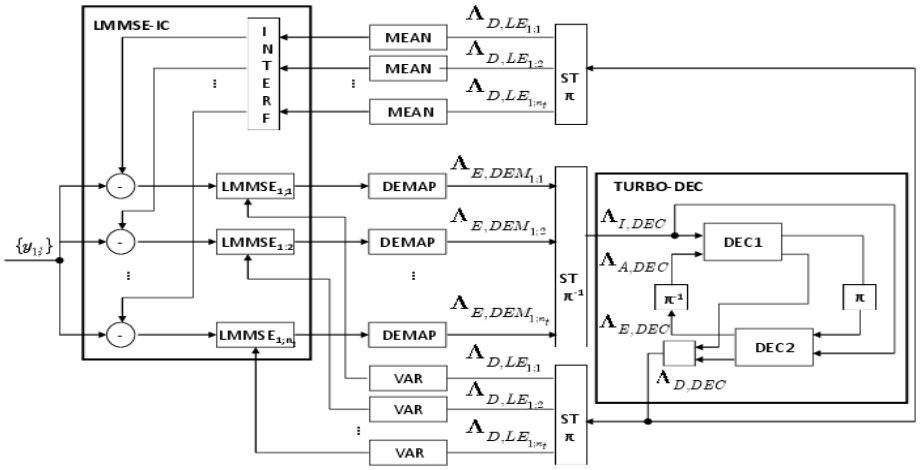

Figure 32 Turbo receiver structure (adapted to STBICM with Gray labelling)

4.1.4 PHY-layer abstraction

An LMMSE-IC based turbo receiver turns out to be a complicated non-linear dynamical system. Our objective is to analyze its evolution as iterations progress as in [39]. The proposed performance prediction method is semi-analytical and relies on ten Brink's stochastic approach of EXIT charts particularly useful in understanding and measuring the dynamics of turbo processing.

4.1.4.1 **Prediction scheme**

The proposed prediction scheme is illustrated in Figure 33. The first step consists in estimating the SINR at the LMMSE output which is a function of the input variance and others given parameters. The estimated SINR allows the computation of the average mutual information (AMI) which is a monotonously increasing function of the SINR, and depends on the MCS index (it is simulated off-line and stored in a look-up table (LUT)). The next step is to stochastically characterize the joint demapper and turbo decoder for the latter proceeds iteratively. This is achieved by introducing a simpler bivariate transfer function which requires as parameters the effective SINR gleaned from the AMI as well as the mutual information that measures the a priori information bits of the last iteration. The transfer functions used for our scheme are the measured BLER $P_e = F_{JDD_\nu}(\gamma, I_A)$, thevariance $\overline{v} = G_{JDD_\nu}(\gamma, I_A)$ which is an indicator on the interference estimation reliability, and the mutual information $I_E = T_{JDD_\nu}(\gamma, I_A)$. They are computed off-line and stored in separate LUTs.

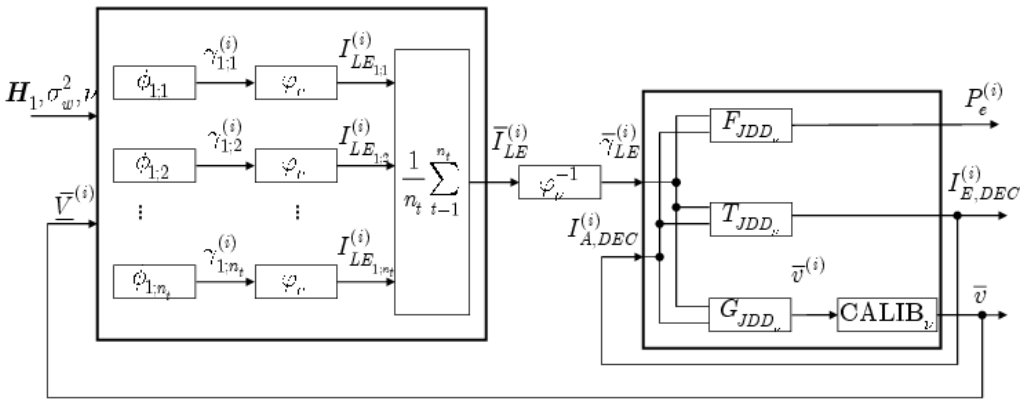

Figure 33 Performance prediction method (with calibration)

4.1.4.2 **Calibration**

A major drawback of this performance prediction method is thatsome of our assupmtions (see [40] for more details) do not hold for LAPPR-based iterative LMMSE-IC. As a consequence, the estimated SINRs at the detectors' outputs are approximated. The true SINRs, if we could have access to them, would be smaller. To solve this problem, we introduce a calibration procedure whose principle is to adjust the variance $\bar{v}$ with a real-valued factor $\beta_v \geq 1$. More specifically, $\bar{v}$ is replaced by $C_v(\bar{v}) = \min(\beta_v \bar{v}, 1)$, which has the effect to artificially reduce the SINRs that are used in the performance prediction method.

4.1.5 Link level performance evaluation

Closed-loop adaptation performs *joint* spatial precoder selection (i.e., antenna selection) and MCS selection. It aims to *maximize* the *average rate* subject to a target BLER constraint assuming LAPPR-based iterative LMMSE-IC at the destination. The number of iterations n_{it} depends on the destination computational capacity.

4.1.5.1 **Problem formulation**

For a given SNR and a given channel outcome $\{\mathbf{H}_b\}$, the problem is to maximize the throughput by selecting the highest MCS and $n_{t,\theta}$ antennas from the n_t transmit antennas with a block error probability less than threshold ε. In practice, retransmission is activated where one block error is detected. Assuming ARQ Type-I retransmission algorithm and retransmissions within the coherence time of the channel, the throughput is defined as

$$T = R(1-P_e)$$

The throughput maximization problem is defined as

$$\max_{\omega \in \Omega} \ \mathrm{T}$$

$$\text{subject to } P_e \leq 0.1 \text{ and } n_{t,\theta} \leq \min(n_t, n_r)$$

where Ω is the set of all possible couples (MCS, $n_{t,\theta}$), and P_e is the predicted BLER.

For comparison, the *simulated* BLER $P_{e,sim}$ and the *simulated* throughput T_{sim} are obtained via Monte Carlo simulation. Then, we evaluate the average predicted rate $\overline{R} = \mathsf{E}[R]$, i.e. the average predicted throughput $\overline{T}_{pred} = \mathsf{E}[T_{pred}]$ and the average simulated throughput $\overline{T}_{sim} = \mathsf{E}[T_{sim}]$ where expectation is w.r.t. $p_{\{\mathbf{H}_b\}}(\{\mathbf{H}_b\})$ (an exhaustive search is described in [40], Algorithm 1).

4.1.5.2 **Numerical results**

The closed-loop link adaptation procedure is tested for two types of channels: 4×4 MIMO flat memoryless channel (i.e., $n_b = 1$, $n_\tau = 0$), 4×4 MIMO 4 - block fading memoryless channel (i.e., $n_b = 4$, $n_\tau = 0$), referred to as CH1, CH2. n_s is fixed to 2040 with $L = 2040$ for CH1 and $L = 510$ for CH2. The target BLER is $\varepsilon = 10^{-1}$. The set of MCS and optimal calibrating factors are reported in Table 1. The maximum number of bits per channel use (bpcu) is 13.33. They are based on two 8-state rate-1/2 recursive systematic convolutional (RSC) encoders with generator matrix $\mathbf{G} = [1, g_1/g_0]$ where $g_0 = [1011]$ and $g_1 = [1101]$ and QAM modulations (Gray labeling). LAPPR-based iterative LMMSE-IC is performed at the destination. The length of the sliding window (in CH3) is $L_{SW} = 33$ with $L_1 = L_2 = 16$. For each SNR, we evaluated the average predicted and simulated throughputs over $n_{ch} = 1000$ channel outcomes. For each channel outcome, Monte Carlo simulation is stopped after 100 block errors. The results in the following channel types CH1, CH2 are shown in Figure 34 andFigure 35,

respectively. For all three types of channels, we observe that the average predicted throughputs match exactly the average simulated ones at every iteration and increase dramatically as iterations progress.

Table 5 Set of MCS and optimal calibrating factors

Index ν	r_ν	Constellation	β_ν
MCS 1	1/3	QPSK	1.7
MCS 2	1/2	QPSK	2.0
MCS 3	2/3	QPSK	2.2
MCS 4	3/4	QPSK	2.5
MCS 5	5/6	QPSK	3.0
MCS 6	1/2	16QAM	3.3
MCS 7	2/3	16QAM	5.0
MCS 8	3/4	16QAM	5.5
MCS 9	5/6	16QAM	6.0

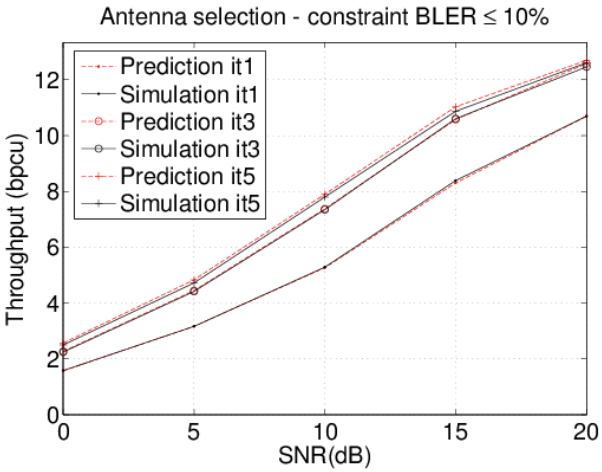

Figure 34 Average predicted and simulated throughputs (in bpcu) vs. SNR (dB) – CH1

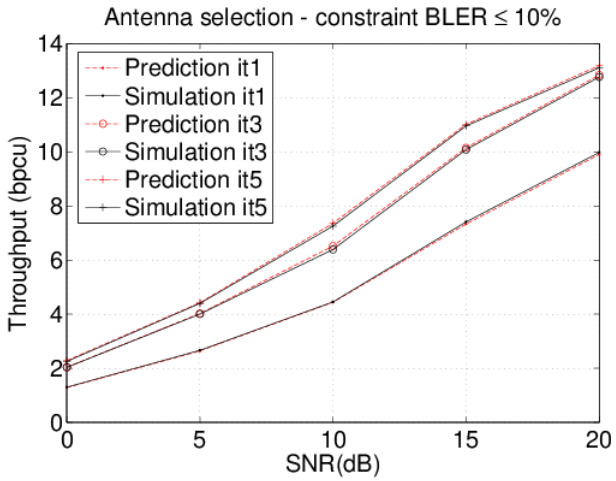

Figure 35 Average predicted and simulated throughputs (in bpcu) vs. SNR (dB) – CH2

4.1.6 Next steps

In this upcoming work, we will propose 2-D and 3-D calibration for the prediction scheme, which plays on the AMI compression and the variance interference estimation.Another ongoing perspective is to integrate the HARQ-Type II Chase Combining scheme in the LMMSE-IC joint decoding receiver which along with the new calibration way results in better BLER and throughput performance.

4.2 Interference Alignment with Incomplete CSIT

Corresponding scenario in D2.2: 2.9.12 "Interference alignment for large dense networks"

Although multi-transmitter coordinated transmission such as interference alignment (IA) constitutes a promising tool to combat interference, coordination benefits go at the expense of acquiring accurate enough channel state information (CSI) at the transmitters (TXs) and sharing it across all TXs whether explicitly or implicitly. In the case of multi-antenna based IA without channel extension, some form of CSI at the TXs (CSIT) is required to compute the precoders at each one of the TXs and can result in a significant overhead in practice. The IA literature for static MIMO channels is rich in methods improving the efficiency of the precoding schemes at finite SNR and reducing the complexity of the algorithms. Yet, the obtaining of the CSIT at the TXs represents a major obstacle to its practical use and the study of how CSIT requirements can somehow be alleviated has become an active research topic in its own right.

Yet, in all the existing works on IA feasibility, it is assumed that every TX knows perfectly the full multi-user channel, which we define as the channel from all the TXs to all the RXs. This assumption is critical as the maximal DoF is known to be significantly lower in the absence of CSIT. However, a simple examination of IA achievability in particular cases of IC reveals that how much CSIT is required at any one TX actually depends on the antenna configuration. Obvious examples include TXs with single antenna which has no alignment capability, hence requires no CSIT, or an IC with many-antenna RXs which eliminate the need for any alignment, hence CSIT. In the general case with heterogeneous antenna distributions, an interesting question is whether an alignment scheme can get away with less than full CSIT. To this end, one needs to revisit the IA feasibility question under the prism of CSIT. We focus in this task on a completely different problem which is the incomplete CSIT sharing, which means that each TX receives its own CSIT. In particular, we will exploit the fact that some channel coefficients are only known at a subset of TXs. We will show that in this case, perfect alignment is still possible despite the lack of full CSIT. More remarkably, we show that as the number of antennas on the devices (BS and terminals) is increasing, the need for CSIT goes down instead of up as was conventionally thought. The contribution and results will be described in the next deliverable.

4.3 Topological Interference Management with Transmitter Cooperation

Corresponding scenario in D2.2: None

4.3.1 Introduction

Most known techniques for interference coordination and cooperation (such as interference alignment, coordinated beamforming and JP-CoMP) rely on the assumption that the transmitters are endowed with an instantaneous form of channel information whose coherence time is similar to that of the actual fading channels, so that a good fraction or the totality of the DoF achieved in the perfect CSIT can be obtained. Such an assumption is hard to realize in many practical scenarios. A closer examination of these pessimistic results however reveals that many of the considered networks are fully connected, in that any transmitter interferes with any non-intended receiver in the network.

Owing to the nodes' random placement, the fact that power decays fast with distance, the existence of obstacles and local shadowing effects, certain interference links are unavoidably much weaker than others, suggesting the use of a partially-connected graph to model, at least approximately, the network topology. An interesting question then arises as to whether the partial connectivity could be leveraged to allow the use of some relaxed form of CSIT while still achieving a substantial DoF performance. In particular the exploitation of topological information, simply indicating which of the interfering links are weak enough to be approximated by zero interference and which links are too strong to do so, is of great practical interest.

The objective of this task is to answer the question whether such topological information can somehow be exploited in the context of an interference network where a message exchange mechanism between transmitters pre-exists. For instance, in future LTE-A cellular networks, a backhaul routing mechanism

ensures that base stations selected to cooperate under the coordinated multi-point (CoMP) framework receive a copy of the messages to be transmitted. Still, the exchange of timely CSI is challenging due to the rapid obsolescence of instantaneous CSI and the latency of backhaul signalling links. In this case, a broadcast channel over distributed transmitters (a.k.a. network MIMO) ensues, with no instantaneous CSIT. The problem raised by this task concerns the use of topology information in this setting.

4.3.2 Problem Description

We consider a network with *K* transmitters (TX), e.g. cells. In each cell the TX (e.g. base station) is equipped with one antenna and serves one single-antenna user (RX). The partial connectivity of the network is modelled through the received signal equation for RX-*j* at time instant t by:

$$Y_j(t) = \sum_{i \in \mathcal{T}_j} h_{ji}(t) X_i(t) + Z_j(t)$$

where $h_{ji}$is the channel coefficient between TX-*i* and RX-*j*, the transmitted signal $X_i(t)$ is subject to the individual power constraint, i.e., $E\left[\left|X_i(t)\right|^2\right] \le P_i$, with P_i being transmit power at TX-*i*, and $Z_j(t)$ is the Gaussian noise with zero-mean and variance N_0 and is independent of transmitted signals and channel coefficients. We denote by T_k the transmit set containing the indices of transmitters that are connected to RX-*k*, and by R_k the receive set consisting of the indices of receivers that are connected to TX-*k*, for $k=\{1,2,\ldots,K\}$. In practice the partial connectivity may be modelled by taking those interference links that are "weak enough" (due to distance and/or shadowing) to zero. For instance in[41], a reasonable model is suggested whereby a link is disconnected if the received signal power falls below the effective noise floor.

Conforming to the so-called topological interference management (TIM) framework [41], the actual channel realizations are not available at the transmitters, yet the network topology (i.e., T_k, R_k, $\forall k$) is known by all transmitters and receivers. A typical transmitter cooperation is enabled [42], where every transmitter is endowed the messages desired by its connected receivers, i.e., TX-*k* has access to a subset of messages W_{R_k}, where W_j ($j \in R_k$) denotes the message desired by RX-*j*. We consider a block-fading channel, where the channel coefficients stay constant during the coherence time. The network topology is fixed throughout the communication.

4.3.3 Preliminary Results: Illustrative Examples

In the following, we present two illustrative examples, with which the main interference management techniques are illustrated. The general results will be detailed in the next deliverable.

4.3.3.1 Interference Avoidance

We focus for example on the network topology shown in Figure 36, and message sharing across transmitters is enabled [42]. The optimal symmetric DoF is pessimistically 1/3 without message sharing. In contrast, if transmitter cooperation is allowed, the symmetric DoF can be remarkably improved to 2/5 even with a simple interference avoidance scheme.

Without message sharing, the interference avoidance scheme consists in scheduling transmitters to avoid mutual interferences. In contrast, with message sharing, scheduling can be done across links rather than across transmitters. A possible link scheduling associated with Figure 36 is shown in Table 6. It can be found that each message is able to be independently delivered twice during five time slots, and hence symmetric DoF of 2/5 is achievable.

Table 6 Link Scheduling

Slot	Scheduled Links (e_{ij}: TX-i → RX-j)	Delivered Messages
A	e_{41}, e_{55}, e_{66}	W_1, W_5, W_6
B	e_{12}, e_{54}, e_{66}	W_2, W_4, W_6
C	e_{13}, e_{54}	W_3, W_4
D	e_{41}, e_{33}	W_1, W_3
E	e_{12}, e_{55}	W_2, W_5

Although the above link scheduling solution provides an achievable scheme for the example inFigure 36, the generalization is best undertaken by reinterpreting the link scheduling into a graph coloring problem, such that the rich graph theoretic toolboxes can be directly utilized to solve our problem. The nature of our problem calls for a distance-2 fractional clustered-graph coloring scheme, which consists of the following ingredients:

- Distance-2 fractional coloring: Both the adjacent links and the adjacency of the adjacent links (resp.edges with distance less than 2) should be scheduled in difference time slots (resp.assigned with different colors).
- Clustered-graph coloring: Only the total number of messages delivered by links with the common receiver (resp.colors assigned to the edges with the same vertex) matters. Thus, the number of assigned colors should be counted by clusters where the edges with common vertices are grouped together.

As such, the reinterpretation of the link scheduling as a distance-2 fractional graph coloring is shown in Figure 36. To ease presentation, we transform graph edge-coloring into graph vertex-coloring of the line graph. We first transform the topology graph G (left) into its line graph G_e (right) and map the links connected to each RX in G to the vertices in G_e. For instance, the four links to RX-2 in G are mapped to Vertices 3,4,5,6 in G_e. Then, we group relevant vertices in G_e as clusters, e.g., Vertices 3, 4, 5, 6 in Ge corresponding to the links to RX-2 are grouped as one cluster. By now, a clustered-graph is generated. The graph coloring can be performed as follows. For instance, if Vertex 2 in G_e receives a color indicated by 'A',then Vertices 13 and 15 can receive the same color, because the distance between any two of them is no less than 2. Try any possible coloring assignment until we obtain a proper one, where each cluster receives m distinct colors out of total n ones, such that any two vertices with distance less than 2 receive distinct colors. There may exist many proper coloring assignments. The fractional chromatic refers to the minimum of n/m among all proper coloring assignments. In this example, we have $m = 2$ and $n = 5$. The vertices (i.e., links in G) with the same color can be scheduled in the same time slot. Accordingly, each cluster receives two out of five colors means every message is scheduled twice during five time slots, yielding the symmetric DoF of 2/5. According to the connection between link scheduling and graph coloring, the inverse of the fractional chromatic number can serve as an inner bound of symmetric DoF of the general cellular networks, although its computation is NP-hard.

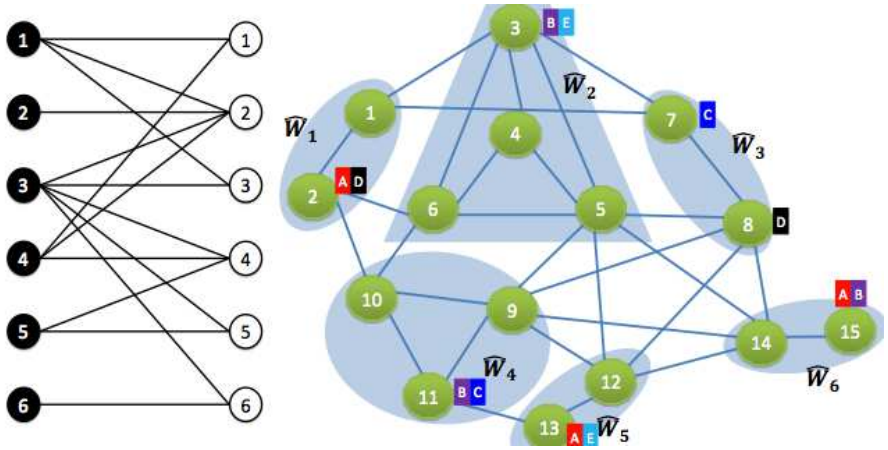

Figure 36 A topology of the 6-cell network. On the left is the network topology graph G, and on the right is its line graph G_e. The distance-2 fractional coloring offers each cluster two out of in total five colors, where any two vertices that receives the same color are set apart with distance no less than 2.

4.3.3.2 **Interference Alignment**

Let us consider the five-TX/RX pair regular network where each receiver is interfered by two other transmitters, as shown in Figure 37. By enabling transmitter cooperation, the symmetric DoF is improved from 2/5 to 1/2. In what follows, we will show an interference alignment scheme to achieve this.

For notational convenience, we denote by a,b,c,d,e the messages desired by five receivers, with the subscript distinguishing different symbols for the same receiver. We use multiple time slots to transmit these symbols, where multiple time slots span a space such that each symbol will be sent along with a specific direction spanned by vector $\boldsymbol{V}$in this space. In this example, we use in total four time slots, and

the symbols are sent along with the directions spanned by five 4x1 random vectors $\boldsymbol{V}_1$, $\boldsymbol{V}_2$, $\boldsymbol{V}_3$, $\boldsymbol{V}_4$, $\boldsymbol{V}_5$, any four of which are linearly independent. The transmitted signals within four time slots are concatenated as

$$\boldsymbol{X}_1 = \boldsymbol{V}_1 c_1 + \boldsymbol{V}_3 d_1, \quad \boldsymbol{X}_2 = \boldsymbol{V}_2 d_2 + \boldsymbol{V}_4 e_1$$
$$\boldsymbol{X}_3 = \boldsymbol{V}_5 a_1 + \boldsymbol{V}_3 e_2, \quad \boldsymbol{X}_4 = \boldsymbol{V}_4 a_2 + \boldsymbol{V}_1 b_2$$
$$\boldsymbol{X}_5 = \boldsymbol{V}_5 b_1 + \boldsymbol{V}_2 c_2$$

Where $\boldsymbol{X}_i$ is the 4x1 vector from TX-i with j-th element being transmitted signal in j-th time slot. With sufficient coherence time (i.e., four time slots in this example), the received signal at RX-1 for example within four time slots can be written as

$$\begin{aligned}\boldsymbol{Y}_1 &= \sum_{i\in\mathcal{T}_1} h_{1i}\boldsymbol{X}_i + \boldsymbol{Z}_1 \\ &= h_{11}\boldsymbol{X}_1 + h_{13}\boldsymbol{X}_3 + h_{14}\boldsymbol{X}_4 + \boldsymbol{Z}_1 \\ &= \underbrace{h_{13}\boldsymbol{V}_5 a_1 + h_{14}\boldsymbol{V}_4 a_2}_{\text{desired signal}} \\ &+ \underbrace{\boldsymbol{V}_1(h_{11}c_1 + h_{14}b_2) + \boldsymbol{V}_3(h_{11}d_1 + h_{13}e_2)}_{\text{aligned interferences}} + \boldsymbol{Z}_1.\end{aligned}$$

Recall that $\{\boldsymbol{V}_i, i=1,2,3,4,5\}$ are 4x1 linearly independent vectors spanning four-dimensional space, by which it follows that the interferences are aligned in the two-dimensional subspace spanned by $\boldsymbol{V}_1$ and $\boldsymbol{V}_3$, leaving two-dimensional interference-free subspace spanned by $\boldsymbol{V}_4$ and $\boldsymbol{V}_5$ to the desired symbols a_1,a_2. Hence, the desired messages of RX-1 can be successfully recovered, almost surely. Applying this to all other receivers, all receivers can decode two messages within four time slots, yielding the symmetric DoF of 1/2.

To illustrate the interference alignment, we describe the transmitted signals geometrically as shown in Figure 37. In this figure, we depict the subspace spanned by $\{\boldsymbol{V}_i, i=1,\ldots,5\}$ as a four-dimensional space, where any four of them are sufficient to represent this space. We also denote the message for example W_j sent from TX-i by $\boldsymbol{X}_i(W_j)$. Let us still take RX-1 for example. Because of $T_1=\{1,3,4\}$, the transmitted signals from the transmitters that do not belong to T_1 will not reach RX-1, and hence the vector $\boldsymbol{V}_2$ is disappeared. In addition, we have the interference-free signals in the directions of $\boldsymbol{V}_4$ and $\boldsymbol{V}_5$, and the aligned interferences carrying messages other than a_1,a_2 in the subspace spanned by $\boldsymbol{V}_1$ and $\boldsymbol{V}_3$. Recall that vectors $\{\boldsymbol{V}_1,\boldsymbol{V}_3,\boldsymbol{V}_4,\boldsymbol{V}_5\}$ are linearly independent, almost surely. As such, the interference alignment is feasible at RX-1, and also it can be checked to be feasible at all other receivers.

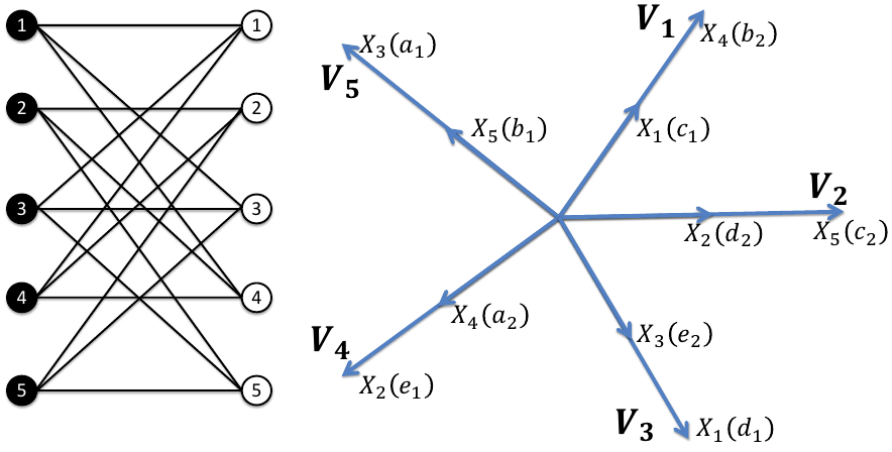

Figure 37 A regular cellular network. On the right is the illustration of the interference alignment scheme

4.3.4 Short Summary and Future Studies

Two illustrative examples are provided for the topological interference management problem with transmitter cooperation. By these two examples, the main interference management techniques, e.g., a fractional graph coloring based interference avoidance and an interference alignment approaches, have

been proposed, shedding light on how to generally exploit the benefits of both topological knowledge and transmitter cooperation.

For the general topological interference management (TIM) problem with transmitter, the fundamental limits of transmitter cooperation remain unclear. The general interference avoidance and interference alignment approaches have to be studied to handle arbitrary network topologies, and the sufficient and/or necessary conditions to achieve a certain amount of symmetric DoF should be identified for a family of network topologies.The further contributions with general results will be described in the next deliverable.

4.4 Joint Location and Interference Prediction for ICIC

Corresponding scenario in D2.2: 2.3.12 "Joint interference and location prediction"

Nowadays, popularity of smart terminals, with their enhanced functionalities and applications, makes the cellular networks facing more and more serious challenges to satisfy the constant growth of traffic. 3GPP LTE networks present a major advance in cellular technology. They offer significant improvements over previous technologies in terms of peak data rate and spectral efficiency. However, in LTE release 8, the cell-edge and average user throughputs are still significantly lower than the peak data rates. 3GPP group is continuously working to improve the LTE networks, proposing new releases. Initial enhancements were included in 3GPP Release 9 such as Self-Organizing Network (SON), Multimedia broadcast/ Multicast service (MBMS), UE positioning, and IP Multimedia Subsystem (IMS) emergency. Then, 3GPP LTE release 10, also known as LTE-Advanced, followed including more significant improvements, exploring ways to extend LTE in order to reach very high data rates up to 1 Gbps and a spectral efficiency equal to 30 b/s/Hz in peak and 2.6 b/s/Hz in average. However, some of the adopted techniques are complex and significant research efforts are needed to bring these techniques to reality. In the meantime, a straightforward but extremely effective way to increase the network capacity is to make the cells smaller and keep the network closer to the user.

Thus future wireless networks are becoming more and more heterogeneous, as we move towards 5G. The heterogeneous networks follow the non-uniform users' distribution, in the sense they are constructed with layers of macro and small cells, and accommodate other technologies e.g. Wi-Fi. Since the inter-cell interference level suffered by users in downlink depends on the relative positions of mobile users and the fixed elements of infrastructure, an increase of cells densification implies an increase of cell edge users' suffering from a high inter-cell interference level. Several techniques of Inter-Cell Interference Coordination (ICIC) and/or Cancellation have been proposed in the literature to mitigate the interference level and improve the users' Signal to Interference plus Noise Ratio (SINR) in heterogeneous networks. In co-channel deployment, where the small cells' base stations operate at the same frequency band as that of the macro cells' base stations, a frequency domain inter-cell interference coordination based on the Soft Frequency Reuse (SFR) approach is proposed in [43] and [44]. Pre-defined power levels are given at each portion of the frequency bandwidth which lead to decrease the impact of the macro cells' base station transmit power on the small cell users downlink. A time domain ICIC introduces blank subframes in the transmission known as "Almost Blank Subframe" where the macro cells' base station stops transmitting to cancel the inter-cell interference caused by the macro cells base stations transmit power at a given subframe [45]. In order to use the time and/or frequency domain ICIC, users are classified into two sets: small cell users and macro cell users. The user's classification is based on the user's long-term SINR which depends also on the users' location. Thus, the ICI Coordination/Cancellation techniques take advantage of external (and most often static) information such as location and/or average interference levels.

On the other hand, to fully exploit the LTE-Advanced network capacity, the major challenge of standard communication in such environments is to provide a good spectral efficiency and fairness among users, even for cell edge users, by adopting an adequate Radio Resource Management (RRM) policy and flexibility between the cells in terms of cell size fluctuation (e.g. cell zooming techniques).

The capability to properly manage and allocate time/frequency resources, to manage the inter-cell interference, to offload the data traffic, to define optimal packet relaying strategies, or to optimize the transmission parameters, is clearly conditioned on the actual levels of interference suffered by the users (at any place and any time). Then, the solution is to provide to these systems with the instantaneous inter-cell interference level information at each pixel of the area of interest. Such maps have already been mentioned in the recent literature. However, the optimal and most practical way to build them is still an open issue. The interference estimation techniques can roughly be divided into three types as given is the next subsections.

4.4.1 Statistical interference estimation

There has been an emerging interest in modeling the inter-cell interference while building an interference map. Providing statistical models of the interference power is essential to allow an accurate evaluation of network management methods performance without the need of lengthy and costly Monte Carlo simulations. The statistical characterization of the inter-cell interference level has been investigated for a long time, under different scenarios, and following several approaches. In [46], an analytical model of the inter-cell interference power in downlink is proposed. The inter-cell interference distribution is derived analytically by modifying the Burr probability distribution. In addition to the fading effect, the authors consider an average value of the channel gain. Then, the channel gain does not depend on the users' position and the inter-cell interference level is averaged and does not take into consideration the users' location information. Unlike the latter, the authors of [47] propose an analytical distance based inter-cell interference distribution model in downlink. The authors model the distribution of the distance between users and the interfering base stations in a regular network, considering a hexagonal grid. Nevertheless, the shadowing and the fading effects are not taken into account. Based on the moment generating function, authors of [48] derive the distribution of the total received power at any given pixel in the central cell of a regular network, which captures the system parameters such as, network load, scheduling, adaptation of the power level, and fading channel.

In [49], an analytical model of the interference level caused by narrowband users to the ultra-wideband users and vice-versa is proposed. Since the stochastic geometry approach is more adapted for heterogeneous network modeling, authors of [49] consider in their simulations a random network, where narrowband users and ultra-wideband users are modeled with homogeneous Poisson Point Processes (PPP). The modeling and analysis of K-tiers downlink heterogeneous cellular networks are given in [50]. The authors derive the expressions of coverage probability, the average rate achieved by a randomly located user and the average load of each tier of base station. The downlink interference estimation, based on the moment generating function, in K-tier heterogeneous network is addressed in [51], where a Rayleigh fading is considered. The authors extend their study in order to estimate the wireless activity according to a measured interference power [52]. Downlink interference statistics are given in [53], where the cumulants of the interference are given in a random punctured process. The authors assume that the randomly punctured PPP keeps its Poisson property. The cumulant expression derivation requires the joint statistics of the distance between the transmitters and the receivers. One and multiple desired transmitters' cases are considered in this study.

The interference map obtained with such methods is able to take into account different network configurations e.g. networks' activity rate which is essential in such scenarios, and radio metrics. The interference map establishes a rough correspondence between inter-cell interference level and position. However, the statistical interference estimates, which are still imprecise and practically challenging to get a priori in real systems due to the statistical model accuracy and the representativeness in operating environments, should be made available and refined while users are communicating and/ or moving around.

4.4.2 Deterministic interference map

The deterministic 2D interference map uses a deterministic approach to evaluate the inter-cell interference level at any pixel of the area of interest. The classical method is the Fingerprint. This method exploits geo-referenced metrics (i.e. learnt at known visited locations) to build the interference map. This method needs a pre-training phase, which can be built offline e.g., with a drive-test that collects the Received Signal Strength (RSS) measured at an exact position and stores them in a database. The RSS is available information at the mobile user, since measurements are continuously performed to select the served base station and to prepare handovers. The user's position can be obtained by the GPS (in outdoor), which the present days smart phones are equipped with, or by any alternative terrestrial positioning system. The later can implement one of the positioning or tracking algorithms available (e.g. trilateration, triangulation, tracking filters, message-passing, etc), while relying on different radiolocation metrics such as the Angle of Arrival (AoA), Round Trip-Time of Flight (RT-ToF), Time Difference of Arrival (TDoA), Observed TDoA (OTDoA), RSS, etc. Surveys on wireless positioning systems are given for indoor and outdoor environment in [54][55] and [56], respectively.

Instead of RSS measurements, ray-tracing/ launching methods can deterministically predict information regarding the rays between emitters and receivers, and thus the level of received power over a given link. The aggregated power can, then, be evaluated at each pixel of the area of interest. These methods need a long run time for the pre-training phase. The computational time of these methods is roughly linearly proportional to the number of receiver locations. Accordingly, a deterministic interference map could be obtained through simulations, following a brute force approach where the inter-cell interference values are computed at each grid location with very high resolution. The interference map obtained by

such methods is discrete. To obtain the inter-cell interference level at almost any location, a high resolution is required, which leads to a high computational time running. In addition, the deterministic interference map is mostly static and not really adapted to heterogeneous network (i.e. switch on/off of small cells). However, these methods can be used as a reference method for comparison and performance evaluation.

4.4.3 Interference map based on fingerprint

Since the fingerprint is complex, and the high resolution increases the run time of the interference map, several works based on a low resolution fingerprint exploit spatial interpolation in order to extend the inter-cell interference level estimation at any location. The spatial interpolation techniques are used to estimate the values *Z* at previously unobserved locations within a certain area, based on a minimal set of collected data Z_i, in our case a minimal set of RSS measurements. The area of interest is partitioned into N convex polygons such that each polygon contains exactly one generating mobile node and every node in a given polygon is closer to its generating node than to any other. This partition can be done using the Voronoi decomposition as illustrated in Figure 38

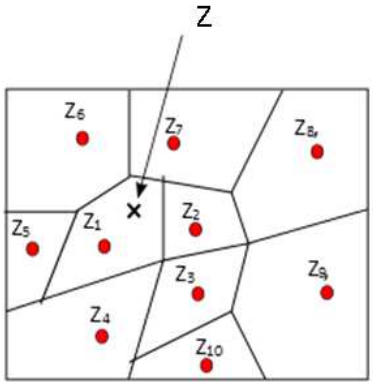

Figure 38 Voronoi decomposition

Several spatial interpolation techniques are investigated in the literature in order to estimate the value of inter-cell interference in arbitrary 2D location that does not belong to the physically unvisited locations. In the following some of these techniques are discussed.

1- Nearest Neighbor

It is a straightforward interpolation technique from a computational point of view once the Voronoi decomposition is obtained. The inter-cell interference value *Z* at a non-visited location is the value of the nearest sample data point to the considered location. Then, the resolution of the interference map depends on the number of sample data points contained in the database.

2- Inverse Distance Weighting

It is a deterministic spatial interpolation technique [57]. The value of the inter-cell interference assigned at the physical unvisited location is calculated based on the weighted average of the sample data point [58]. The interpolated value *Z at* a given position *x* is given as a function of λ_i the weights corresponding at each sample data point as follows:

$$\boldsymbol{Z(x)} = \sum_{i=1}^{N} \frac{\boldsymbol{\lambda_i(x) Z_i}}{\sum_{i=1}^{N} \boldsymbol{\lambda_j(x)}}$$

where,

$$\lambda_i(x) = \frac{1}{d(x, xi)^p}$$

is the Shepard's weighting function given according to the distance between the new location xi and the location of the RSS measurements, and the real positive power p.

3- **Kriging**

It is a linear spatial interpolation technique. Similarly to the inverse distance weighting, the Kriging interpolation technique uses a weighted average of sample data points by exploiting their spatial correlation. Then, the new inter-cell interference value *Z* is given as:

$$Z(x) = \sum_{i=1}^{N} \lambda_i (x) Z_i$$

Where the weights λ_i are chosen such that the variance of the estimator is minimized, and the weight vector is computed as a function of the statistical dependence between the new location and the sample data points, expressed as:

$$\lambda(x) = K^{-1} k(x)$$

with $K_{ij} = \gamma(\|x_i - x_j\|)$, and $k(x) = \gamma(\|x - x_i\|)$ are the spatial variance between all the sample points $\{x_i, x_j\}$, and between $\{x, x_i\}$ respectively, and $\lambda(x)$ is a vector whose elements are $\lambda_i(x)$. $\gamma$is a function which depends on the variogram model. In [57] an exponential variogram model is used.

4- Polynomial interpolation based on Delaunay triangulation

This method is based on the Delaunay triangulation [59]. Then, in addition to a Voronoi decomposition, a triangulation of the network is needed. The inter-cell interference value estimated at the new location *x* is obtained with a polynomial interpolation which considers only the nodes of the triangle that contains *x*. Then, *the* new value Z is expressed as:

$$Z(x) = \sum_{i=1}^{3} \Phi_i(x) Z_i$$

whereΦ_i is the interpolating basis function.

5- Spatio-temporal interpolation

An additional dimension is considered in [60]. The authors investigate a spatio-temporal interpolation in order to obtain an expected value of the inter-cell interference at any location, and any time using the Kriging Kalman Filtering spatio-temporal interpolation. This method uses a Kriging spatial interpolation to estimate the inter-cell interference in 2D space, whilst a Kalman filtering is used for the temporal dimension. An auto-regressive model for temporal evolution of the shadowing is defined in [61][62]. This method is based on particle filters approximation and Kalman filter for shadowing tracking.

The different techniques cited before could be adapted and extended in order to determine the inter-cell interference level according to a users' position, in a heterogeneous networks.

4.4.4 Proposed joint location and interference prediction

In the frame of the envisaged study, we aim to estimate the inter-cell interference level suffered by users in the downlink of a heterogeneous network, according to their locations. The main idea is to create a 2D interference map. A third dimension representing time will be incorporated to the interference map with the user's tracking mechanism. A joint location and interference prediction will be proposed in order to assist subsequent location-based ICIC mechanisms, and enable better in-site dynamic spectrum access. The temporal aspect of the joint location and interference prediction will be exploited in radio resource allocation, handover decisions and traffic offload. Figure 39 presents our main contributions in order to build a space/time interference prediction.

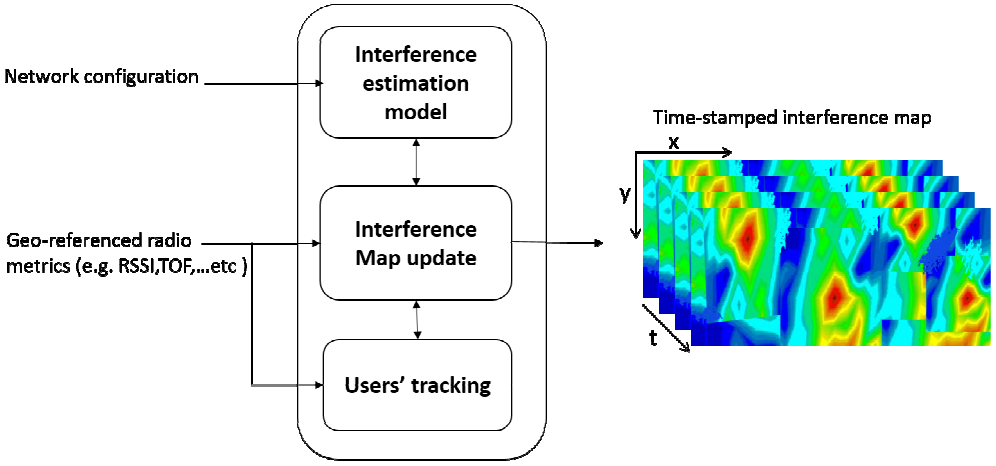

Figure 39 Space/time interference prediction

Initially, as a preliminary step of our investigation, we will consider the user's position as known, with a given uncertainty (delivered through any radiolocation means, including solutions relying on the interfering/ interfered systems it-self, i.e. LTE). Firstly, an analytical model of the inter-cell interference based on the user's position will be proposed. This model will consider the distance dependent path loss when the small cells and macro cells antennas' positions are known, as well as the radio environment, the networks activity rate, the interferers transmission power (different transmission power levels are allocated to macro and small cells base stations), geo-referenced metrics such as RSS, and the networks' configuration.

A stochastic geometry approach will be investigated, in order to model the heterogeneous network. Its flexibility and a large arsenal of mathematical tools will cope with heterogeneous network complexity, especially for the small cells configuration (e.g. small cells' sleep mode) and allow an interference map initialization when starting from scratch where only a spatial density of the network's nodes is available.

Secondly, a self-learning solution will be explored. The interference map will be initialized through coarse statistical model assumptions and then they will be refined and updated retrospectively, according to the geo-referenced metrics collected in the locations physically visited by the mobile terminal. As an example, in relevant approaches from the recent state of the art most of them exploit the RSS measured by users moving around in the area. In our case, this metric can be exploited in order to refine the interference map.

Then, user tracking will be performed using the user's location information, the collected radiolocation metrics and their a priori mobility models. With the interference map and the MT tracking process, the inter-cell interference suffered by users at the location visited in the next Transmission Time Interval (TTI) will be estimated. This inter-cell interference level will be considered as an input to the location-based ICIC mechanisms.

The semi-deterministic inter-cell interference model will be evaluated according to the uncertainty of estimated positions (mobile users and fixed elements). Afterwards, the minimum required position accuracy will be determined, delivering insights about the adequate positioning methods and radiolocation technologies. In particular the additional resources to be committed to achieve sufficient interference map accuracy will be derived with respect to the primary system deployment scenarios (i.e. radio relying on LTE only, or LTE+UWB, of UWB only… radiolocation involving non-cooperative with respect to fixed anchors only or also cooperative links, etc.).

The proposed methods and the analytical inter-cell interference estimation model will be evaluated in realistic scenarios in compliance with the SHARING context. In particular, the quality of the semi-deterministic interference map prediction will be compared with deterministic propagation estimation tools such as the ray-tracing/ launching, and/or brute force methods.

4.5 Relay-Aided Interference Mitigation

In the current work, we focus on a simple version of the two-user Interference Relay Channel (IRC) which still captures the rather complex interplay between interference and relaying: an Interference Channel (IC) with a relay station (may be fixed or mobile) connected to both destinations but to only one transmitter (Figure 40). In this way, we expect to provide some useful insights into the underlying

regimes, and their coding, for the general IRC which is not well understood yet. This setup captures, e.g., a scenario in which one transmitter is far away from the relay.

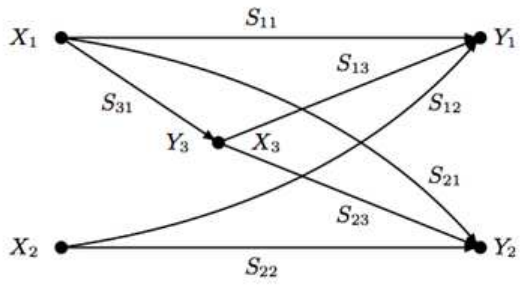

Figure 40 Gaussian model of the IRC. The values S_{ij} represent the SNR between nodes j and i.

Our results involve a novel outer bound for a class of IRCs and three relaying strategies based on Decode-Forward (DF) and Compress-Forward (CF). The main outcome of this work is the identification of three different regimes in the Gaussian case, in which different transmission strategies seem to be needed in order to obtain constant gap results. In particular, when the source-relay link is stronger than the direct link, full DF is used. As the strength of this link reduces, it is preferable to only decode part of the message, thus partial DF is used. When the source-relay link is weaker than the interfering link, CF is needed instead.

The main outcome for the moment is as follows. We evaluate the gap between the achievable regions and the outer bound in the Gaussian case. Then, we identify the strategies that achieve a constant gap to the capacity region for any SNR value.

A. *Full DF Scheme Achieves Capacity to Within* 1 *Bit*

When the relay is close to the source, i.e., when S31 is high enough, the relay is able to decode the entire message without penalizing the rate R1.

Proposition 1: If S31 ≥ S11, the full DF scheme, with which the relay fully decodes the source signal and then re-encodes and forwards it to the receivers, achieves capacity to within 1 bit.

B. *Partial DF Scheme Achieves Capacity to Within* 1.5*Bit*

If the source-relay link is not good enough for the relay to decode the entire message, it should only decode the message partially. However, the relay should still be able to decode the common message in order to help both end users.

Proposition 2: If S31 < S11 and S31 ≥ S21, the partial DF scheme, with which the relay decodes parts of the source signal and then re-encodes and forwards it to the receivers, achieves capacity to within 1.5 bit.

C. *CF Scheme Achieves Capacity to Within* 1.43*Bit*

In the remaining regime, when the relay cannot even decode the common layer, its best strategy is to forward its channel observation to both destinations.

Proposition 3: If S31 < S11 and S31< S21 the CF scheme, with which the relay compressed its received signal and then re-encodes and forwards it to the receivers, achieves capacity to within 1.43 bit.

D. *Usefulness of the Relay*

Furthermore, it sounds reasonable that for a really low SNR in the source-relay link, the use of relaying has limited benefit. In this case, the best strategy is to shut the relay down and fall back to the much simpler Han-Kobayashi [15] scheme for the IC.

Proposition 4: If S31 ≤ S11/ (1 + S12) and S31 ≤ S21/(1 + S22), the Han-Kobayashi scheme achieves capacity to within 1 bit.

The two conditions over the source-relay link presented above can be interpreted as follows. In the first case, S31 ≤ S11/(1 + S12) implies that, by treating the interference from source 2 as noise, destination 1 can still have a better observation on source 1's signal than the relay does. Therefore, the relay's observation cannot help much for destination 1 to decode its own signal.
On the other hand, S31 ≤ S21/(1+S22) implies that, by treating its own signal as noise, destination 2 can still have a better observation on source 1's signal than the relay does. Therefore, the relay's observation cannot help much for destination 2 to learn/decode the interference from source 1.

5 REALISTIC CHANNEL AND NETWORK SIMULATION

Before being standardized, all new features are exhaustively debated between companies using theoretical analysis and large simulation campaigns to support their technological candidates. For this purpose simplified models are used to bound the run-time of the simulations, but also to offer an objective basis for comparison between features in competition. However, when being deployed in the field, technology performances may differ from the simulated ones. Therefore, it is not easy for network operators to properly plan their future deployments and assess either the network capacity or user's satisfaction. In the aim of reducing the gap between real network performance and simulations with simplified models, a simulation framework including realistic environment and network deployment is proposed with ray-based propagation modelling.

5.1 Channel Modelling

Corresponding scenario in D2.2: 2.3.6 "LTE-A multi-layer network in urban/suburban environments"

Progress in propagation and stochastic channel models in the past two decades has allowed for the design of sophisticated methods, capturing and modelling multi-path and scattering phenomena with always more realism. These predictions offer relevant data for the evaluation of new wireless network techniques sensitive to wideband channel estimate, multi-antenna systems (MIMO precoding, geo-location, etc.) and small-scale time variations (resource management). Small-cell densification, which is viewed as a major factor for network capacity rise, brings even more challenges in terms of channel prediction. Several environments (outdoor, indoor multi-floor) and configurations (macro, micro and pico-cells) must be managed jointly and coherently, while multi-RAT and multi-carrier systems make the resource management dependent on the propagation conditions in a wide range of frequency bands (e.g. from 800 MHz LTE to unlicensed 5 GHz). That is even more obvious with carrier aggregation as the allocation of data and control messages is then spread over several carrier components. In this context, the ability of ray-tracing to compute all channel properties in complex environments and for different frequencies is a real asset. Ray-tracing constitutes a solid basis that can be exploited in advanced algorithm evaluation and network dynamic simulation.

However, ray-tracing suffers from high computational times. With the aim of predicting the network coverage of large areas, SIRADEL developed a highly efficient ray-based propagation model, Volcano [63], for radio network planning and optimization usage. Implementation choices make it possible to get fast prediction of the main multi-path contributions, suitable for accurate prediction of the narrowband received power in a time-constrained operational process and thus for network coverage simulation.

With the aim of assessing Radio Resource Management (RRM) algorithms, Volcano ray-based model can be used as a channel model to predict the frequency selectivity or small-scale time fluctuations. Its main advantage compared to stochastic approaches is its ability to address a large range of different scenarios and the inherent correlation between different channel realizations. Volcano channel predictions can be exploited as well for evaluation of MIMO schemes by the prediction of the MIMO channel matrix.

Assessment of the RRM or MIMO algorithms requires the multi-path channel prediction to be highly realistic (e.g. in terms of delay spread, coherency bandwidth or angular spread). The implementation choices or parameterization adapted to the narrowband power simulation are obviously not sufficient. In the frame of the SHARING project, SIRADEL is developing extensions of the Volcano ray-tracing algorithm and is evaluating different settings to refine the channel model.

In the following, two different levels of modelling complexity are compared, named 'Basic' and 'Full'. The basic-complexity model that is precisely described in [63] generates the strongest specular contributions that we may consider as appropriate for precise and time-optimized assessment of the narrowband received power. The full-complexity model is the outcome of recent enhancements in the model implementation, allowing for a richer multi-path prediction with additional allowed combinations between reflections and diffractions, and the construction of long-delay contributions. Finally, the model is extended with the introduction of the diffuse scattering contribution proposed in [64] to capture a more realistic angular diversity around terminals.

The channel characteristics computed from the two levels of modelling complexity are compared on a dense urban case study (Paris), where a single sectored Macro Base Station transmits a vertically-polarized signal to a User Equipment (UE) having an isotropic antenna. Several outdoor UE locations are computed, distributed over a 500 m x 500 m grid with a 5 m resolution. Figure 41 summarizes the scenario and shows the simulated ray paths reaching one of the in-street receivers for the 'Basic' model (multi-path richness with the 'Full" model leads to such a large number of rays that there was no real interest to plot it). Figure 42 shows that the "Full" model leads to be a far richer channel impulse

response thanks to diffuse scattering. In addition, distant dominant buildings contribute to non-negligible propagation paths with large excess delay, increasing the delay spread and, consequently, reducing the coherence bandwidth. Figure 42 shows also the increase in angular diversity, which is of great importance for an accurate MIMO channel prediction. Figure 43confirms this channel prediction enrichment all around the base station with increased angular spreads in both the horizontal and vertical planes thanks to interactions with more buildings. At the receiver side, the vicinity of the buildings makes the diffuse scattering in the 'Full' model increase the horizontal and vertical arrival spread even more.

Frequency band
2.6 GHz

Macro Base Station (BS)
Height 30 m
60° sector antenna with max gain 14 dBi
Tx Power17.8 dBm

User Equipment (UE)
Height 1.5m
In the street
Isotropic antenna

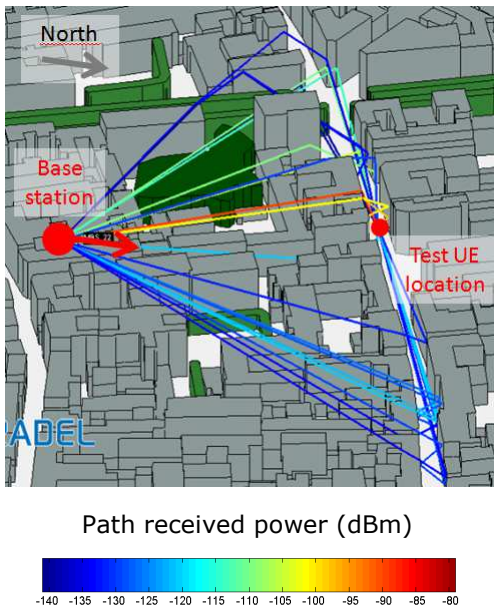

Figure 41 Channel modelling scenario

Basic-complexity model	Full-complexity model
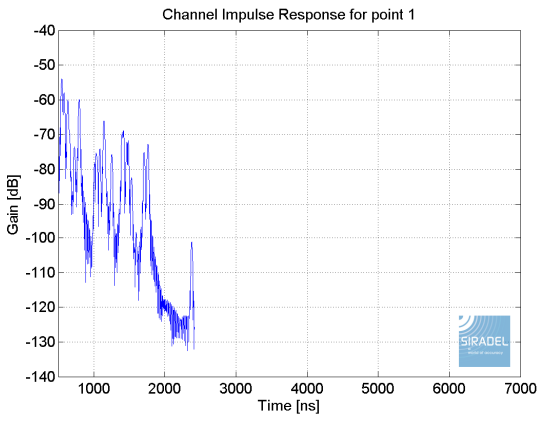	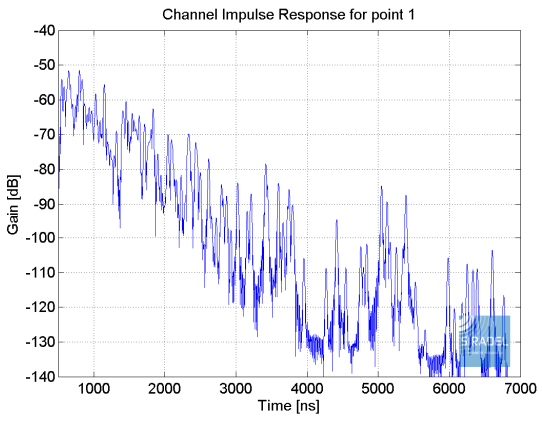

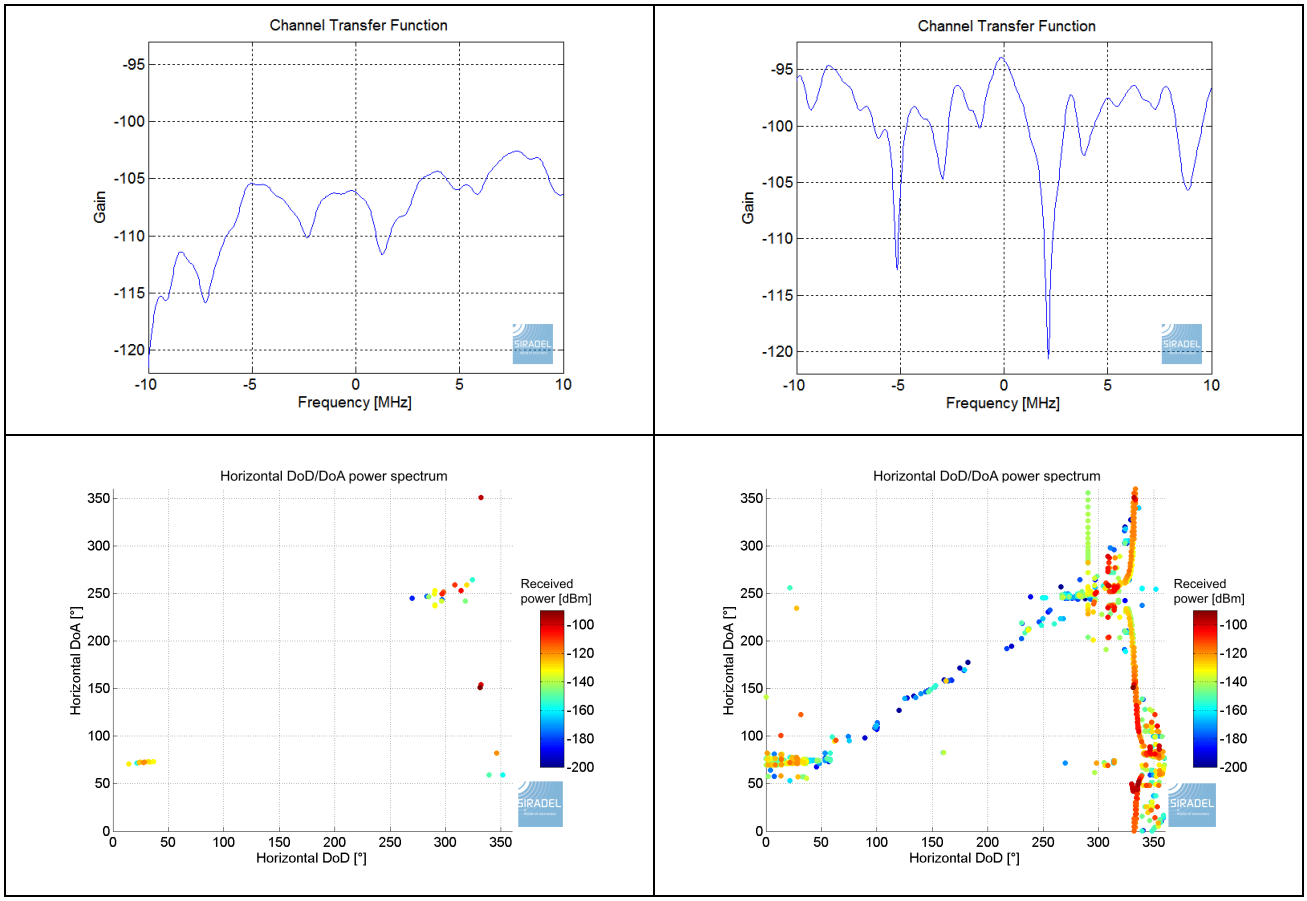

Figure 42 Channel impulse response, Transfer function and Directional of Departure (DoD) / Direction of Arrival (DoA) dispersion at test UE location with basic (left) and full (right) complexity models

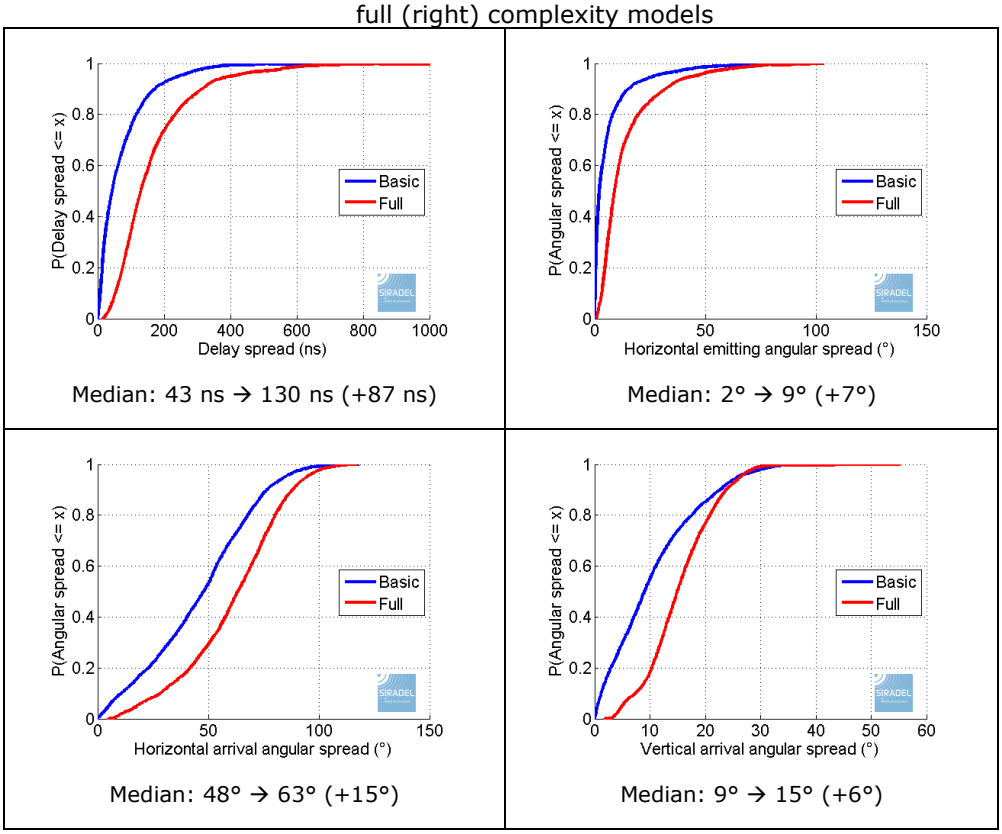

Figure 43 Channel statistics predicted in the streets surrounding the macro base station

The frequency selectivity of the channel is further explored by comparing the predicted coherency bandwidth. Figure 44 shows the CDF of the coherency bandwidth (defined for 50% and 90% correlation) obtained in the study area. The full-complexity model predicts lower coherency bandwidth, below 5MHz in roughly all cases. The median value is 0.75 MHz with the full-complexity model, while it is 1.18 MHz with basic-complexity (for the 90% correlation). The difference is expected to significantly impact the simulated signal and SINR variations within a LTE band, that is typically 5 MHz or above.

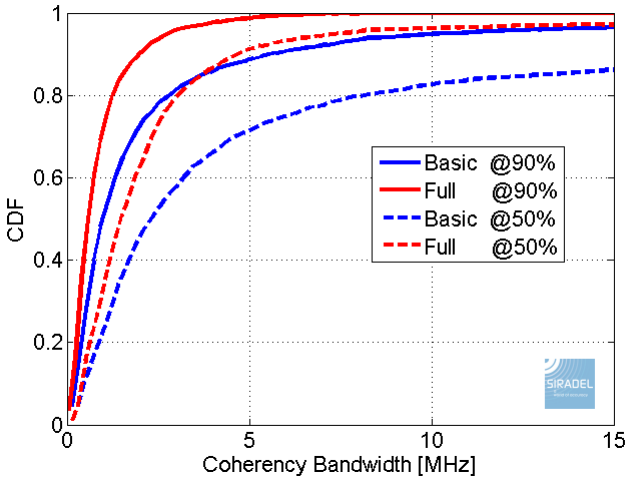

Figure 44 Statistics of the coherency bandwidth simulated in the study area with basic and full complexity models

A typical consequence of the channel enrichment can be observed on the prediction of the channel rank. The rank is an indicator of how many data streams can be spatially multiplexed on the MIMO channel. The rank is obtained through the Singular Value Decomposition (SVD) of the channel matrix and corresponds to the number of non-zero singular values [65]. In a 2×2 MIMO system, another key indicator is the Condition Number (CN) of the MIMO matrix, defined as $20.\log_{10}(\sigma_1/\sigma_2)$ in dB, where σ_1 and σ_2 are the two singular values given by the SVD. A well-conditioned matrix with CN close to 0 dB allows for reliable multi-layer reception. We define the mean CN as an average of the CN over N_f sub-bands:

$$CN_{mean} = 20.log_{10}\left(\frac{1}{N_f}\sum_{f=1}^{N_f}\frac{\sigma_{1,f}}{\sigma_{2,f}}\right)$$

Figure 45shows the mean CN from the MIMO channel computed between the base station already presented in Figure 41and the UE moving along a street perpendicular to the direct path. The base station antenna system is composed of 2 elements separated by 2λ, while 2 antenna elements are separated by λ at the UE. The mean CN is averaged over several locations in order to smooth out the fluctuations. The basic-complexity model shows the highest mean CN, indicating high correlation in the spatial modes due to poor channel predictions. This is especially true when the UE is in Non-Line of Sight where the additional contributions from the full-complexity model impact largely the angular diversity.

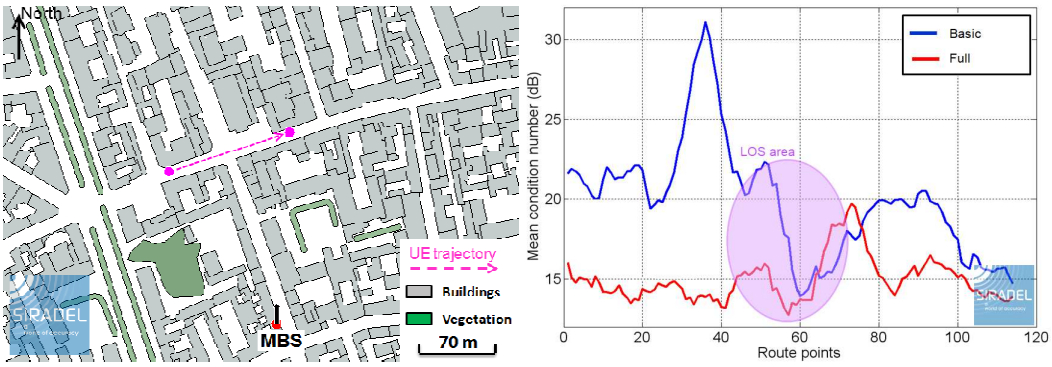

Figure 45 Condition Number (CN) prediction

The enrichment of the deterministic channel predictions in the temporal and angular domain impact very significantly the predicted wideband and MIMO channel parameters. This is expected to be a key improvement for the creation of realistic scenarios dedicated to the evaluation of 3D beamforming, MIMO precoding, interference cancellation and RRM.

5.2 Scenario for HetNet simulation

Corresponding scenario in D2.2: 2.3.6 "LTE-A multi-layer network in urban/suburban environments"

The construction of highly realistic multi-cell, multi-user scenarios is essential in the evaluation methodology to get valuable results. SIRADEL will elaborate dynamic scenarios as a basis for HetNet network evaluation, relying on a real environment (e.g. an existing urban area represented by 3D buildings), including non-uniform, multi-service and multi-environment user traffic, multi-cell and multi-layer network deployments, site-specific path-loss models, advanced channel models and prediction of the wireless backhaul links.

5.2.1 Definition of the scenario

Based on realistic macro cellular configurations, we define scenarios matching the future challenges of cellular operators on their wireless HetNet. Scenarios are proposed to tackle different network configurations and management techniques, and investigate the impact on radio network performances.

The simulation environment that has been selected so far characterizes a typical European dense urban city (note that other environments could be considered later during the project, e.g. suburban residential, if required). The environment is modelled by 3D buildings over a Digital Terrain Model (DTM). The following network layouts will be considered either separately or combinations of them to form a HetNet:

- Macro network
- Outdoor Small-cells (oSC)
- Indoor Femto-cells (Femtos)
- Indoor WiFi Access Points (APs)

The main parameters of the different network layouts are described in Table 7.

Table 7 HetNet topology parameters

Macro	Hexagonal site deployment: two rings around the central site, i.e. 19 sites corresponding to 57 cells. Three cells per site. Inter-site distance (ISD): 450 m. Average antenna height: 32 m above ground. Maximum total transmit power: 40 W per antenna.Antenna: directional, 14 dBi gain. Antenna electric down-tilt: 6°.
Small-cell	Location: outside (typically on poles). Antenna height: 8 m. Deployment: different setups will be considered (several density, uniform vs non-uniform) Maximum total transmit power: 5 W. Antenna: omnidirectional with 5 dBi gain or smart antenna.
Femto-cell/WiFi AP	Location: Inside the different building floors. Antenna height: 1m above floor. Deployment: partly random, different setups will be considered (several densities, uniform vs non-uniform). Maximum total transmit power: 250 mW. Antenna: omnidirectional with 5 dBi gain or smart antenna. Access type: Open or closed or restricted to a group of users.

The Macro-cells are deployed on two rings around a central three-sector site. These are not located on real sites, but dominant locations have been selected that are representative of an operational network.

Figure 46 shows an example of a multi-layer network based on a uniform SC deployment in a real dense urban environment. As explained in Table 7, other deployments and strategies may be defined to evaluate the impact on network topology such as hotspot deployments.

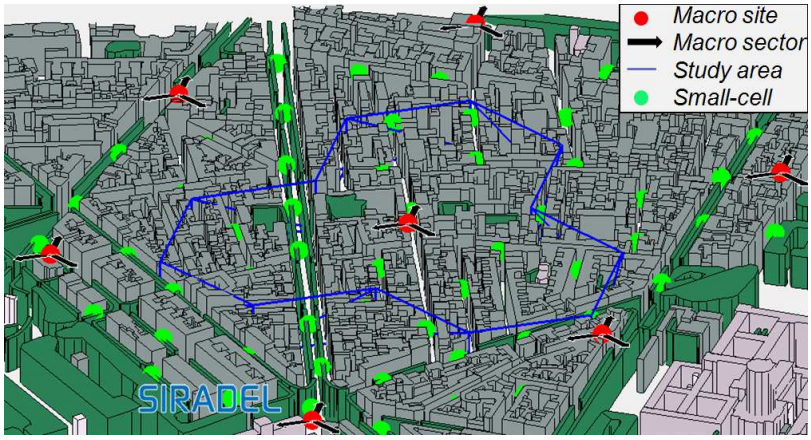

Figure 46 Example of a multi-layer deployment in a real dense urban environment

Femtos and APs can be deployed over the whole study area, in order to integrate the potential customer indoor solutions into the HetNet simulations. Different deployment strategies can be realized, considering a uniform density over the study area, or a density depending on the distance to the macro-cell and the presence of hotspots. Locations inside the buildings are generated randomly, with, if needed, the possibility to control the average distance to external walls. This will make it possible to get a general overview of the challenges raised by indoor deployments in a HetNet context. Figure 47 illustrates a typical uniform Femtos/APs deployment in a whole building block.

A study case in a specific building may be also envisaged, where only Femtos and APs deployed in this building are simulated.

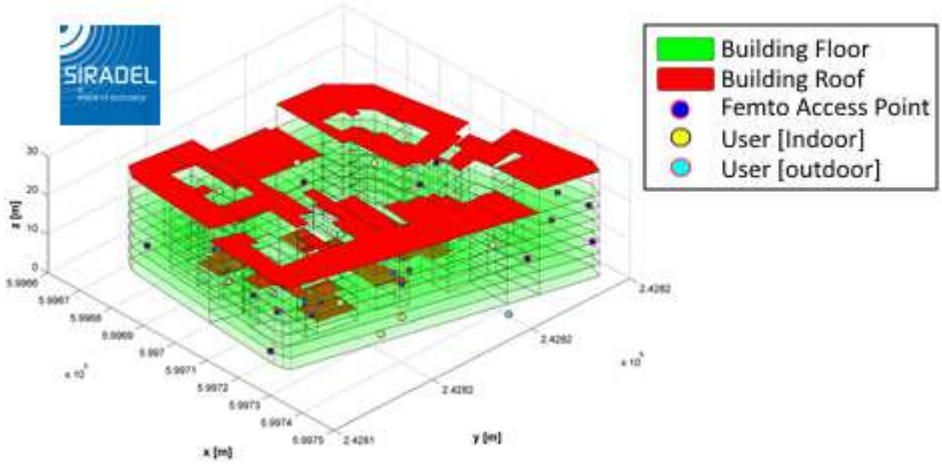

Figure 47 Typical femto-cells deployment in a building

Path loss is a major input of the simulation process and is critical in the complex multi-layer environment presented here-above. The propagation model must be able to address very different radio link configurations (Figure 48):

1 - Macro outdoor BS to outdoor UE

2 - Macro outdoor BS to indoor UE

3 – Indoor Femto/AP to indoor UE

4 - Indoor Femto/AP to outdoor UE

5 - Indoor Femto/AP to indoor UE in another building

6 - Outdoor SC to outdoor UE

7 - Outdoor SC to indoor UE

BS: Base-station; SC: Small-Cell; UE: User Equipment.

The Volcano ray-based propagation model, along with 3D high resolution geographical map data, is able to deal with this heterogeneity and bring realistic spatial correlation and variability in path-loss. This approach enables the realization of large-scale HetNet performance evaluation.

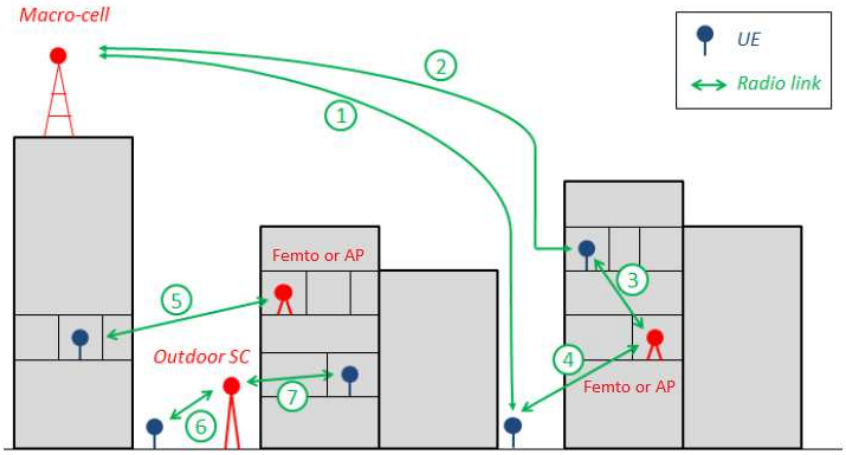

Figure 48 Radio links in a HetNet

The scenario is complemented with time-variant traffic maps to model the spatial and temporal user traffic variations. These maps make it possible to distribute multi-floor indoor users and outdoor users in the study area (Figure 49) with specific situations at working time, evening or night. Traffic maps also provide user profiles (list of services for specific user categories) and mobility models (indoor, outdoor pedestrian, outdoor vehicular).

Based on innovative concepts expressed in D4.1, generated traffic maps will include hotspot areas as well as realistic multi-floor indoor repartition. Those advanced features will exploit study area characteristics merged from different sources: building footprints, enriched information (e.g. office building, apartment building or shop opening hours) embedded in the geographical data bases or retrieved from the web and if available, network monitoring data. By processing multiple simulations based on user distribution snapshots representative of potential user locations, we will be able to derive statistics on network performance metrics.

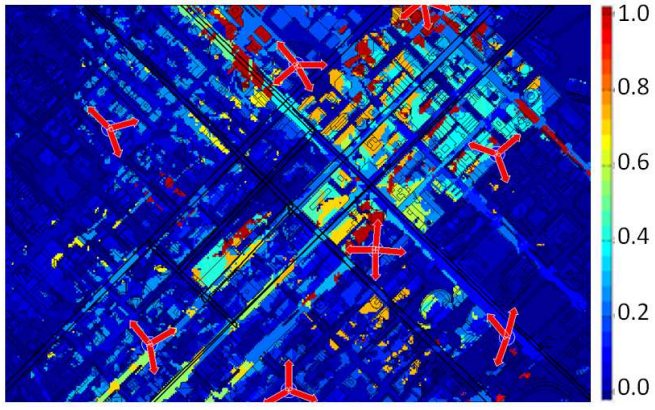

Figure 49 2D display of relative user densities extracted from a 3D traffic map [66].

5.2.2 Exploitation in system simulations

The network setup, user traffic distribution and multi-cell multi-user 3D radio predictions compose together a reference evaluation framework that can be interfaced with third-party system-level simulators, as illustrated in Figure 50. It may be used (and customized) in the innovation WPs for simulation and assessment of HetNet deployment and algorithm performance in terms of service coverage, network capacity, energy efficiency and fairness. More precisely it could target the

assessment of advanced transmission and reception schemes in WP3 but also offloading and SON mechanisms in WP4.

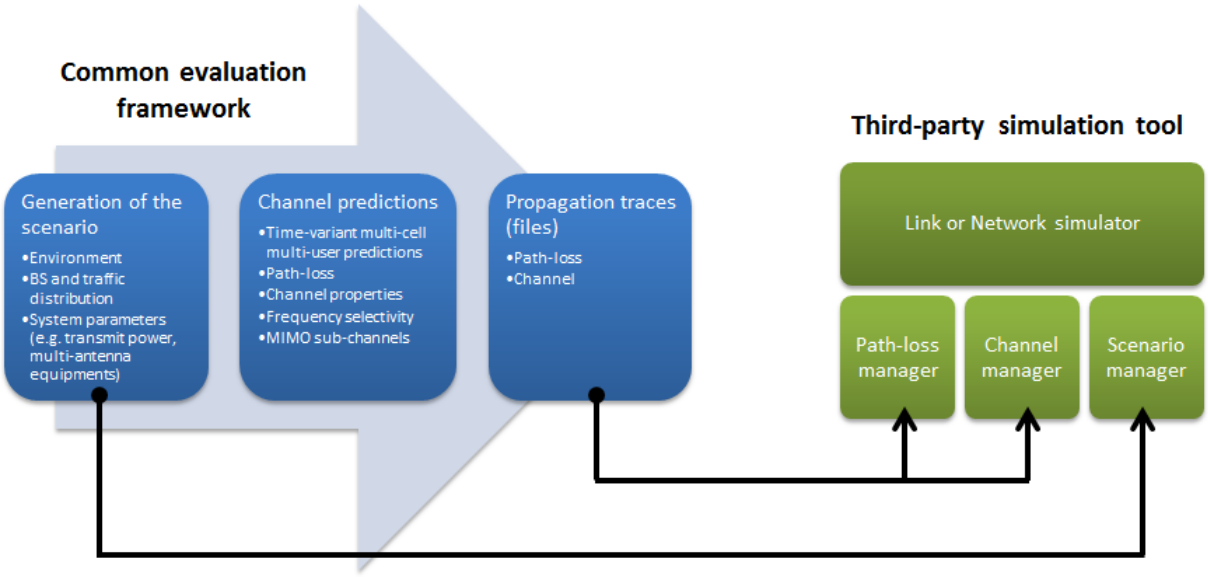

Figure 50 Outline of the common evaluation framework

System-level simulations might lead to the elaboration of site-specific interference or performance statistical models that characterize the impact of an innovative algorithm(s). Integrated into operational simulation processes (based on simplified and time-efficient system modelling), these abstraction models would permit the new techniques to be considered in large-scale network simulation, network design and optimization. The evaluation of the implemented techniques (and combination of them) may be then conducted on large realistic scenarios. Figure 51 illustrates the integration of such abstraction models into the SIRADEL coverage-based simulation process. Actually abstraction models can be implemented in different blocks that rely on simplified system algorithms: network/cell selection, resource allocation, power control, interference modelling, or link performance modelling.

Finally, the assessment of the network performance with the selected algorithms will lead to the elaboration of initial guidelines for an efficient HetNet design and deployment.

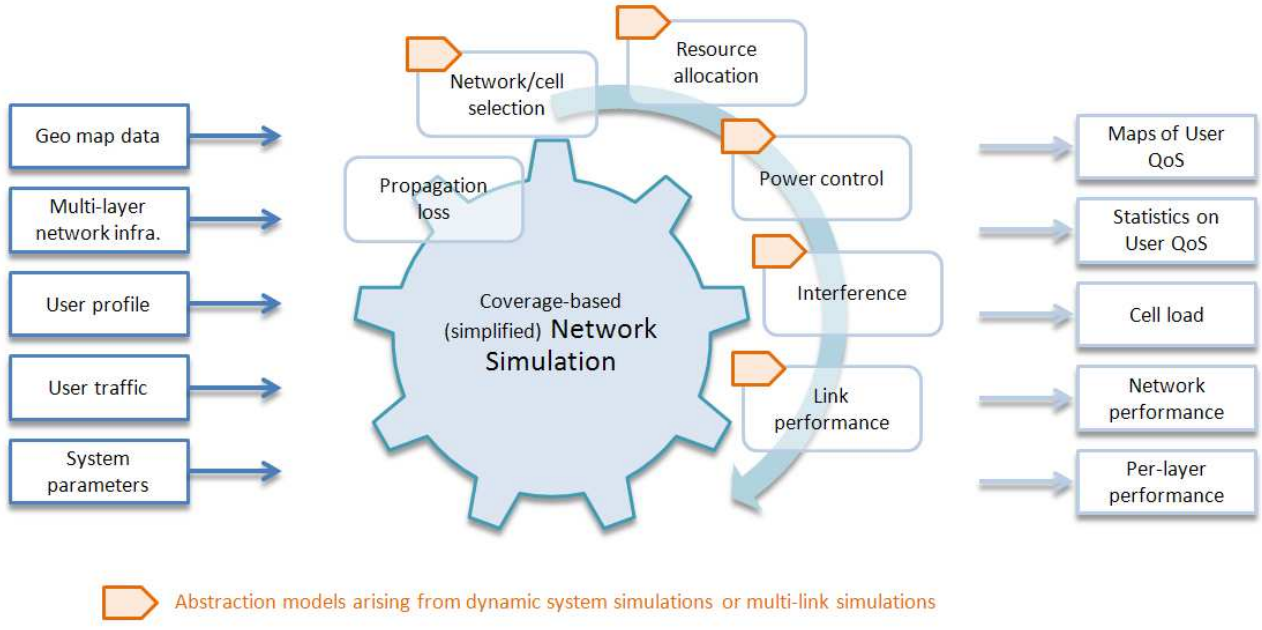

Figure 51 Outline of SIRADEL operational simulation chain that will be used and extended in the project

5.2.3 Case study

The first envisaged case study relying on this scenario aims at analyzing the performance of 3D beamforming in LTE-A multi-layer networks.

The investigated LTE-A network topology is composed of a usual macro layer and of small-cells equipped with traditional or beamforming antennas. The interference is supposed to be managed by ICIC (Inter-Cell Interference Coordination) or eICIC (enhanced ICIC) techniques, like ICIC FFR (Fractional Frequency Reuse) in the macro layer, eICIC ABS (Almost Blank Subframe) between macro and small-cell layers and UL ICIC to coordinate power control. The usage of beamforming is expected to enhance the user throughput and network capacity by further reducing interference levels. Its benefit will be evaluated first on the downlink and possibly on the uplink.

Beamforming is a multiple antenna technology used in transmission and/or reception. The objective is to dynamically adapt the antenna pattern to orient the beam towards users in order to reduce interference in other directions and possibly increase the useful signal (if the antenna maximum gain can be increased). Thereby, the base station uses a specific beam (a specific set of complex weights) for each user according to his transmission condition.

Although the horizontal beamforming has been implemented in networks such as TD-SCDMA (3G technology used in Asia) or WiMax, and is proposed in LTE and LTE-A, the 3D beamforming is a recent technique that has been introduced in 3GPP LTE Release 11. It aims at steering the antenna beam not only in the horizontal plane but also in the vertical plane, taking benefit of the 3D distribution of users (in streets and at all building floors) and of the largest user elevation angle discrimination in small cells compared to macro cells.

In order to enable accurate assessment of beamforming, a realistic evaluation framework is essential. Standard system-level simulations based on 2D channel model and 2D user distribution are not able to capture the benefits of these transmission techniques. In particular, mandatory features are realistic environments (including indoor and outdoor), realistic user distributions (3D and non-uniform) and 3D radio channel models for all types of link met in the proposed evaluation framework.

In terms of radio planning, the coverage prediction for each pixel (or user location) must be calculated with the specific beam chosen for it, and must consider the reduced interference coming from neighbour cells. Thus, the traditional prediction method based on a fixed transmission antenna is no longer applicable. New models (so-called abstraction models) will thus be derived to achieve the goal of this case study.

6 RF AND ANTENNA TECHNOLOGIES

Different key aspects related to RF front-ends and antennas to support carrier aggregation (CA) will be addressed in the context of small cells. CA will play an important role to increase the bandwidth up to 100MHz providing flexibility for using the available spectrum.

Innovative RF architecture solutions will be studied to handle bandwidths up to 100MHz allowing reconfigurability in terms of bandwidth and frequency of operation from an energy efficiency perspective. Apart from that, the antenna design will be focused on the development of reduced size solutions for multi-band applications. Meta-materials will be considered to optimize the radiation properties of the antenna over different frequency bands.

In this section, the requirements and challenges of reconfigurable RF front-ends and antennas for CA are discussed.

6.1 Reconfigurable RF Front-ends for CA

Corresponding scenario in D2.2: 2.7.1"Carrier aggregation using reconfigurable RF front-ends"

One of the key features of LTE-Advanced (LTE-A) is to support peak data rates that reach as high as 1Gbps for low mobility applications and 100Mbps for high mobility. These peak rates targeted for LTE-A have fundamental repercussions on the system design. Achieving the downlink peak data rate of 1Gbps will require wider channel bandwidths. At the moment, LTE supports channel bandwidths up to 20MHz, and it is unlikely that spectral efficiency can be improved much beyond current LTE performance targets. Therefore, the only way to achieve significantly higher data rates is to increase the channel bandwidth. LTE-A extends up to 100MHz of bandwidth when five 20MHz component carriers (CCs) are aggregated (currently only 2 CCs are allowed). As a result, carrier aggregation (CA) can improve network efficiency and user performance by dynamically allocating traffic across the entire available spectrum.

As most of the spectrum is occupied and 100MHz of contiguous spectrum is not typically available, the creation of wider bandwidths through the aggregation of contiguous and non-contiguous CCs has been allowed. The CA technique can be used either with frequency-division duplex (FDD) or time-division duplex (TDD), and can be developed over 3 different modes depending on the way that the CCs are placed over the spectrum:

- Intra-band contiguous
- Intra-band non-contiguous
- Inter-band

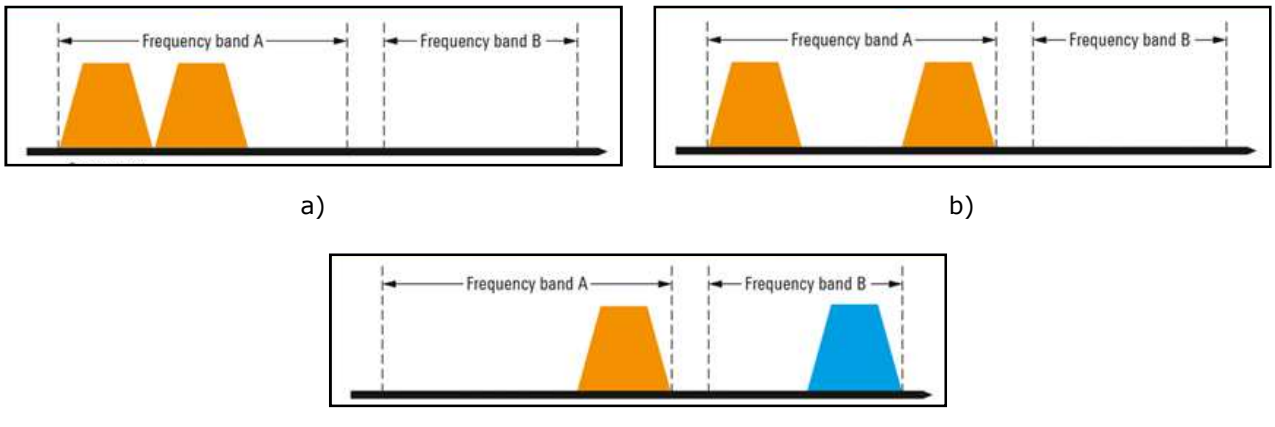

Figure 52 Different CA modes: a) Intra-band contiguous, b) Intra-band non-contiguous and c) Inter-band

Figure 52 represents the occupied spectrum of each CA mode. Intra-band CA uses a single LTE-A frequency band, while inter-band CA combines two different LTE-A frequency bands. In addition, the CCs can be adjacent or not, performing contiguous or non-contiguous CA respectively. The allowed channel bandwidths for each CC are 1.4 MHz, 3 MHz, 5 MHz, 10 MHz, 15 MHz and 20 MHz. Nowadays the maximum aggregated bandwidth is 40 MHz for intra-band contiguous CA and inter-band CA [67].

Beyond these current bandwidth configurations, RF front-ends should be designed to deal with up to 100 MHz.

LTE-A is defined to operate in certain frequency bands depending on the use of FDD or TDD [67]. In Europe, the operating bands for FDD are bands 1, 3, 7, 8 and 20, while bands 33, 34, 38 and 40 are available for TDD.

To support CA and its bandwidth flexibility, RF blocks should fulfil certain characteristics because RF components have to work in a higher bandwidth. That implies some constraints in components typically found in a narrow band design, such as power amplifiers, circulators, etc. Furthermore, reconfigurable components are required to fit the different operating bands and CA modes. Depending on the CA mode, various architecture options can be found according to where the CCs are combined, i.e., at digital baseband, or in analog waveforms before the RF mixer, or after the mixer but before the power amplifier (PA), or after the PA. Figure 53 presents the transmitter architecture options defined in 3GPP [68].

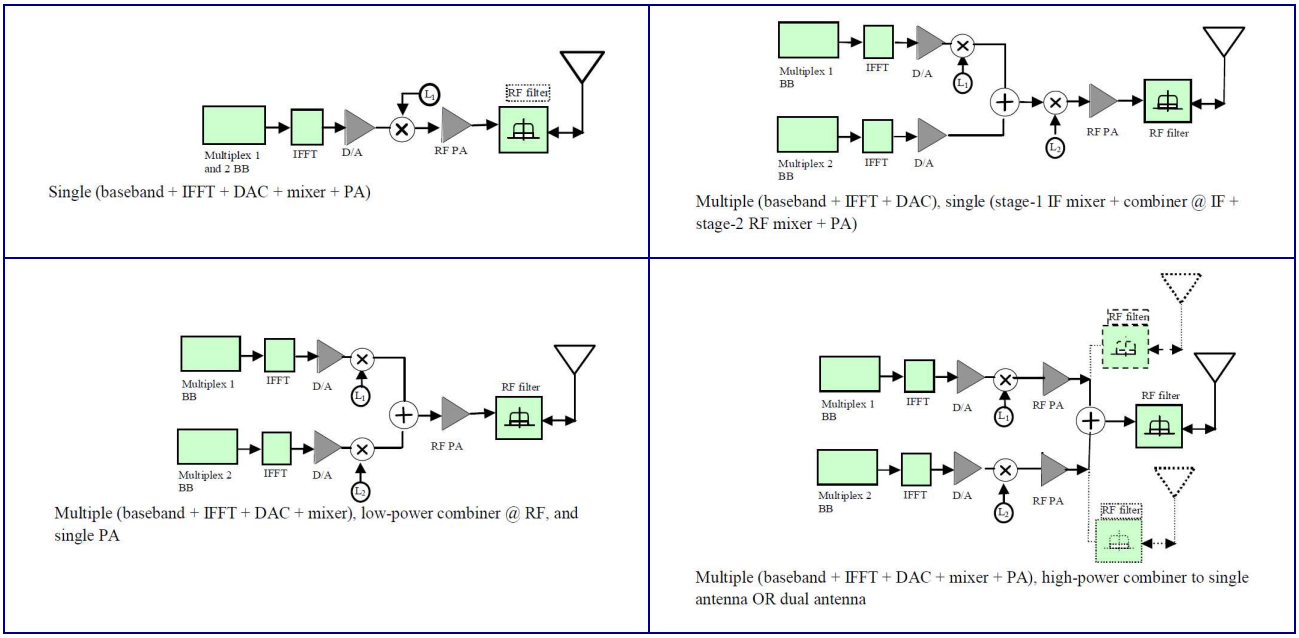

Figure 53 Different transmitter architecture options to implement CA [68]

In all options, the RF PA is a relevant component because it is one of the most power consuming components in an RF front-end. The study will focus on it, proposing a reconfigurable PA to adapt to the different CA modes from an energy efficiency perspective. The solution proposes a unique reconfigurable PA for each LTE-A frequency band adapting its performance according to the number of carriers handled and the bandwidth combination set.

The study refers to the base station (BS) case because it presents a higher power level tunability. According to 3GPP standard [69], a maximum mean power level per carrier for BS operating in CA configuration is defined. This power level is 46dBm for macro cells, 38dBm for micro cells, 24dBm for pico cells and 20dBm for femto cells. Taking into account that the maximum level is defined per carrier instead of BS, a femto BS performing CA with 2 CCs has 23dBm maximum mean power level, 24.8dBm with 3CCs, 26dBm with 4CCs and 27dBm with 5CCs.

A reconfigurable PA is a suitable solution to adapt to the different CA configurations providing energy savings versus a conventional PA. In small cell scenarios, it is reasonable to use a unique PA per various CCs to reduce the size and the cost because the power levels that PA handles are not strongly challenging as in macro cell scenarios. In those latter scenarios, a PA is usually developed per CC due to high power level constraints.

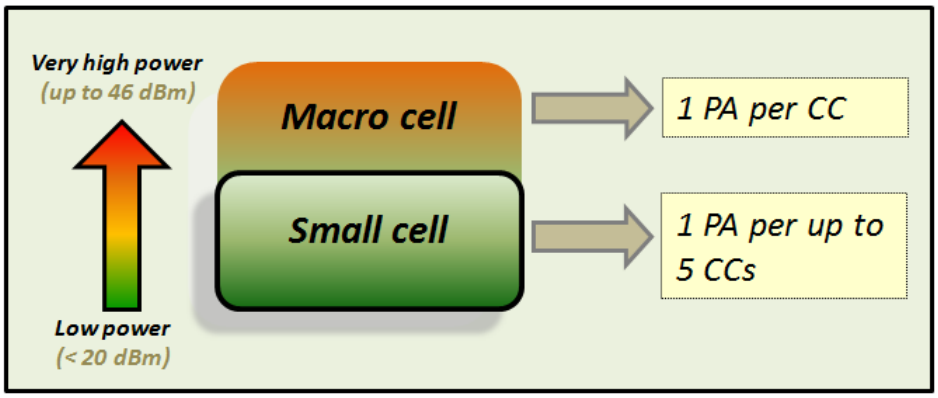

Figure 54 PA reuse according to the maximum power level in CA developments

In Figure 55, both possible transmitter architectures focusing on PA reuse are presented. The first configuration is optimal for macro cell scenarios and the second one for small cell scenarios which will be the purpose of this study.

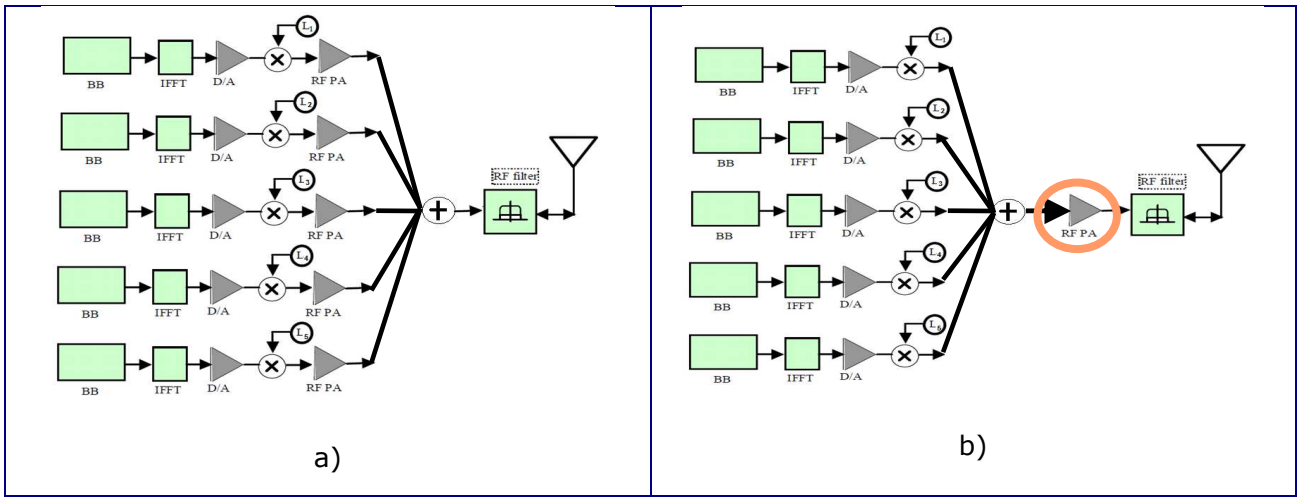

Figure 55 Transmitter architecture for CA: a) using a PA per CC and b) using a unique PA for various CCs

The study will examine the PA performance when a unique PA is implemented for CA in a small cell scenario. The target will be to evaluate its performance concerning the number of CCs for CA and CA modes in order to fulfil 3GPP specifications in terms of PA linearity and intermodulation constraints [69].

Moreover, LTE signals use digital modulation techniques which present signals with high peak-to-average-power ratio (PAPR). Typical PAPR for LTE signals could be estimated around 8-10 dB for each CC. These systems require PAs with superior performance, requiring large back-off power levels to avoid spectral spreading. The PA design is usually optimized in terms of energy efficiency at maximum output power. Meanwhile energy efficiency gets worse at lower output power levels. To meet these stringent linearity requirements and at the same time operating the amplifiers at their highest possible efficiency becomes a challenging issue.

Furthermore when CA is implemented using a unique PA which is the scope of this study, there are additional linearity requirements depending on the number of CCs and CA mode. Therefore a reconfigurable PA could be an appropriate solution to adapt to different possible configurations. In this study, we will evaluate different PA requirements which are mandatory for implementing CA with a unique PA and at the same time we will evaluate how provide energy savings through PA reconfigurability.

Some of the PA requirements which will be evaluated are the unwanted emissions [69]. They consist of out-of-band emissions and spurious emissions. Out-of-band emissions are immediately outside the channel bandwidth resulting from the modulation process and non-linearity in the transmitter. There are out-of-band emissions requirements for the BS transmitter which are specified in terms of Adjacent Channel Leakage power Ratio (ACLR) and operating band unwanted emissions. The ACLR requirement constrained by 3GPP standard [69] is defined to be at least 45 dB. Spurious emissions are emissions

which are caused by unwanted transmitter effects such as harmonics emission, parasitic emission, intermodulation products and frequency conversion products, but exclude out of band emissions. All these requirements should be taken into account during the PA design.

Some preliminary simulations have been done for five 10 MHz CCs performing intra-band contiguous CA, showing the effects of PA characteristics over ACLR performance. A common 20 dB gain PA was used varying its output power at 1dB compression (P1dB) to show its influence over ACLR performance. Figure 56presents CA spectrum for five 10MHz CCs before and after a 20 dB gain PA adjusting P1dB to achieve 45 dB ACLR. Comparing both results, out-of-band emissions are clearly present related to non-linearity effects from PA performance. Nevertheless this performance is adequate to fulfil 3GPP specifications.

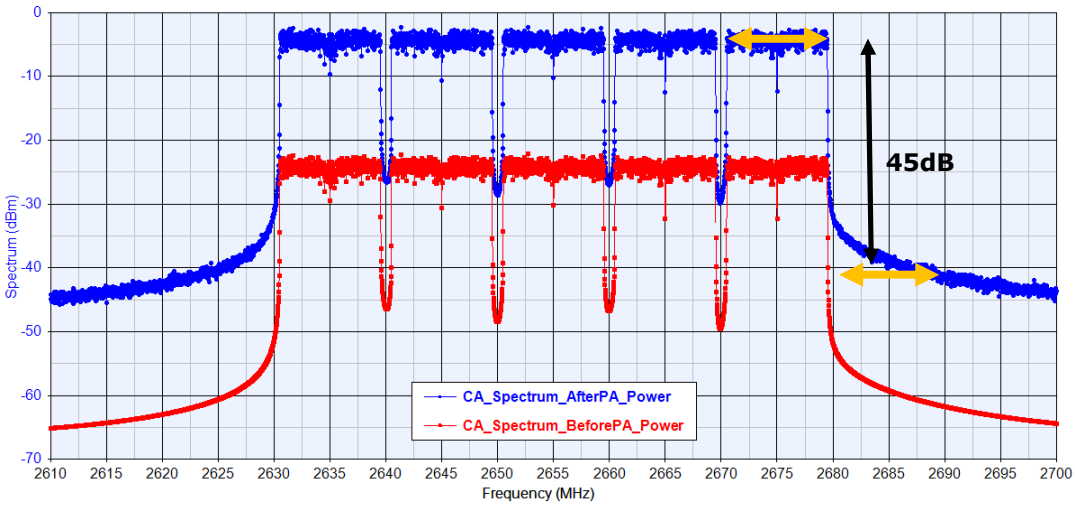

Figure 56 CA spectrum showing the performance before and after 20dB gain PA for 45 dB ACLR

On the other hand, Figure 57 presents CA spectrum when 3GPP specifications are not fulfilled, achieving only 35 dB ACLR. In this particular case, P1dB at PA was reduced by 5 dB providing only 35 dB ACLR.

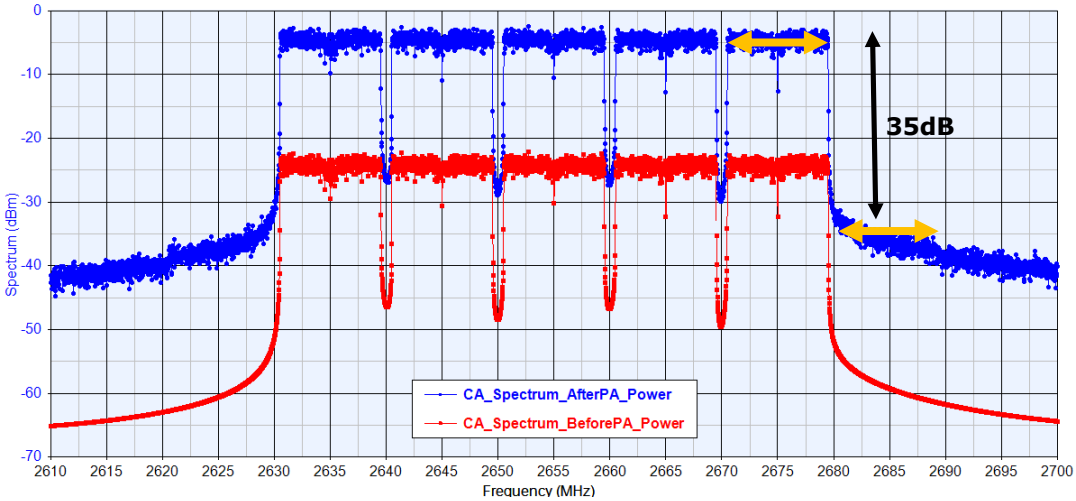

Figure 57 CA spectrum showing the performance before and after 20 dB gain PA for 35 dB ACLR

In this example, out-of-band emissions increase due to PA linearity deterioration. This performance doesn't fulfil 3GPP specifications and would require a PA with higher back-off power level. However, this back-off power level enhancement provides lower energy efficiency at PA due to PA characteristics.

Therefore during the evaluation the target will be to optimize the energy efficiency as much as possible at PA while 3GPP specifications are fulfilled. We will evaluate the PA performance concerning the number of CCs and CA modes, and in terms of back-off power level needed as a function of the PAPR and

intermodulation constraints. A reconfigurable PA will be analysed in different CA configurations, evaluating the potential energy savings versus a conventional PA.

6.2 Compact Frequency Agile Antenna

Corresponding scenario in D2.2: 2.7.2"Antenna design: small antenna for femto-cell, compatible with 4G systems bandwidths"

6.2.1 Introduction

6.2.1.1 Frequency Agile Antennas

Reconfigurable antennas have a versatile behavior needed in the always more complex communication systems. A classic antenna offers fixed characteristics and can only operate at frequencies for which it has been originally designed. On the contrary, the characteristics of a reconfigurable antenna can be adjusted to match different communications standards. It is even possible to imagine reconfiguring the antenna on a standard non-existent at the time of the design. Thus, it permits to access to new standards (with the possibility of fast switching between the different frequencies) and extends antenna life by following the evolution of communication systems.

The frequency agility of reconfigurable antennas allows in some instances to replace a bulky broadband antenna by a more compact antenna having a narrow instantaneous frequency bandwidth associated with a control device to adjust the band and the operating frequency. This solution often results in antenna size reduction. Beyond the compactness resulting from the integration of new functions in the antenna, the use of reconfigurable antennas may allow a single structure to replace multiple antennas. It results in a saving of space at a system level. Moreover, this solution inherently facilitates the coexistence of multiple radios despite their proximity with pre-filtering performed by the antenna.

It can be noted that by acting on the radiation of the antenna, it is also possible to achieve a polarization or radiation pattern diversity with a single antenna [70][71] but will not be discussed in this document.

6.2.1.2 Drawbacks

The first drawback of reconfigurable antennas is a higher cost compared to conventional antennas. The additional cost is directly related to the use of active components on the structure. It can either be due to the high performance required for the device or due to a more expensive specific manufacturing process (etching of semiconductor components, MEMS directly on antenna, etc.).

The second drawback is the energy consumption both in the continuous and in the RF domain. These additional losses must be taken into account at the design stage and the energy required by the system must be sized in accordance. Active components are often DC biased which necessarily consumes energy. Furthermore, these components often have resistive impedance and absorb the high frequency power which directly affects the antenna performance and its efficiency.

Another issue is to handle the RF power with the non-linear behavior of the active components. It also implies non-classical constraints on the design process. It leads to the last drawback which is the design complexity due to the non-conventional antenna structures, especially due to the biasing circuit, which can result in a fragile device and in additional cost. Moreover, this technical complexity, mainly due to the integration of active components in the radiating structure or the tuning circuit, causes conceptual and simulation difficulties, in particular for electromagnetic calculations.

6.2.1.3 Performance Criteria

There are several criteria to characterize properties of antennas agile in frequency. The first criterion is the frequency Tuning Range (TR) defined by:

$$TR = 2.\frac{f_{sup} - f_{inf}}{f_{sup} + f_{inf}} \times 100\ \%$$

With f_{sup} et f_{inf} the maximum and minimum frequencies of operation for the considered reconfigurable antenna, respectively. In addition, there are two distinct categories of frequency agility: discrete and continuous. The discrete frequency agility allows the antenna to operate at discrete values, while the continuous frequency agility allows a scanning of frequencies continuously inside the overall band.

The second criterion characterizing reconfigurable antennas is the radiation efficiency. This parameter plays a key role in reconfigurable antenna design as inserted active components, used to vary the electrical properties or reduce the physical dimensions, generally reduce the antenna efficiency.

Another important criterion, related to the efficiency of the system, is the consumption or the maximum voltage required to obtain the required frequency sweep for the device. This parameter is extremely important for handheld devices with batteries whose life time is limited and low DC voltage value is available.

The last criterion is about the linearity of the reconfigured characteristic with respect to the input or radiated power. The additional active components can induce non-linear effect in the antenna behavior such as harmonics, saturation, null of radiation, etc.

Other parameters such as the antenna size, the complexity of the biasing circuit and the cost generated are among other criteria to care and relate to the considered application.

6.2.2 Compact Antenna Reconfiguration Techniques

6.2.2.1 Introduction

There are several techniques to provide frequency reconfigurability to a compact antenna. The three main techniques used are presented in the following sections. They are composed of switches or variable elements on the radiating element or on its matching circuit or the use of tunable materials to affect the electrical characteristics of the RF structures. The choice of a specific technique depends on the type of antenna and the desired characteristics to achieve.

Many configurations can be found in the literature [72][73] but only microstrip, slot and monopole antennas (compact antennas) are considered in this study. Frequency agility can be obtained by adjusting the matching of the antenna without changing its electrical length. Active devices are usually used to adjust the matching between the antenna and the feed allowing the desired behavior. It can also be obtained by modifying the equivalent length of the antenna which generally acts as a resonator or by loading the antenna with a variable capacity/inductance. To control the resonant frequency of microstrip antennas, slots are usually used to adjust the current path and thus change its resonant frequency. The advantage of slots is the ease to introduce switches and vary the length of the slots by their activation. This comment is also valid for slot antennas. In the case of Planar Inverted F Antenna (PIFA) structures, the location of the feed or the short circuit is the main characteristic to control the antenna impedance. Regarding monopole antennas, the resonant frequency is defined by its arm length. To change the length of the arms, an active device can be added either to connect extra length or load. The loads used to modify antenna characteristics can be electronically controlled by active components such as varactor, digital tunable capacitor or electronic switch (PIN diode, FET or MEMS). It implies variable capacitance/inductance at well-chosen locations on the radiating element [74][75].

Tunable materials can also be used to modify the resonator properties. Different physical properties of material (permittivity or permeability) can be controlled and used to modify the electrical length of the antenna. The modification of these properties is based on their specific physical characteristics such as ferroelectric, ferromagnetic, piezoelectric, etc.

6.2.2.2 Active Component on the Matching Circuit

To optimize power transmission between the transmitter output or the receiver input and the antenna, an impedance matching circuit can advantageously be added between them. The matching circuit can be used to provide reconfigurability to the system using active components such as switches, varactors, etc. [76]. A typical block diagram of a transmitter integrating an impedance matching circuit is shown in Figure 58.

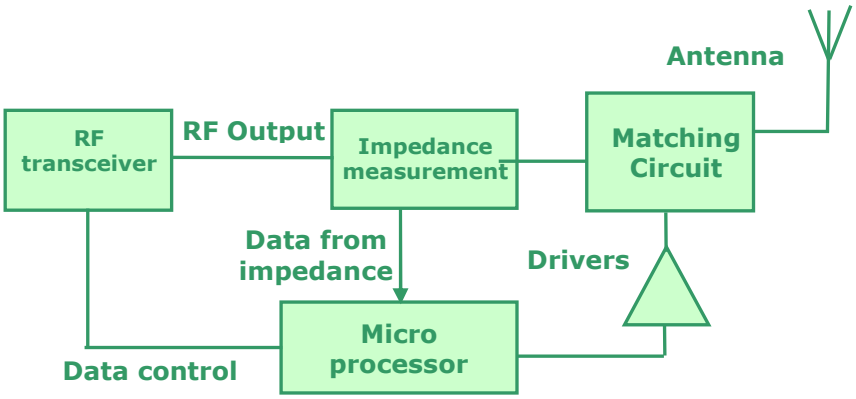

Figure 58 Reconfiguration system between the transmitter and the antenna [76]

In [77], an antenna based on a reconfigurable matching circuit is studied. The fabricated antenna is presented in Figure 59-c. It operates both in GSM band and the band used for US cellular. A matching circuit is associated to antenna to switch the system from a frequency band to another (Figure 59-b). The antenna is connected through the line l_1 to either the line l_{21} for the GSM band or the line l_{22} for the other band via a FET switch. The length of the lines l_{21} and l_{22} are different which affects the load presented to the antenna and thus affects its frequency response. It can be seen in Figure 59-d that the operating frequency band depends on the line connected to the antenna (l_{21} or l_{22}). The measured radiated efficiency is about 79% and 72% for the US band and the GSM900 respectively (Figure 60). For this antenna, simulated results show a maximum radiated efficiency not greater than 85%. The losses introduced by the matching circuit have been assessed in simulation and are low (88% radiated efficiency without matching circuit).

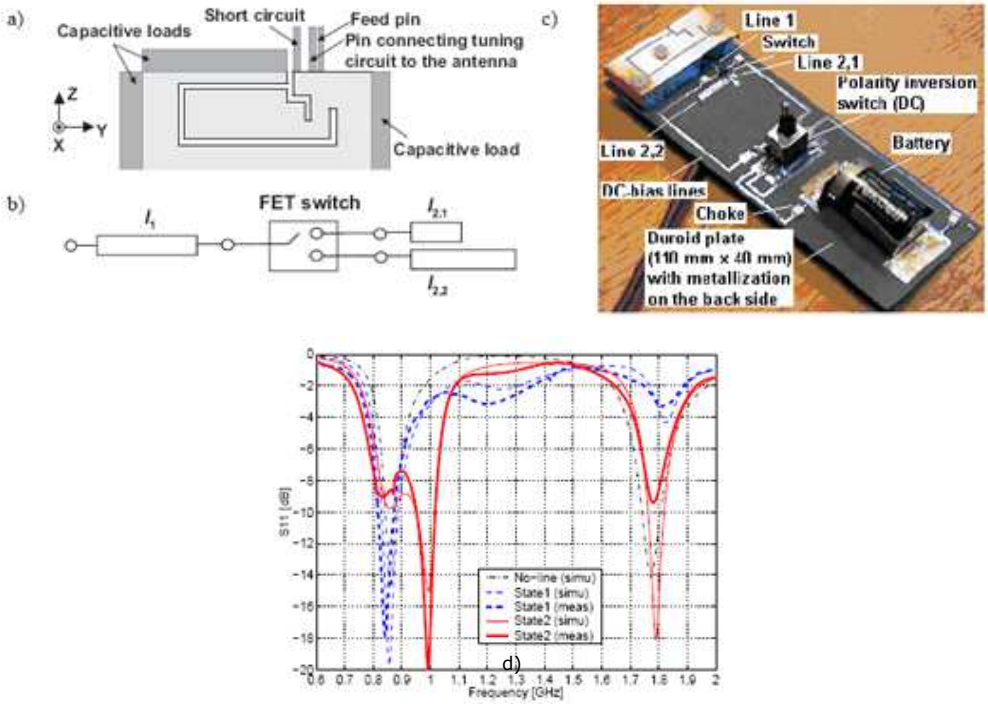

Figure 59 Antenna structure (a), use of the FET switch (b), realized prototype photograph (c) and reflection coefficients (d) [77]

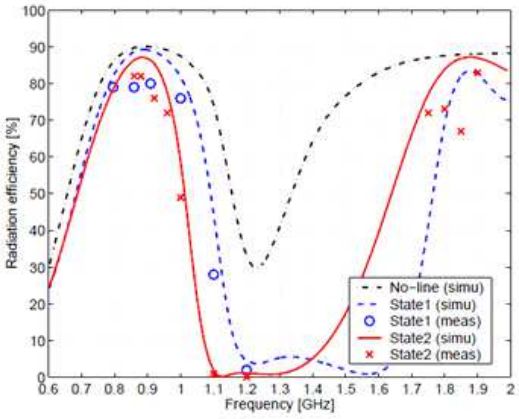

Figure 60 Simulated and measured radiated efficiency [77]

Recently, in [78], a PIFA antenna (Figure 61-a) has been associated to a matching circuit composed of 3 varicap diodes A, B and C (Figure 61-b). These diodes are used to adjust the impedance presented to the antenna, controlling its frequency response. Without impedance matching circuit, the antenna operates at 2.4 GHz. Depending on the bias on each diode, the antenna can operate over a wide frequency band ranging from 900 MHz to 2.4 GHz. In Table 8, the operating frequencies that can be achieved by the PIFA antenna are related to different diode configurations. Reflection coefficients for a few configurations are presented in Figure 62. The dimensions of the antenna are 4.96 mm x 9.93 mm x 23.57 mm which makes the largest dimension as $\lambda_0/14.1$ (λ_0 is the wavelength at 2.4 GHz). The dimensions of the ground plane are not taken into consideration in this study. This technique results in a reconfigurable antenna 62.5% smaller than the initial antenna ($\lambda_0/2$).

The measured radiated efficiency of the antenna without matching circuit is 91% which corresponds to the typical order of magnitude for PIFA efficiencies. After integration of the matching circuitry, the operating frequency changes to 2.45 GHz and the measured radiating efficiency drop to 75%. The authors claim that the efficiency can be improved by a better fabrication quality of the system.

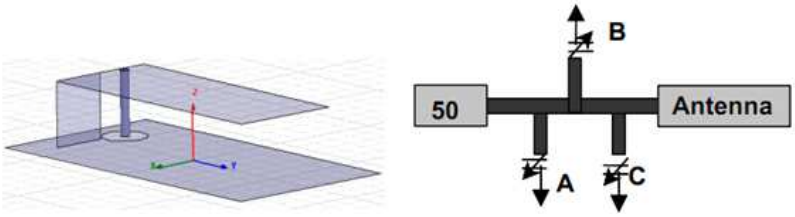

a) b)

Figure 61 PIFA antenna operating at 2.4GHz (a) and impedance matching circuit (b) [78]

Table 8 Operating frequencies related to the diodes configurations [78]

Tuner	Diode A (pF)	Diode B (pF)	Diode C (pF)	BW (MHz)
900 MHz	2.089	3.113	3.467	175
1176 MHz	1.625	1.8615	0.626	50
1227 MHz	1.071	1.668	1.8179	125
1575 MHz	0.705	0.943	1.065	50
1.8 GHz	0.6	0.643	0.7925	40
2.4 GHz	1.139	0.029	0.334	55

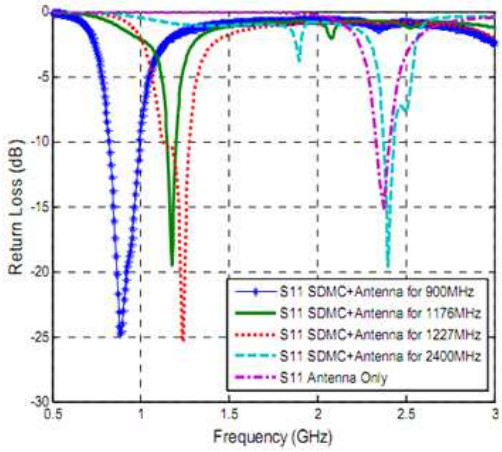

Figure 62 Reflection coefficients for different antenna configurations [78]

The use of active components in the matching circuit shows interesting reconfigurability properties but is limited in term of operating frequencies.

6.2.2.3 **Active Component on the Radiating Structure**

In this section, the use of the main active components for antenna agility is described with different examples. These components are all used to change the electrical characteristic of the antennas.

6.2.2.3.1 MEMs

A widely studied technique is to use Micro ElectroMechanical System (MEMS) as switch or variable capacitance [74]-[84] to control the antenna characteristics. Simons et al. have shown in [82] an example of patch antenna using two MEMS as variable capacitance. The geometry and the reflection coefficient of this structure are presented in Figure 63(a) and (b) respectively.

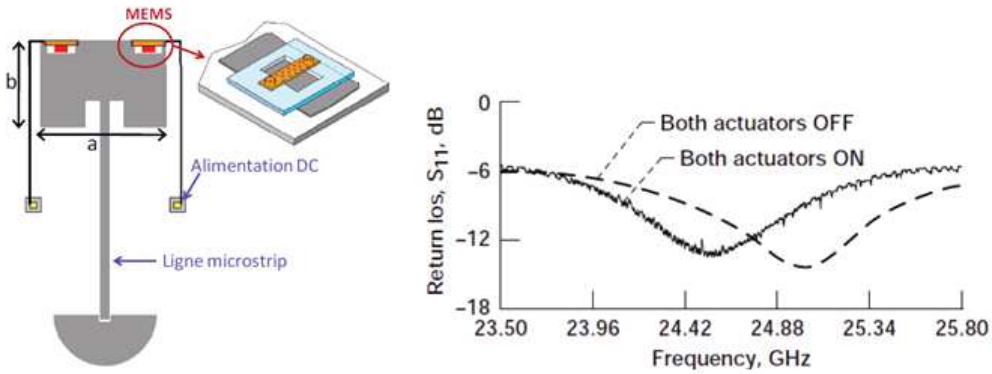

(a) (b)

Figure 63 (a) Geometry of a frequency reconfigurable antenna using MEMs and (b) its measured reflection coefficients when the MEMs are activated or not [82]

The patch antenna is printed on a 400 µm thick silicon wafer which is put on top of a substrate used as a support for measurement. The operating frequency is defined by the length of the patch *b*. The MEMs on the top sides of the patch shunt or not the parasitic capacitance and the resonant frequency of the patch is shifted by 1.6 % when the MEMs goes from the ON to the OFF state Figure 63-b).

6.2.2.3.2 PIN Diode

One possible use of PIN diodes is to short-circuit part of the arm of a slot antenna to electrically change the arm length. An example of PIN diodes used in slot dipole antenna is depicted in Figure 64[85]. The combination of eight diodes controls the length of the radiating slot and allows a discrete scanning over a frequency band from 2.8 GHz to 8 GHz depending on the ON and OFF states of the diodes. The reflection coefficients for the four considered combination of diodes are presented in Figure 64.

8% and 21% of impedance bandwidths are achieved according to the considered combination of switches with a realized gain in the range of 3.5 to 5.2 dBi. Finally, this antenna has relatively large dimensions since its length is greater than $\lambda_0/2$ at 2.8 GHz. Other works present more compact antennas with main dimensions smaller than $\lambda_0/2$, but with a significantly smaller achievable frequency range.

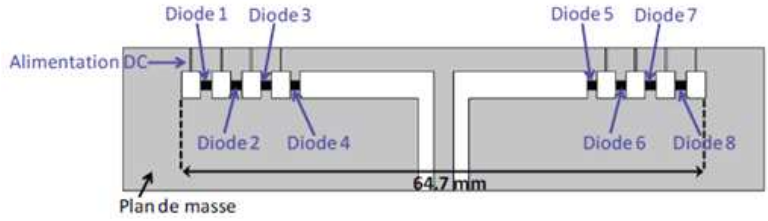

Figure 64 Geometry of frequency agile antenna incorporating PIN diode [85]

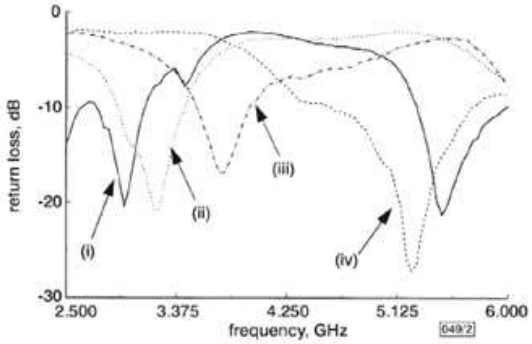

Figure 65 Reflection coefficients of the antenna for different states of the diodes. All diodes OFF (i), diodes 1 & 8 ON (ii), diodes 1, 2, 7 & 8 ON (iii), and diodes 1, 2, 3, 6, 7 & 8 ON (iv) [85]

6.2.2.3.3 Varactor Diode

A varactor is a type of diode whose capacitance varies as a function of the voltage applied to it and can be used for reconfigurable antennas. When a varactor diode is used as localized load, the input impedance of the antenna is affected and makes it possible to sweep the operating frequency [86]-[91]. In [86], Behdad and Sarabandi present a slot antenna loaded by a varactor diode. The antenna geometry is presented in Figure 66.

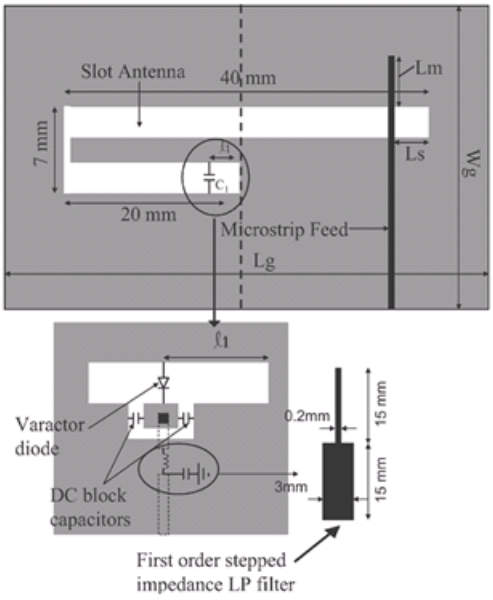

Figure 66 Geometry of the slot antenna incorporating varactor diode [86]

The bias voltage applied to the varactor diode controls the value of its equivalent capacitance and thus the electrical length of the slot antenna. The antenna can then be matched to the feed in desired frequency bands as shown in Figure 67. It can be noticed that, in this case, the frequency agility is limited within the lower frequency band due to the miniaturization of the antenna [86] and the use of large capacitance values.

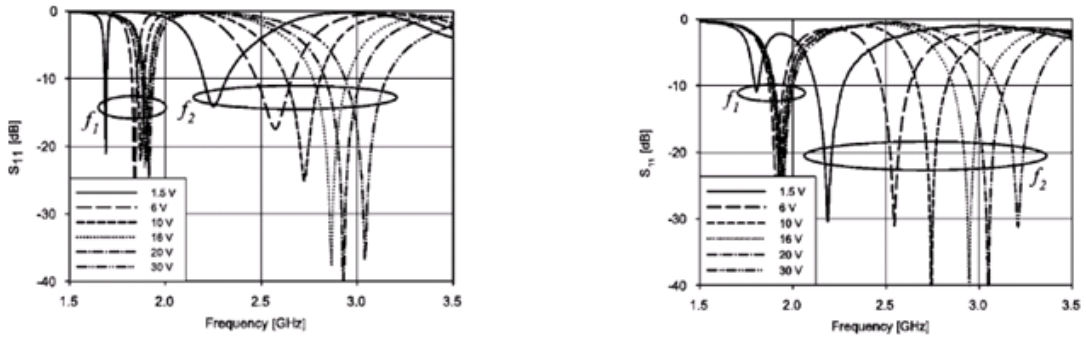

(a) (b)

Figure 67 (a) Simulated and (b) measured reflection coefficients for different bias values [32]

6.2.2.3.4 PIN and Varactor Diodes Combination

The combination of PIN diode and varactor diode is usually chosen when a large frequency range of operation is required. A PIFA antenna structure using both PIN and varactor diodes are presented in Lim et al. work [92]. The antenna structure is shown in Figure 68.

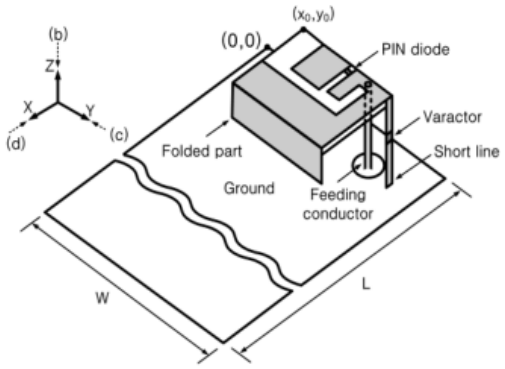

Figure 68 PIFA antenna structure using PIN and varactor diode [92]

The specificity of this structure is its ability to cover a whole range of frequencies whatever the configuration set to the PIN diodes. For configuration 1, the PIN diode is in the OFF state and by varying the value of the varactor diode, the antenna operates over the following bands: USPCS (1.85–1.99 GHz), WCDMA (1.92 – 2.18 GHz) and WLAN (5.15–5.825 GHz). In configuration 2, the PIN diode is in the ON state and the bias voltage of the varactor diode is set to 0 V. The antenna operates in both USPCS and m-WiMAX (3.4–3.6 GHz) bands. It can be noticed that the antenna efficiency is affected by the state of the diode. The radiation efficiency is about 90% and drop to 63% when the diode is in the OFF and ON state respectively. The effect of a parasitic resistance in series with an ideal diode on the antenna efficiency is presented in Figure 69. As expected, it can be observed that the less resistive the diode, the more efficient the antenna.

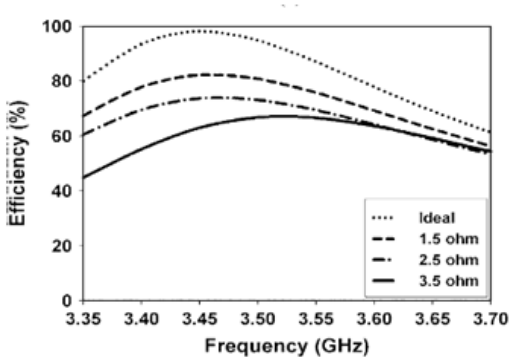

Figure 69 Simulated antenna efficiency in the m-WIMAX band for different parasitic resistance in series with an ideal diode [92]

6.2.2.3.5 Digital Tunable Capacitor

A new kind of tunable capacitor has recently been developed: the Digitally Tunable Capacitors (DTC). It consists of interconnected integrated Metal Insulator Metal (MIM) capacitors using RF switches to get a switched capacitor bank. The resulting capacitance is controlled by a digital word applied to the device.

As an example, the DTC from Peregrine uses a serial interface to control FET switches that connect or disconnect High-Q MIM capacitors. The technology employed for these DTC is Silicon on Insulator (SOI) [94] or more recently Silicon on Sapphire [93].

A block diagram of the DTC by Peregrine and a graph of Capacitance versus Tuning State are shown in Figure 70-a and b respectively.

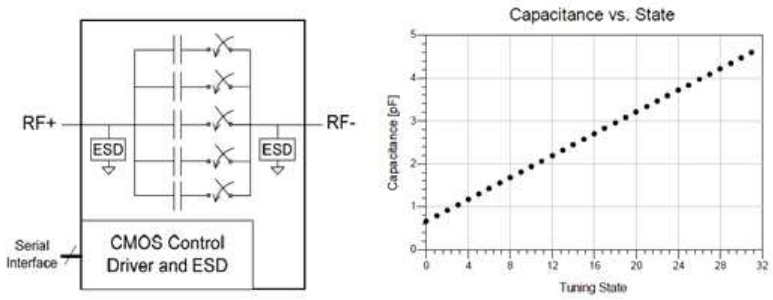

Figure 70 (a) Block diagram of Peregrine DTC and (b) Capacitance vs Tuning State of the DTC – Peregrine Application Note 29 [94]

Current state-of-the-art DTCs exhibit improved RF performance as compared to early commercial versions. The improvements are mainly on Q values, tuning ratio and the minimum capacitance (C_{min}). Low C_{min} improves matching network coverage in a shunt configuration and higher Q factor minimizes RF insertion loss.

6.2.2.3.6 Variable Inductors

In the previous reported cases, the active elements were acting on the antenna impedance adding a capacitive part. These elements are the most widely studied and used thanks to the ease of use and control of their values. Very few papers present variable inductors.

In [95], a monopolar wire patch antenna [96] is using a variable inductor for its reconfigurability. The variable inductors are based on MEMs technology whose magnetic characteristics provide inductance tunability. The inductively loaded antenna geometry is presented in Figure 71.

The metallic top hat is short circuited by a cylindrical conductor which introduces a low frequency parallel resonance where the new operating mode is obtained. This square antenna has typical dimension of $\lambda_0/4$($\lambda_0$being the free space operating wavelength). The inductor is introduced between the short circuiting wire and the antenna ground plane. It means that the variable inductor is set in series with the shorting wire. Changing the inductance value implies a variation of antenna input impedance and modifies the resonant frequency as shown in Figure 72.

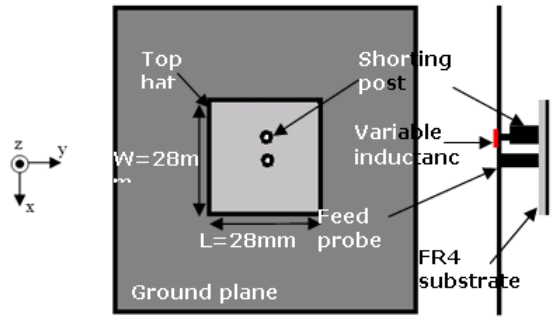

Figure 71 Description of the inductively loaded antenna structure

For the basic antenna structure without inductor, the maximum gain is about 0 dBi. When an inductance of 2.2nH is added to the antenna, the maximum measured gain is about -8 dBi. The gain decreases because of the size reduction of the antenna which is in accordance with the fundamental limits of miniature antennas and the losses induced by the inductor. However, the typical radiation pattern and the vertical main polarization of the Monopolar Wire Patch antenna are maintained.

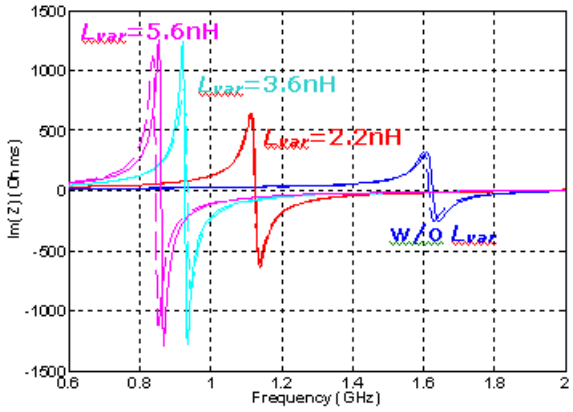

Figure 72 Illustration of the evolution of the frequency resonance versus Lvar in simulation and measurement

6.2.2.4 **Tunable Material**

Many compact antennas are printed on simple dielectric substrates. The use of a substrate with variable parameters would give agility to the antenna by modifying its electrical properties. In this section, four types of tunable materials are presented and their potentials and limitations discussed.

6.2.2.4.1 Metamaterial

Metamaterials are artificial materials with interesting electromagnetic properties that cannot be obtained with natural materials (permittivity and permeability simultaneously negative, etc.). These materials consist of periodic structures made of dielectric or metal which behave like a homogeneous material. An example of a patch antenna on top of a Split Ring Resonator (SRR) structures loaded substrate is shown in Figure 73.

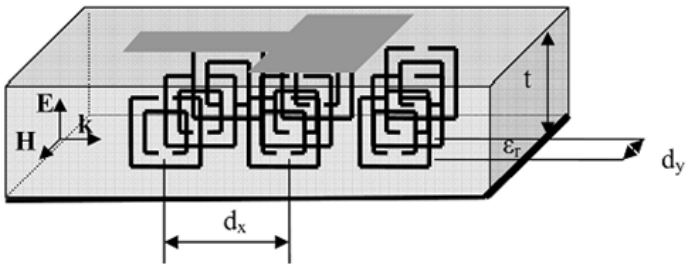

Figure 73 Printed microstrip antenna on Split Ring Resonator (SRR) structures loaded substrate [97]

Recently, several studies have shown the ability of these new materials to provide agility of antenna structures [98]-[100]. In [99], Lin et al present a loop antenna printed on top of a substrate loaded by Split Ring Resonator (SRRs) structures. Each SSRs are loaded by heterojunction phototransistors (HPT) as shown in Figure 74-a. The resonant frequency of the loop antenna depends on the local capacity of the SRR which is controlled by the phototransistors and, therefore, makes it possible to reconfigure this inductive antenna. With this design, the resonant frequency can be adjusted from 41.5 GHz to 44 GHz with a DC voltage ranging from 0 to 12V respectively. The disadvantage of this technique is the manufacturing complexity and losses induced by the parasitic elements.

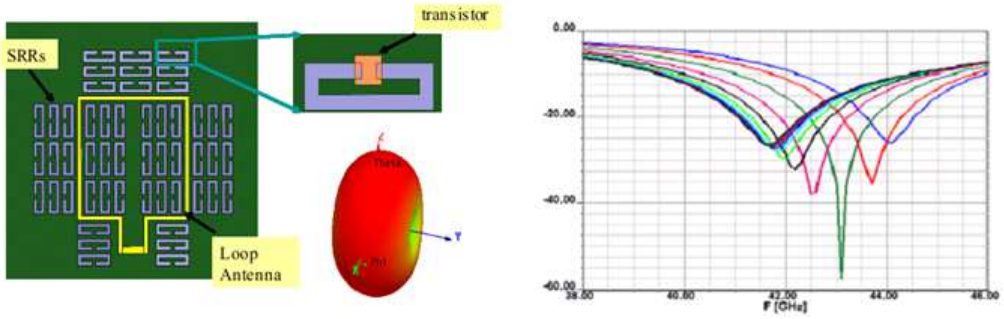

(a) (b)

Figure 74 a) Loop antenna on top of HPT loaded SRR and its radiation pattern, b) reflection coefficient for different voltages applied on the HPT (0 to 12V) [99]

6.2.2.4.2 Ferromagnetic Material

Ferromagnetic materials have a permeability which depends on the magnetic field applied to it. These materials are defined by the saturated magnetization, the remanent magnetization and the coercive field. For a use in microwave devices, the coercivity of the material must be as low as possible.

The most widely used magnetic material in microwave devices is the ferrite. Several examples of microstrip antennas designed on ferrite substrates have demonstrated significant variations on the resonant frequency (about 40 %) [101]-[103]. Radiated efficiencies are not explicitly given but the reported values of gain indicate that high efficiencies can be obtained with low-loss ferrites. In [101], a microstrip antenna deposited on a ferrite substrate is presented (Figure 75). The size of the antenna is 1.4 cm x 1.8 cm and is fed through a coaxial probe. The ferrite substrate is 1.27 mm thick with a permittivity of 15 and a saturated magnetization $4\pi M_s$ of 1720 G.

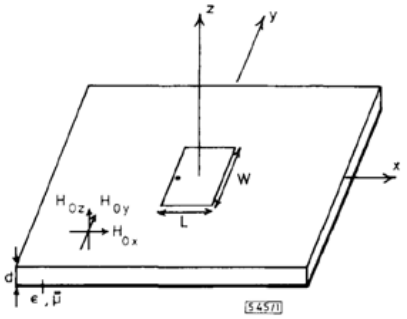

Figure 75 Antenna geometry on top of a ferrite substrate

To magnetize the ferrite, an external magnet located at a variable distance from the substrate (different magnetic field) is needed. The orientation and magnitude of the magnetic field applied to the substrate affects the field confined between the radiating element and the ground plane and leads to a variation of the operating frequency. In Table 9, it can be noticed that a maximum agility of 40% can be achieved when the field is oriented along the y axis.

The antenna gain and the radiation pattern are closed to conventional microstrip antennas. However, a larger cross-polarization is observed in this work (Figure 76).

Table 9 Agility of a patch antenna on ferrite substrate as a function of the magnetization orientation [101]

Magnetization axis	Frequency variation (GHz)	Agility (%)
X	4.6 – 5.5	16
Y	4.6 – 2.8	39
z	4.6 – 5.5	16

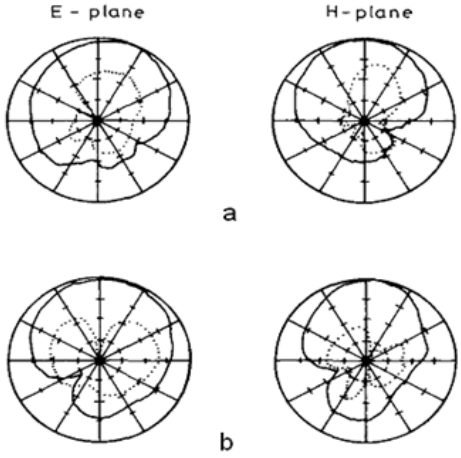

Figure 76 Measured radiation pattern of the antenna a) without (4.6GHz) and b) with DC bias (2.81GHz). The co- and cross-polarization are represented with solid and dotted lines respectively [101]

However, the use of ferrite materials in microwave devices is limited by the low magnetization values obtained, but especially by their high electrical conductivity which induces significant losses by leakage current [104]. Various studies have addressed this issue: [104][105] proposed to use these materials as composite associating insulating materials to minimize the overall losses.

In addition, the limitation provided by integration into magnetic control devices (coils are bulky and heavy) is problematic and has also motivated several studies in progress to overcome this constraint [106].

6.2.2.4.3 Ferroelectric Materials

Ferroelectric materials have the same behavior as ferromagnetic ones (seen in the previous section) except that their permittivity is controlled by means of an external electric field instead of a magnetic field. This property is used for reconfigurable devices.

There are numerous advantages to use ferroelectric materials in reconfigurable device. First of all, the electric control is easier to integrate to a system than a magnetic control. Moreover, the low values of the electric field required to control the electrical characteristics allow a fairly short switching time and makes these materials ideal candidates for reconfigurable devices. However, the major disadvantage comes from the very important dielectric losses. Many studies are working on techniques to limit these intrinsic losses either by doping [107]-[109], by creating composite ferroelectric-dielectric material [110]-[112] or to reduce the overall losses of the device by choosing the location of these materials in active areas of the device [113], [114].

6.2.2.4.3.1 Ferroelectric Material based Substrate

As shown in Figure 77, a radiating structure can be located on a ferroelectric substrate with variable permittivity. The considered substrate can be used either in a volume form (ceramics) [130] or in a thin film form (another substrate is needed as support) [131]. The variation of the substrate permittivity results in a variation of the antenna radiation pattern or a variation of the resonant frequency. In Castro Vilaro's work [131], the resonant frequency of a slot antenna is shifted from 27.46 GHz to 25.65 GHz when the permittivity of the thin film changes from 400 and 1200 respectively. This solution has potentially good properties for reconfigurable RF devices but is for now limited due to fabrication issues and technology maturity and also the difficulty to apply sufficient electric field for the command.

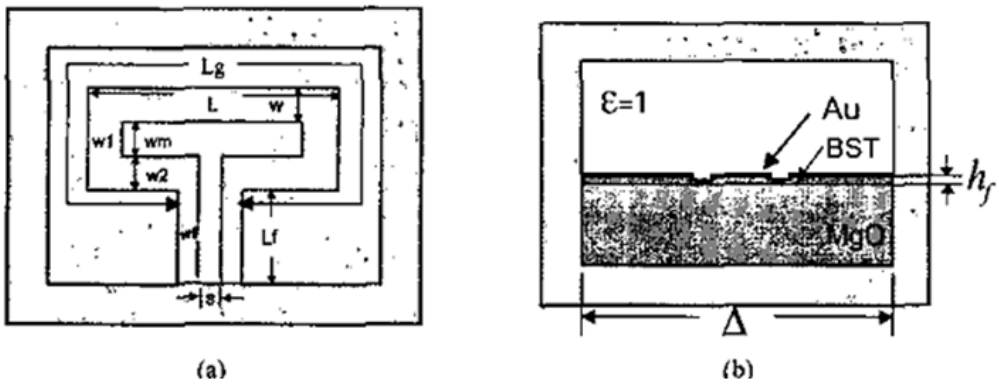

Figure 77 Slot antenna on ferroelectric substrate [130]

6.2.2.4.3.2 Ferroelectric Material based Discrete Components

Instead of using ferroelectric material as a substrate for the whole structure, it can be used to integrate ferroelectric based reconfigurable devices. However, only few studies have demonstrated, fabricated and integrated such devices because of the very recent development of thin film technology for ferroelectric which must be compatible with the standards RF standards [117]. The most used solution is to create a local capacitor. This element is used to change the electrical length of the antenna [133][134]. In Cardona's work [120], a reconfigurable antenna design using a thin BST layer (Ba_xSr_1-xT_iO_3) based capacitance is presented. The antenna design is described inFigure 78. The antenna can cover a wide frequency band ranging from 700 MHz to 960 MHz for mobile applications.

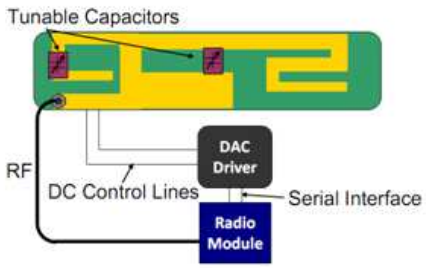

Figure 78 BST reconfigurable capacitance based antenna for mobile applications [120]

6.2.2.4.3.3 Monolithic Solution

Another implementation is to design a monolithic reconfigurable component with the antenna [121]-[124], usually a capacitor. In [124], Li et al. use an interdigitated capacitor on a 200 nm thick BST substrate. These capacitors are located in different positions in the slot loop antenna (shown in Figure 79). The DC voltage applied to the capacitors is ranging from 0 to 39V (a maximum electric field of 1950 kV/cm). It results in a shift of the resonant frequency ranging from 15.18 GHz to 15.36 GHz respectively.

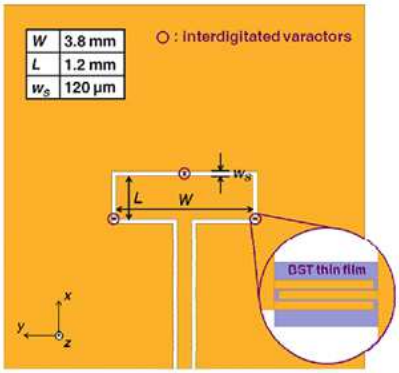

Figure 79 Slot antenna with varactors on a thin film of BST [124]

In [122], Jiang et al. has also demonstrated an antenna integrating nine capacitors based on thin film of BST in a rectangular slot antenna (Figure 80). The capacitance values can be set using a DC voltage giving frequency agility to the antenna. A frequency sweep ranging from 5.3 GHz to 5.8 GHz is achieved when the voltage applied to the BST thin film varies from 0 to 7 V (the maximum static field is about 280 KV/cm). The maximum measured antenna gain is - 3 dBi (Figure 81-b).

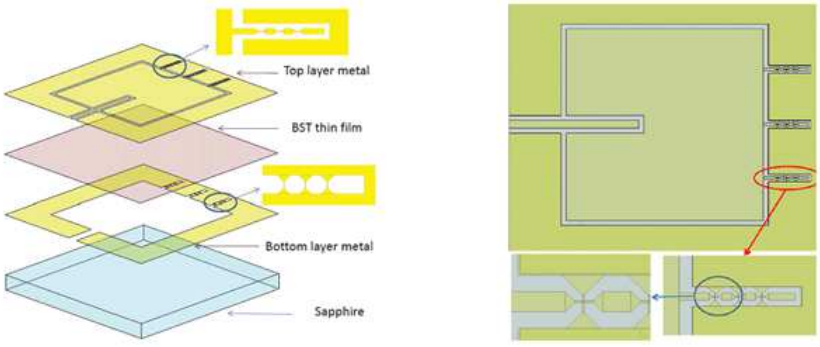

(a) (b)

Figure 80 Rectangular slot antenna with integrated capacitance on thin film of BST [122]: a) stack of layers and b) zoom on the capacitances

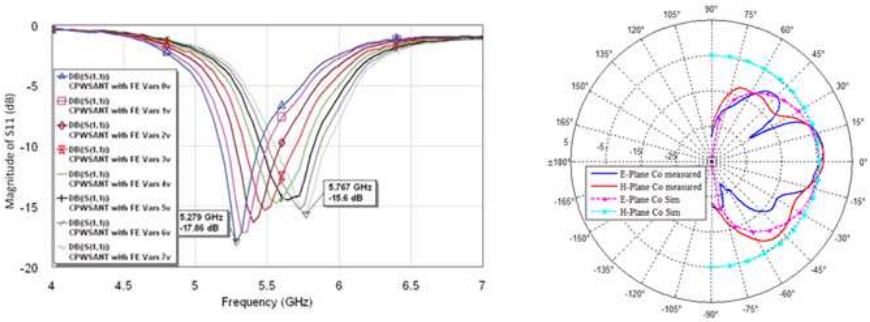

(a) (b)

Figure 81 a) Reflection coefficient versus the applied continuous voltage and b) radiation pattern of the antenna with ferroelectric capacitances (V = 0V)

The drawback of this solution is that the testing of the antenna (feed and biasing) is done through micro-probing. Consequently, the measurements of the radiation pattern becomes challenging.

6.2.2.4.4 Liquid Crystal

Liquid crystals are materials combining the properties of the liquid state and the solid crystal state in their metastable state (usually called mesophase). Generally, they are used for their optical properties and for display applications such as LCDs. However, the dielectric properties of these materials are very sensitive to electric or even magnetic fields making them interesting to use in reconfigurable systems.

The liquid crystal state most commonly used in microwave applications is the nematic state [125]. This state consists of elongated shape molecules with an averaged orientation in a well-defined direction (Figure 82-a). It is maintained by the presence of a PVA layer (PolyVinylAlcohol). Molecules are tilted when an external electric field is applied (Figure 82-b) and aligned along field orientation. The electric field applied to this substrate controls its permittivity and thus gives agility to the device designed on it.

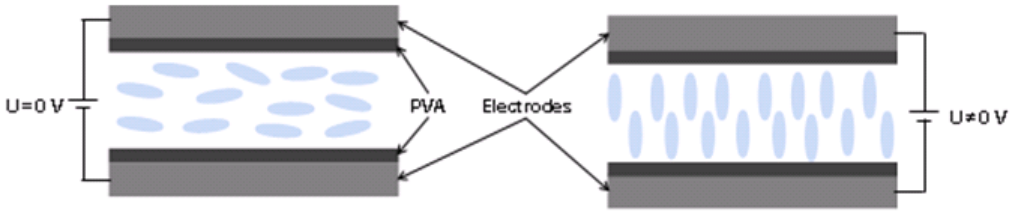

(a) (b)

Figure 82 Schematic diagram of a liquid crystal based capacitance, without electric field (a) and with electric field (b)

Several studies have shown agile devices using this technology [126]-[130]. In [127], Liu and Langley present a liquid crystal based microstrip antenna operating at 5 GHz. 4% agility is achieved using a voltage ranging from DC to 10 V (Figure 83). However, the material exhibits important losses (0.12) which significantly affect the antenna efficiency with 20% and 35% for control voltages of 0 V and 10V respectively. With a 0.51 mm thick substrate, the electric field used in this study is low with 0.2 KV/cm.

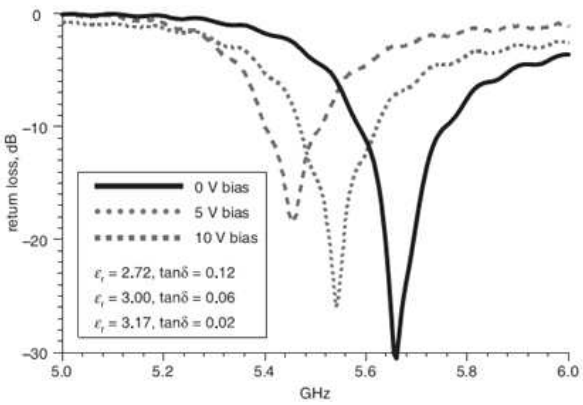

Figure 83 Reflection coefficient of a liquid crystal based microstrip antenna [127]

The main advantage of these materials is the low electric field required to control the material characteristics. This sensitivity to electric field leads to the major drawbacks for its use in microwave reconfigurable devices. First the losses of these materials are too high for most of the applications and then the response time of several seconds can also be an issue for lots of applications.

6.2.2.5 **Liquid Metal**

As shown in the previous sections, to change the resonant frequency of an antenna its electrical dimensions must be modified. The first idea is to change its physical dimensions. This simple idea was not easy to implement as it requires stretchable materials which keep their electrical or mechanical properties. Recent works focus on lightweight, flexible, and stretchable antennas for low cost applications [131]. Flexible antennas can be used in wearable health-monitoring devices or for sensors and security applications such as RFIDs. In these applications, flexibility is desired but usually without changing the antenna parameters. However, this technology is well-suited for reconfigurable antennas.

An example of reconfigurable dipole antenna using a liquid metal and a stretchable substrate is presented in [131]. The bendable, frequency-reconfigurable dipole antenna is implemented by embedding a liquid metal alloy (Galinstan) micro-channeled in a polydimethylsiloxane (PDMS) substrate. It is shown that the resonant frequency of the liquid metal antenna can be tuned by stretching the substrate, thereby altering the physical length of the antenna. A hybrid substrate has later been presented to increase the strain by up to 120% by incorporating a more elastic substrate around the rigid components while maintaining the PDMS substrate [132]. Fabrication of the hybrid substrate is more complicated and requires extra steps.

In [133], experimental results of a frequency-reconfigurable microstrip patch antenna using a new flexible material are reported. The proposed design is a patch antenna implemented using a planar reservoir of Galinstan inserted in the substrate (Figure 84-a). The substrate can be stretched by up to 300% (Figure 84-b). To enhance the strain, a new TC5005 silicone substrate structure and a slot-aperture-coupled feeding technique are incorporated.

It is shown that by stretching the substrate along the length of the antenna, its operating frequency can be reconfigured as a smooth transition. It demonstrates a narrowband behavior which operates from 1.3 to 4 GHz depending how the substrate is stretched (Figure 85).

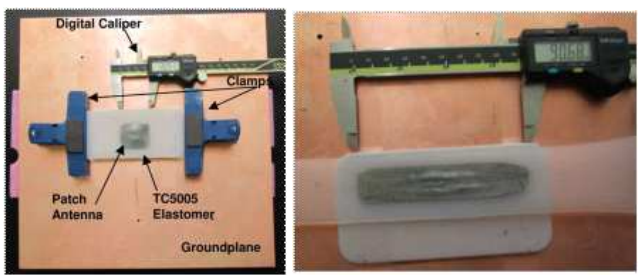

a) b)

Figure 84 a) Relaxed (non-stretched) and b) stretched state patch antenna prototype

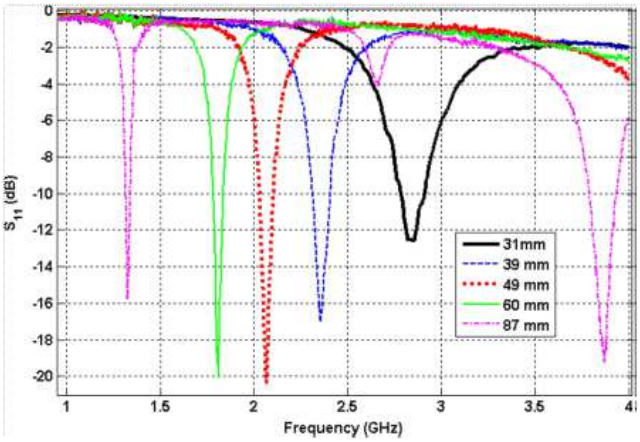

Figure 85 Variations of the Galinstan patch antenna when altering its geometrical length by stretching

6.3 Compact antenna solution investigations

Mainly two challenging issues will be addressed in this work. Firstly, it deals with the extension of antenna operating frequency band towards low frequency. Classically, broad operating frequency band at lower frequency leads to larger antenna dimensions [134]– [136]. Secondly, carrier aggregation asks for multi-band antenna solutions able to operate simultaneously in each band. In accordance with front-end architecture, a particular configuration of compact multiband antenna has to be investigated. The main guideline is to keep compact the antenna dimensions in spite of the multifunctional and low frequency requirements.

6.3.1 Preliminary requirements

In accordance with the development of the RF transmitter and receiver, the demonstrator is planned to operate in LTE-A bands 7 (2.5 – 2.69 GHz) and 20 (791-862 MHz). Different scenarios of communications are envisaged based on 3GPP TS36.521 Release 10 in Europe such as:

- Intra band CA in band 7
- Inter band CA in bands 7 and 20

Dedicated RF front-end will support each frequency band. Two antenna ports are necessary for connection to distinct front-ends dedicated to each LTE-A frequency band. First antenna demonstrator deals with compact sectorial antenna typically used for access points of small cells.

6.3.2 Strategy of antenna topology development

To limit the dimension of the antenna while addressing lower operating frequencies, the strategy of frequency agile antenna solution has been selected. By limiting the instantaneous bandwidth, it is expected to obtain correct antenna efficiency with miniature antenna dimensions. Based on the state of the art of the frequency agile techniques, we have selected the solution using tunable components (varactor, DTC) on compact resonator, as first approach.

Carrier aggregation needs multiband antenna solution with different RF access in our case. To limit antenna size, cohabitation of miniature frequency agile low band radiating element is investigated with more classical broad high band antenna structure (where miniaturization work is not necessary). The imbrication of dual port radiating element is of particular interest to obtain compact structure with similar performance in each operating band. Moreover, specific studies have to be performed concerning combination of radiating structures, including command of the frequency agile miniature antenna, to limit possible alterations.

An illustration of the proposed concept is presented in Figure 86. The described structure is developed for directional radiation (sectorial) antenna properties but version for omnidirectional radiation can be equally investigated, if needed. The overall antenna system dimension is given by the upper band antenna where no miniaturization effort is required. As an example, a patch antenna can be used to cover the upper frequency band using specific arrangement to obtain the broadband behavior. The typical dimensions for this antenna are between half and quarter wavelength (6 – 3 cm). A miniaturized frequency agile radiating structure is studied in order to operate over 790-870 MHz with similar

dimensions (that means operating wavelength divided by 6 – 12). A modified loop antenna over limited ground plane illustrates one of the investigated radiating structures to obtain this kind of performances.

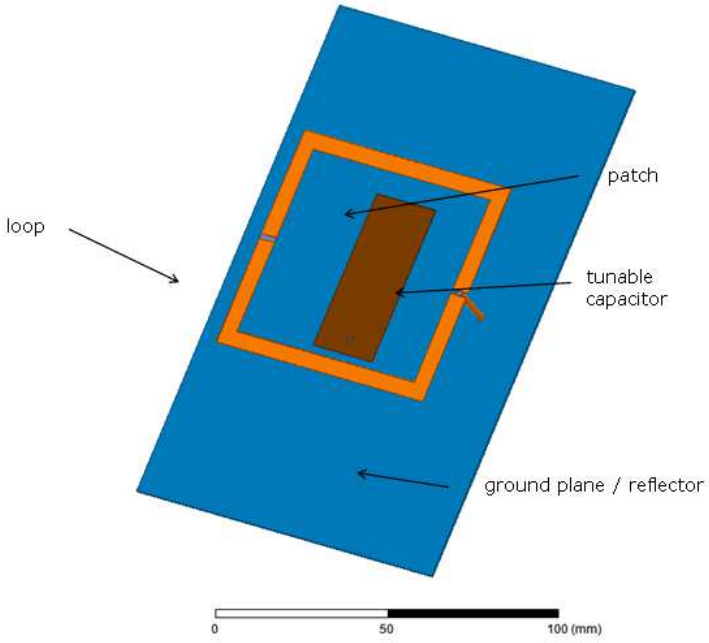

Figure 86 Illustration of possible antenna structure

7 CONCLUSIONS AND THE WAY FORWARD

This document describes the main challenges and objectives for the innovations on multi-point transmission and reception schemes, which are contained in WP3 of the SHARING project. Hence, detailed descriptions of the problems and the targeted solutions as well as the challenges related to these solutions are presented. Furthermore, some initial evaluation results, where available, have been shown.

The purpose of WP3 is to investigate the benefits of cooperation in multi-point transmission and reception schemes, and to determine to what extent these schemes bring performance and capacity gains in near-future wireless networks. To this end, the work in WP3 will achieve this purpose by addressing the problem from different points of views: transmitter cooperation (chapter 2), interference mitigation at the receiver (chapter 3) and cross-layer interference mitigation within a transmitter-receiver cooperation framework (chapter 4). In addition, these innovations are accompanied by the following studies: a realistic simulation framework to assess the real benefits of the studied solutions (chapter 5), and an innovative RF front-end and antenna solution as an enabler for the challenging RF issues involved in carrier aggregation for small cells (chapter 6).

The information contained in this report will help the other WPs to get information on the studies/innovation, more precisely on their objectives and the incurred challenges; thus paving the way for fruitful cross-WP discussions and possible innovative solutions.

REFERENCES

[1] Thien-Toan Tran, Yoan Shin, Oh-Soon Shin, "Overview of Enabling Technologies for 3GPP LTE-Advanced, " EURASIP Journal on Wireless Communications and Networking, 2012

[2] TR 36.814 3GPP Release 9, "Technical Specification Group Radio Access Network; Evolved Universal Terrestrial Radio Access (E-UTRA); Further advancements for E-UTRA physical layer aspects"

[3] TR 36.819 3GPP Release 11, "Technical Specification Group Radio Access Network; Coordinated multi-point operation for LTE physical layer aspects"

[4] Report ITU-R M.2135-1 (12/2009) Guidelines for evaluation of radio interface technologies for IMT-Advanced (http://www.itu.int/pub/R-REP-M.2135-1-2009/fr)

[5] Kottath, Sandeep; Gesbert, David; Khanfir, Hajer; Hardouin, Eric "Broadcast channel feedback in multiple-antenna transmitter cooperation networks: Accuracy or consistency?" EW2014, 20th European Wireless Conference, May 14-16, 2014, Barcelona, Spain

[6] Irmer, R.; Droste, H.; Marsch, P.; Grieger, M.; Fettweis, G.; Brueck, S.; Mayer, H. -P; Thiele, L.; Jungnickel, V., "Coordinated multipoint: Concepts, performance, and field trial results,", IEEE Communications Magazine, vol.49, no.2, pp.102,111, February 2011

[7] 3GPP TS 36.211 Release11, Physical channels and modulation

[8] 3GPP TR 36.829 V11.1.0 (2012-12). 3rd Generation Partnership Project; Technical Specification Group Radio Access Network; Enhanced performance requirement for LTE User Equipment (UE) (Release 11)

[9] 3GPP TR 36.866 V2.0.0 (2014-02). 3rd Generation Partnership Project; Technical Specification Group Radio Access Network; Network-Assisted Interference Cancellation and Suppression for LTE (Release 12)

[10]Bai, Z.; Badic, B.; Iwelski, S.; Scholand, T.; Balraj, R.; Bruck, G.; Jung, P., "On the Equivalence of MMSE and IRC Receiver in MU-MIMO Systems," Communications Letters, IEEE , vol.15, no.12, pp.1288,1290, December 2011

[11]Ghaffar R.; Knopp R., "Interference-aware receiver structure for multi-user MIMO and LTE," EURASIP Journal on Wireless Communications and Networking 2011

[12]Jung Hyun Bae; Sungsoo Kim; Jungwon Lee; Inyup Kang, "Advanced downlink MU-MIMO receiver for 3GPP LTE-A," Communications (ICC), 2012 IEEE International Conference on , vol., no., pp.7004,7008, 10-15 June 2012

[13]Latif, I.; Kaltenberger, F.; Knopp, R., "Link abstraction for multi-user MIMO in LTE using interference-aware receiver," Wireless Communications and Networking Conference (WCNC), 2012 IEEE, vol., no., pp.842,846, 1-4 April 2012

[14]P.Chevalier, F.Dupuy, "Widely Linear Alamouti Receiver for the Reception of Real-Valued Constellations Corrupted by Interferences—The Alamouti-SAIC/MAIC Concept", IEEE Transactions on signal processing, Vol. 59, No. 7, July 2011

[15]T. S. Han and K. Kobayashi, "A New achievable rate region for the interference channel," IEEE Trans. Inf. Theory, vol. 27, no. 1, pp. 49–60, Jan. 1981.

[16]M. Ali Maddah-Ali and D. Tse, "Completely stale transmitter channel state information is still very useful," Information Theory, IEEE Transactions on, vol. 58, no. 7, pp. 4418–4431, 2012

[17]S. Yang, M. Kobayashi, D. Gesbert, and X. Yi, "Degrees of freedom of time correlated miso broadcast channel with delayed csit," Information Theory, IEEE Transactions on, vol. 59, no. 1, pp. 315–328, 2012.

[18]S. Jafar, "Interference alignment: A new look at signal dimensions in a communication network," Foundations and Trends in Communications and Information Theory, vol. 7, no. 1, pp. 1–136, 2011.

[19]X. Yi, S. Yang, D. Gesbert, and M. Kobayashi, "The degrees of freedom region of temporally-correlated MIMO networks with delayed □CSIT," IEEE Trans. Inf. Theory, vol. 60, no. 1, pp. 494 – 514, Jan. 2014.

[20]S. Yang, M. Kobayashi, P. Piantanida, and S. Shamai, "Secrecy degrees of freedom of MIMO broadcast channels with delayed CSIT," IEEE Trans. Inf. Theory, vol. 59, no. 9, pp. 5244–5256, Sept. 2013.

[21]S. Park and C. G. Kang, "Complexity-reduced iterative MAP receiver for interference suppression in OFDM-based spatial multiplexing systems," IEEE Trans. Veh. Technol., vol. 53, no. 5, pp. 1316–1326, 2004.

[22]D. Asztly and B. Ottersten, "MLSE and spatio-temporal interference rejection combining with antenna arrays," in Proc. Ninth European Signal Processing Conference (Eusipco'98), 1998.

[23]R. Narasimhan and S. Cheng, "Channel estimation and co-channel interference rejection for LTE-advanced mimo uplink," in Proc. IEEE Wireless Communications and Networking Conference (WCNC'12), 2012.

[24]M. Di Renzo, H. Haas, A. Ghrayeb, S. Sugiura, and L. Hanzo, "Spatial modulation for generalized MIMO: Challenges, opportunities, and implementation," Proceedings of the IEEE, vol. 102, no. 1, pp. 56–103, 2014.

[25]R. Mesleh, H. Haas, Y. Lee, and S. Yun, "Interchannel interference avoidance in MIMO transmission by exploiting spatial information," in Proc. IEEE Personal, Indoor and Mobile Radio Communications (PIMRC'05), 2005.

[26]S. Ganesan, R. Mesleh, H. Haas, C. W. Ahn, and S. Yun, "On the performance of spatial modulation OFDM," in Proc. Signals, Systems and Computers (ACSSC '06), 2006.

[27]J. Jeganathan, A. Ghrayeb, and L. Szczecinski, "Spatial modulation: optimal detection and performance analysis," IEEE Commun. Lett., vol. 12, no. 8, pp. 545–547, Aug 2008.

[28]J. Jeganathan, A. Ghrayeb, L. Szczecinski, and A. Ceron, "Space shift keying modulation for MIMO channels," IEEE Trans. Wireless Commun., vol. 8, no. 7, pp. 3692–3703, 2009.

[29]J. Jeganathan, A. Ghrayeb, and L. Szczecinski, "Generalized space shift keying modulation for MIMO channels," in Proc. IEEE Personal, Indoor and Mobile Radio Communications (PIMRC'08), 2008.

[30]F. Pipon, P. Chevalier, P. Vila et J.J. Monot, "Joint Spatial and Temporal Equalization for Channels with ISI and CCI - Theretical and Experimental results for a base station reception », Proc. IEEE Signal Processing Workshop on Signal Processing Advances in Wireless Communications, pp. 309-312, Paris, France, 1997

[31]R.W. Heath, D.J. Love, "Multimode antenna selection for spatial multiplexing systems with linear receivers," *IEEE Trans. Sig. Proc.*, vol. 53, no. 8, pp. 3042–3056, Aug. 2005.

[32]E. Ohlmer, G. Fettweis, "Link adaptation in linearly precoded closed-loop MIMO-OFDM systems with linear receivers," *Proc. IEEE ICC'09*, Dresden, Germany, Jun. 2009.

[33] K.M. Varanasi, T. Guess, "Optimum decision feedback multiuser equalization with successive decoding achieves the total capacity of the Gaussian multiple access channel," *Proc. Asilomar Conf.*, Pacific Grove, CA, USA, Nov. 1997.

[34] C. Berrou, A. Glavieux, P. Thitimajshima, "Near Shannon limit error-correcting coding and decoding: Turbo codes," *Proc. IEEE ICC'93*, Geneva, Switzerland, May 1993.

[35]S. ten Brink, "Convergence behavior of iteratively decoded parallel concatenated codes," *IEEE Trans. Commun*, vol. 49, no. 10, pp. 1727–1737, Oct. 2001.

[36]S. ten Brink, "Convergence of multi-dimensional iterative decoding schemes," *Proc. IEEE ACSSC'01*, Pacific Grove, USA, Nov. 2001.

[37]M. Tüchler, "Convergence prediction for iterative decoding of threefold concatenated systems," *Proc. IEEE GLOBECOM'02*, Taipei, Taiwan, R.O.C., Nov. 2002.

[38]S. ten Brink, G. Kramer, A. Ashikhmin, "Design of low-density parity-check codes for modulation and detection," *IEEE Trans. Commun.*, vol. 52, no. 4, pp. 670–678, Apr. 2004.

[39]R. Visoz, A.O. Berthet, M. Lalam, "Semi-analytical performance prediction methods for iterative LMMSE-IC multiuser MIMO joint decoding," *IEEE Trans. Commun.*, vol. 58, no. 9, pp. 2576–2589, Sep. 2010.

[40]B. Ning, R. Visoz, A.O. Bethet, "Link adaptation in closed-loop MIMO systems of LTER with LMMSE-IC based turbo receivers," *Proc. IEEE WIMOB*, Lyon, France, Oct. 2013

[41]Jafar, S.A., "Topological Interference Management Through Index Coding," *IEEE Transactions on Information Theory*, vol.60, no.1, pp.529,568, Jan. 2014.

[42]X. Yi and D.Gesbert, "Topological interference management with transmitter cooperation,'' in Proc. of IEEE International Symposium on Information Theory (ISIT'14), Hawaii, USA, July 2014.

[43]L. Brunel, M. Plainchault, M. Gresset, N. Dammann, C. Mensing, and R. Raulefs, «Inter-Cell Interference Coordination and Synchrinization based on Location Information», in Proc. *Positioning Navigation and Communication workshop (WPNC'10)*, Dresden, Germany, 2010.

[44]J. Guillet, L. Brunel, and N. Gresset, «Downlink femto-macro ICIC with blind long-term power setting», in Proc. *Personal Indoor and Mobile Radio Communications (PIMRC'11)*, Toronto, canada, 2011.

[45]S. Deb, P. Monogioudis, J. Miernik, and J.P. Seymour, «Algorithms for Enhanced Inter-Cell Interference Coordination (eICIC) in LTE HetNets», in *IEEE/ACM transactions on networking, vol. 22, NO. 1,* pp. 137-150, 2014.

[46]B. Pijcke, M. Zwingelstein-Colin. M. Gazalet, M. Gharbi, and P. Corlay, «An analytical model for the intercell interference power in the downlink of wireless cellular networks», in *EURASIP journal on Wireless Communication and Networking,* pp. 1-20, 2011.

[47]Y. Zhuang, Y. Luo, L. Cia, and J. Pan, «A Geometric probability Model for Capacity Analysis and Interference Estimation in Wireless Mobile Cellular Systems», in Proc. IEEE Globecom workshop (G*lobecom'11)*, Houston, USA, 2011.

[48]N. Akl, and Z. Dawy, «Statistical Interference Maps for Opportunistic Spectrum Access in OFDMA Cellular Networks», in Proc. Global Conference on Signal and Information Processing (G*lobalSIP'13)*, Austin, USA, 2013.

[49]P.C. Pinto, A. Giorgetti, M.Z. Win, and M. Chiani, «A Stochastic Geometry Approach to Coexistence in Heterogeneous Wireless Networks», in *IEEE journal on selected areas in communications, Vol. 27, NO. 7,* pp. 1268-1282, 2009.

[50]H.S. Dhillon, R.K. Ganti, F. Baccelli, and J.G. Adrews, «Modeling and Analysis of K-tier Downlink Heterogeneous Cellular Networks», in *IEEE journal on selected areas in communications,* vol. 30, n° 13, pp. 550-560, 2012.

[51]S. Wang, W. Guo, and M.D. McDonnell, «Downlink Interference Estimation without Feedback for Heterogeneous Network Interference Avoidance», in Proc. *International Conference on telecommunications*, Lisbon, Portugal, May 2014.

[52]S. Wang, and W. Guo, «Mobile Corwd-sensing Wireless Activity with Measured Interference Power», in *IEEE wireless communications letters,* vol. 2, n° 15, pp. 539-542, october 2013.

[53]A. Babaei, M. Haenggi, P. Agrawal, and B. Jabbari, «Interference Statistics of a Poisson Field of Interferers with Random Puncturing», in Proc. Military Communications Conference (*MILCOM'11)*, Baltimore, MD, USA, November 2011.

[54]Y. Gu, A. Lo, and I. Niemegeers, «A survey of indoor positioning systems for wireless personal networks», in *IEEE communications surveys and tutorials, Vol. 11, NO. 1,* pp. 13-32, 2009.

[55]A. Boukerche, H.A.B.F. Oliveira, E.F. Nakamura, and A.A.F. Loureiro, «Vehicular Ad Hoc networks: A new challenge for localization-based systems», in *Science direct computer comunications,* 2008.

[56]A. Roxin, J. Gaber, M. Wack, and A. Nait-Sidi-Moh, «Survey of wireless geolocation techniques», in Proc. IEEE Globecom workshops, Washington DC, USA, December 2007.

[57]R.C. Darakanath, J.D. Naranjo, and A. Ravanshid, «Modeling of Interference Map for Licensed Shared Access in LTE-Advanced Networks Supporting Carrier Aggregation», in *Wireless Day – IFIP*, Niagara falls, Canada, 2013.

[58]D. Shepard, «A tow dimentional interpolation function for irregularly space data», in *ACM national conference,* pp. 517-524, 1968.

[59]S. Üreten, A. Yongaçoglu, and A. Petriu, «Interference Map Generation Based on Delaunay Triangulation in Cognitive Radio Networks», in IEEE workshop in Signal Processing Advances in Wireless Communications (*SPWAC'12)*, Cesme, Turkey, 2012.

[60]S-J. Kim, E. Dann'Anese, and G.B. Giannakis, «Cooperative Spectrum Sensing for Cognitive Radios Using Kriged kalman Filtering», in *IEEE journal of selected topics in signal processing, Vol. 5, NO. 1,* 2011.

[61]H. Noureddine, N. Gresset, D. Castelain, R. Pyndiah, "Auto-Regressive Modeling of the Shadowing for RSS Mobile Tracking," in Proc. IEEE International Conference on Communications (ICC'11), Kyoto, Japan, June 2011.

[62]H. Noureddine, D. Castelain, R. Pyndiah, "Train Tracking and Shadowing Estimation Based on

Received Signal Strength", in Communication Technologies for Vehicles, Lecture Notes in Computer Science Volume 6596, pp 23-33, 2011

[63]Y. Corre and Y. Lostanlen, "Three-dimensional urban EM wave propagation model for radio network planning and optimization over large areas", IEEE Transactions on Vehicular Technology, vol. 58, no. 7, pp. 3112-3123, Sept. 2009.

[64]V. Degli-Esposti, F. Fuschini, E. M. Vitucci and G. Falciasecca, "Measurement and Modelling of Scattering From Buildings", IEEE Transactions on Antennas and Propagation, vol. 55, no. 1, Jan. 2007.

[65]D. Tse And T. Viswanath, Fundamentals of wireless communication, Ed. PramodViswanath. Cambridge university press, Chap. 7, 2005.

[66]F. Letourneux, S. Guivarch and Y. Lostanlen, "Tools on outdoor small-cell deployment cost in a realistic urban scenario", accepted for 80th IEEE Vehicular Technology Conference (VTC 2014-Fall), Sept. 2014.

[67]3GPP TS36.521 Release 12, "User equipment conformance specification radio transmission and reception".

[68]3GPP TR36.815 Release 9, "LTE-Advanced feasibility studies in RAN WG4"

[69]3GPP TR36.104 Release 12, "Base station (BS) radio transmission and reception"

[70]D. Schaubert, F. Farrar, A. Sindoris, and S. Hayes, "Microstrip antennas with frequency agility and polarization diversity," IEEE Transactions on Antennas and Propagation, vol. 29, no. 1, pp. 118 – 123, Jan. 1981.

[71]T. Korosec, P. Ritos, and M. Vidmar, "Varactor-tuned microstrip-patch antenna with frequency and polarisation agility," Electronics Letters, vol. 42, no. 18, pp. 1015–1016, Aug. 2006.

[72]R. N. Simons, D. Chun, and L. P. B. Katehi, "Reconfigurable array antenna using microelectromechanical systems (MEMS) actuators," IEEE Antennas and Propagation Society International Symposium, vol. 3, pp. 674 –677, 2001.

[73]C. Zhang, S. Yang, H. K. Pan, A. E. Fathy, S. El-Ghazaly, and V. Nair, "Development of reconfigurable mini-nested patches antenna for universal wireless receiver using MEMS," in IEEE Antennas and Propagation Society International Symposium, pp. 205–208, July 2006.

[74]Z. Liu, K. Boyle, JoonasKrogerus, M. de Jongh, K. Reimann, R. Kaunisto, and J. Ollikainen, "MEMS-Switched, Frequency-Tunable Hybrid Slot/PIFA Antenna," IEEE Antennas and Wireless Propagation Letters, vol. 8, pp. 311–314.

[75]J.-C. Chiao, Y. Fu, I. M. Chio, M. DeLisio, and L.-Y. Lin, "MEMS reconfigurable Vee antenna," IEEE MTT-S International in Microwave Symposium Digest, vol. 4, pp. 1515–1518, 1999.

[76]J.R. Moritz and Y. Sun, "Frequency Agile Antenna Tuning and matching", HF Radio Systems and Techniques, 2000. Eighth International Conference on (IEE Conf. Publ. No. 474), 2000, pp. 169-174

[77]O. Kivekãs , J. Ollikainen and P. Vainikainen "Frequency-tunable internal antenna for mobile phones", 12th International Symposium on Antennas, Nice, France, volume 2, pages 53-56, November 2002.

[78]Fankem, B.K.; Melde, K.L.; Zhen Zhou; , "Frequency reconfigurable planar inverted F antenna (PIFA) with software-defined match control," IEEE Antennas and Propagation Society International Symposium, 2007, pp.81-84, 9-15 June 2007.

[79]P. Panaia, R. Staraj, C. Luxey, G. Kossiavas, and G. Jacquetmod, "Antenne pifa commutable à fente," Proc. 13èmes Journées Nationales Microondes, pp. 446–447, 2003.

[80]J.-C. Chiao, Y. Fu, I. M. Chio, M. DeLisio, and L.-Y. Lin, "MEMS reconfigurable Vee antenna," IEEE MTT-S International in Microwave Symposium Digest, vol. 4, pp. 1515–1518, 1999.

[81]K. F. Sabet, L. P. B. Katehi, and K. Sarabandi, "Modeling and design of mems-based reconfligurable antenna arrays," Proceedings in IEEE Aerospace Conference, vol. 2, pp. 2_1135–2_1141, March 2003.

[82]R. N. Simons, D. Chun, and L. P. B. Katehi, "Reconfigurable array antenna using microelectromechanical systems (MEMS) actuators," in IEEE Antennas and Propagation Society International Symposium, vol. 3, pp. 674 –677, 2001.

[83]C. Zhang, S. Yang, H. K. Pan, A. E. Fathy, S. El-Ghazaly, and V. Nair, "Development of

reconfigurable mini-nested patches antenna for universal wireless receiver using MEMS," International Symposium in IEEE Antennas and Propagation Society, pp. 205–208, July 2006.

[84]L. Le Garrec, R. Sauleau, and M. Himdi, "Frequency-and polarization-agile reconfigurable antennas," in 6th Conference on Telecommunications, pp. 49–52, 2007.

[85]J.-M. Laheurte, "Switchable CPW-fed slot antenna for multifrequency operation," Electronics Letters, vol. 37, no. 25, pp. 1498 –1500, Dec. 2001.

[86]N. Behdad and K. Sarabandi, "A varactor-tuned dual-band slot antenna," IEEE Transactions on Antennas and Propagation, vol. 54, no. 2, pp. 401– 408, Feb. 2006.

[87]M. Berg, M. Komulainen, V. Palukuru, H. Jantunen, and E. Salonen, "Frequency-tunable DVB-H antenna for mobile terminals," International Symposium in IEEE Antennas and Propagation Society, pp. 1072 –1075, 2007.

[88]B. R. Holland, R. Ramadoss, S. Pandey, and P. Agrawal, "Tunable coplanar patch antenna using varactor," Electronics Letters, vol. 42, no. 6, pp. 319 – 321, March 2006.

[89]M. C. Scardelletti, G. E. Ponchak, J. L. Jordan, N. Jastram, and J. V. Mahaffey, "Tunable reduced size planar folded slot antenna utilizing varactor diodes," IEEE Radio and Wireless Symposium (RWS), pp. 547–550, 2010.

[90]T. Korosec, P. Ritos, and M. Vidmar, "Varactor-tuned microstrip-patch antenna with frequency and polarisation agility," Electronics Letters, vol. 42, no. 18, pp. 1015–1016, Aug. 2006.

[91]Cheng-Shong Hong, "Small annular slot antenna with capacitor loading," *Electronics Letters*, vol. 36, no. 2, pp. 110–111, Jan. 2000.

[92]J.-H. Lim, G.-T. Back, Y.-I. Ko, C.-W. Song, and T.-Y. Yun, "A Reconfigurable PIFA Using a Switchable PIN-Diode and a Fine-Tuning Varactor for USPCS/WCDMA/m-WiMAX/WLAN," IEEE Transactions on Antennas and Propagation, vol. 58, no. 7, pp. 2404 –2411, Jul. 2010.

[93]Baxter, B.; Ranta, T.; Facchini, M.; Dongjin Jung; Kelly, D., "The state-of-the-art in silicon-on-sapphire components for antenna tuning," 2013 IEEE MTT-S International Microwave Symposium Digest (IMS), pp.1,4, 2-7 June 2013.

[94]https://www.psemi.com/pdf/app_notes/an29.pdf

[95]S. Sufyar, C. Delaveaud, R. Staraj, "Frequency agility investigations on compact omnidirectional antennas using variable inductors," 14th International Symposium on Antenna Technology and Applied Electromagnetics & the American Electromagnetics Conference, pp.1,4, 5-8 July 2010.

[96]C. Delaveaud, P. Leveque, B. Jecko, "Small-sized low-profile antenna to replace monopole antennas", Electronics Letters, Vol. 34, Issue: 8, pp. 716-717, 16 Apr 1998.

[97]V. I. Slyusar, "Metamaterials on antenna solutions," in International Conference on Antenna Theory and Techniques, Lviv, Ukraine, pp. 19–24, 2009.

[98]O. Reynet and O. Acher, "Voltage controlled metamaterial," Applied Physics Letters, vol. 84, no. 7, pp. 1198–1200, Feb. 2004.

[99]C. Lin, I. O. Mirza, S. Shi, and D. W. Prather, "Tuneable Meta-Material Split-Ring Resonators for Impedance Matching Antennas for Broadband Applications," DTIC Document, 2008.

[100] M. A. Abdalla and Z. Hu, "Comapct and tunable metamaterial antenna for multi-band wireless communication applications," IEEE International Symposium on Antennas and Propagation (APSURSI), pp. 1054 –1057, 2011.

[101] D. M. Pozar and V. Sanchez, "Magnetic tuning of a microstrip antenna on a ferrite substrate," Electronics Letters, vol. 24, no. 12, pp. 729 –731, Jun. 1988.

[102] H. How, P. Rainville, F. Harackiewicz, and C. Vittoria, "Radiation frequencies of ferrite patch antennas," Electronics Letters, vol. 28, no. 15, pp. 1405 –1406, Jul. 1992.

[103] R. K. Mishra, S. S. Pattnaik, and N. Das, "Tuning of microstrip antenna on ferrite substrate," IEEE Transactions on Antennas and Propagation, vol. 41, no. 2, pp. 230 –233, Feb. 1993.

[104] ErwanSalahun, "Etude et réalisation de dispositifs micro-ondes agiles à commandemagnétiqueutilisant des matériauxcompositesferromagnétiques," l'Université de BretagneOccidentale, 2002.

[105] E. Salahun, G. Tanné, P. Quéffélec, M. Lefloc'h, A.-L. Adenot, and O. Acher, "Application of

ferromagnetic composite in different planar tunable microwave devices," Microwave and Optical Technology Letters, vol. 30, no. 4, pp. 272–276, 2001.

[106] G. F. Dionne, D. E. Oates, D. H. Temme, and J. A. Weiss, "Ferrite-superconductor devices for advanced microwave applications," IEEE Transactions on Microwave Theory and Techniques, vol. 44, no. 7, pp. 1361–1368, Jul.

[107] M. W. Cole, P. C. Joshi, and M. H. Ervin, "La doped Ba1−xSrxTiO3 thin films for tunable device applications," Journal of Applied Physics, vol. 89, no. 11, pp. 6336–6340, Jun. 2001.

[108] K. B. Chong, L. B. Kong, L. Chen, L. Yan, C. Y. Tan, T. Yang, C. K. Ong, and T. Osipowicz, "Improvement of dielectric loss tangent of Al2O3 doped Ba0.5Sr0.5TiO3 thin films for tunable microwave devices," Journal of Applied Physics, vol. 95, no. 3, pp. 1416–1419, Feb. 2004.

[109] Q. Simon, V. Bouquet, W. Peng, J.-M. Le Floch, F. Houdonougbo, S. Députier, S. Weber, A. Dauscher, V. Madrangeas, D. Cros, and M. Guilloux-Viry, "Reduction of microwave dielectric losses in KTa1 − xNbxO3 thin films by MgO-doping," Thin Solid Films, vol. 517, no. 20, pp. 5940–5942, Aug. 2009.

[110] M. Jain, S. B. Majumder, R. S. Katiyar, and A. S. Bhalla, "Structural and dielectric properties of heterostructured BST thin films by sol–gel technique," Thin Solid Films, vol. 447–448, pp. 537–541, Jan. 2004.

[111] E. A. Nenasheva, N. F. Kartenko, I. M. Gaidamaka, O. N. Trubitsyna, S. S. Redozubov, A. I. Dedyk, and A. D. Kanareykin, "Low loss microwave ferroelectric ceramics for high power tunable devices," Journal of the European Ceramic Society, vol. 30, no. 2, pp. 395–400, Jan. 2010.

[112] L. Tang, J. Zhai, H. Zhang, and X. Yao, "Microwave dielectric properties of tunable Ba0.5Sr0.5TiO3 and scheelite AMoO4 (A = Ba, Sr) composite ceramics," Journal of Alloys and Compounds, vol. 551, pp. 556–561, Feb. 2013.

[113] Y. Corredores, "Etude et amélioration des performances de dispositifshyperfréquencesaccordables à base de films mincesferroélectriques KTN et diélectriques BZN," Thèsesoutenue à Université de Rennes 1, 2012.

[114] G. Houzet, X. Malique, D. Lippens, L. Burgnies, G. Velu, and J.-C. Carru, "Microstrip Transmission Line Loaded by split-ring resonators tuned by ferroelectric thin film", Progress In Electromagnetics Research C, vol. 12, pp. 225–236, 2010.

[115] Y. Yashchyshyn and J. Modelski, "The leaky-wave antenna with ferroelectric substrate," in 14th International Conference on Microwaves, Radar and Wireless Communications, 2002. MIKON-2002, 2002, vol. 1, pp. 218–221 vol.1.

[116] A. M. Castro-Vilaro and R. A. R. Solis, "Tunable folded-slot antenna with thin film ferroelectric material," in IEEE Antennas and Propagation Society International Symposium, 2003, 2003, vol. 2, pp. 549–552 vol.2.

[117] S. Gevorgian, Ferroelectrics in Microwave Devices, Circuits and Systems Physics, Modeling, Fabrication and Measurements. London: Springer London, 2009.

[118] E. Lourandakis, M. Schmidt, S. Seitz, and R. Weigel, "Reduced Size Frequency Agile Microwave Circuits Using Ferroelectric Thin-Film Varactors," IEEE Transactions on Microwave Theory and Techniques, vol. 56, no. 12, pp. 3093 –3099, Dec. 2008.

[119] J. Nath, W. M. Fathelbab, P. G. Lam, D. Ghosh, S. Aygiin, K. G. Gard, J. P. Maria, A. I. Kingon, and M. B. Steer, "Discrete barium strontium titanate (BST) thin-film interdigitalvaractors on alumina: design, fabrication, characterization, and applications," in Microwave Symposium Digest, 2006. IEEE MTT-S International, 2006, pp. 552–555.

[120] A. H. Cardona, "Tunable BaSrTiO3 applications for the RF front end," in Microwave Symposium Digest (MTT), 2012 IEEE MTT-S International, 2012, pp. 1 –3.

[121] Hai Jiang, M. Patterson, Chenhao Zhang, and G. Subramanyam, "Frequency tunable microstrip patch antenna using ferroelectric thin film varactor," in Aerospace & Electronics Conference (NAECON), Proceedings of the IEEE 2009 National, 2009, pp. 248–250.

[122] H. Jiang, M. Patterson, D. Brown, C. Zhang, K. Pan, G. Subramanyam, D. Kuhl, K. Leedy, and C. Cerny, "Miniaturized and Reconfigurable CPW Square-Ring Slot Antenna Loaded With Ferroelectric BST Thin Film Varactors," IEEE Transactions on Antennas and Propagation, vol. 60, no. 7, pp. 3111 –3119, Jul. 2012.

[123] K. C. Pan, H. Jiang, D. Brown, C. H. Zhang, M. Patterson, and G. Subramanyam, "Frequency tuning of CPW bowtie antenna by ferroelectric BST thin film varactors," in Aerospace and Electronics Conference (NAECON), Proceedings of the 2011 IEEE National, 2011, pp. 1 –4.

[124] H.-Y. Li, H.-P. Chen, S.-C. Chen, C.-H. Tai, and J.-S. Fu, "A tunable slot loop antenna using interdigitated ferroelectric varactors," in 2012 IEEE Antennas and Propagation Society International Symposium (APSURSI), 2012, pp. 1–2.

[125] C. Janot and B. Ilschner, Matériaux émergents. Lausanne: Presses polytechniques et universitaires romandes, 2001.

[126] S. Missaoui, M. Kaddour, and A. Gharbi, "Design and simulation reconfigurable liquid crystal patch antennas on foam substrate," Journal of Chemical Engineering and Materials Science, vol. 2, no. 7, pp. 96–102, 2011.

[127] L. Liu and R. J. Langley, "Liquid crystal tunable microstrip patch antenna," Electronics Letters, vol. 44, no. 20, pp. 1179 –1180, 2008.

[128] A. Gaebler, A. Moessinger, F. Goelden, A. Manabe, M. Goebel, R. Follmann, D. Koether, C. Modes, A. Kipka, and M. Deckelmann, "Liquid crystal-reconfigurable antenna concepts for space applications at microwave and millimeter waves," International Journal of Antennas and Propagation, vol. 2009, 2009.

[129] W. Hu, M. Y. Ismail, R. Cahill, J. A. Encinar, V. Fusco, H. S. Gamble, D. Linton, R. Dickie, N. Grant, and S. P. Rea, "Liquid-crystal-based reflectarray antenna with electronically switchable monopulse patterns," Electronics Letters, vol. 43, no. 14, 2007.

[130] R. Bose and A. Sinha, "Tunable patch antenna using a liquid crystal substrate," in IEEE Radar Conference, pp. 1 –6, 2008.

[131] J.-H. So, J. Thelen, A. Qusba, G.J. Hayes, G. Lazzi, and M. D. Dickey, "Reversibly deformable and mechanically tunable fluidic antennas," Adv. Func. Mater, vol. 19, pp. 3632–3637, 2009.

[132] M. Kubo , X. Li , C. Kim , M. Hashimoto , B. J. Wiley , D. Ham and G. M. Whitesides "Stretchable microfluidic radiofrequency antennas", Adv. Mater., vol. 22, pp.2749 -2752, 2010.

[133] S.J. Mazlouman, X.J. Jiang, A. Mahanfar, C. Menon, R.G. Vaughan, "A Reconfigurable Patch Antenna Using Liquid Metal Embedded in a Silicone Substrate," *IEEE Transactions on Antennas and Propagation,* vol.59, no. 12, pp. 4406-4412, Dec. 2011.

[134] H. A.Wheeler, "Fundamental limitations of small antennas," Proc. IRE., vol. 35, pp. 1479-1484, Dec. 1947.

[135] L. J.Chu, "Physical limitations on omni-directional antennas," J. Appl. Phys., vol. 19, pp. 1163-1175, Dec. 1948.

[136] J. S. McLean, "A re-examination of the fundamental limits on the radiation Q of electrically small antennas", IEEE Trans. Antennas Propagat. vol. 44, pp. 672–675, May 1996.

GLOSSARY

ACRONYM	DEFINITION
3GPP	Third Generation Partnership Project
ABS	Almost Blank Subframe
ACLR	Adjacent Channel Leakage Ratio
AMI	Average Mutual Information
AP	Access Point
AWGN	Additive White Gaussian Noise
BC	Broadcast Channel
BER	Bit Error Rate
BS	Base Station
CA	Carrier Aggregation
CB	Coordinated Beamforming
CC	Component Carrier
CCUE	CoMP candidate User Equipment
CDF	Cumulative Distribution Function
CN	Condition Number
CO	Confidential
CoMP	Coordinated Multi-Point
CRS	Cell-specific Reference Signal
CS	Coordinated Scheduling
CSI	Channel State Information
CSIT	Channel State Information at Transmitter
CQI	Channel Quality Indication
D2D	Device to Device
DL	Downlink
DM-RS	DeModulation Reference Signal
DoA	Direction of Arrival
DoF	Degree of Freedom
DPS	Dynamic Point Selection
DTC	Digitally Tunable Capacitor
eICIC	enhanced Inter-Cell Interference Coordination
eNB	evolved Node B
FDD	Frequency Division Duplex
FET	Field Effect Transistor

FFR	Fractional Frequency Reuse
FIR	Finite-length Impulse Response
GSSK	Generalized Space Shift Keying
HetNET	HETerogeneous NETwork
HO	Hand Over
IA	Interference Alignment
IC	Interference Cancellation
ICI	Inter-Cell Interference
ICIC	Inter-Cell Interference Coordination
IMS	IP Multimedia Subsystem
IRC	Interference Rejection Combining
IS	Interference Suppression
ITU	International Telecommunication Union
HPT	Heterojunction Phototransistor
JP	Joint Processing
JT	Joint Transmission
LD	Linear Dispersive
LAPPR	Log *A Posteriori* Probability Ratio
LEXTPR	Log Extrinsic Probability Ratio
LMMSE	Linear Minimum Mean Square Error
LTE	Long Term Evolution
LTE-A	Long Term Evolution - Advanced
LUT	Look Up Table
MAC	Medium Access Control
MAIC	Multiple Antenna Interference Cancellation
MAP	Maximum A Posteriori
MBMS	Multimedia Broadcast Multicast Service
MCS	Modulation-Coding Scheme
MEMS	Micro Electro-Mechanical System
MIM	Metal Insulator Metal
MIMO	Multiple Input Multiple Output
MISO	Multiple Input Single Output
ML	Maximum Likelihood
MMSE	Minimum Mean Square Error
MU-MIMO	Multiple User MIMO
NAIC	Network Assisted Interference Cancellation

NAICS	Network Assisted Interference Cancellation and Suppression
NCUE	Non-CoMP User Equipment
OFDM	Orthogonal Frequency Division Multiplexing
PA	Power Amplifier
PAPR	Peak to Average Power Ratio
PF	Proportional fairness
PHY	Physical Layer
PIC	Parallel Interference Cancellation
PIFA	Planar Inverted-F Antenna
PIN	Positive Intrinsic Negative
PMI	Precoding Matrix Indication
QoS	Quality of Service
RAN	Radio Access Network
RAT	Radio Access Technology
RB	Resource Block
RF	Radio Frequency
RI	Rank Indication
RRM	Radio Resource Management
RS	Reference Signals
RSC	Recursive Systematic Convolutional
RSSI	Received Signal Strength Indication
RX	Reception
SAIC	Single Antenna Interference Cancellation
SC	Small Cell
SDoF	Secrecy Degree of Freedom
SFR	Soft Frequency Reuse
SIC	Successive Interference Cancellation
SINR	Signal to Interference plus Noise Ratio
SLIC	Symbol Level Interference Cancellation
SM	Spatial Modulation
SMX	Spatial Multiplexing
SNR	Signal to Noise Ratio
SON	Self-Organizing Network
SRR	Split Ring Resonator
SSK	Space Shift Keying
STBC	Space-Time Block Code

STBICM	Space Time Bit Interleaved Coded Modulation
SU-MIMO	Single User MIMO
SVD	Singular Value Decomposition
TDD	Time Division Duplex
TIM	Topological Interference Management
TR	Tuning Rate
TTI	Transmission Time Interval
TX	Transmission
UE	User Equipment
UL	Uplink
UMTS	Universal Mobile Telecommunication System
WCDMA	Wideband Code Division Multiplexing Access
Wi-Fi	Wireless Fidelity
WLAN	Wireless Local Area Network
WP	Work Package
WSN	Wireless Sensor Network